



# Book of Abstracts

of the

XI annual meeting

of the **ESB-ITA**

Massa, 6-7 October 2022

Centro Congressi della Provincia di Massa-Carrara  
Via S. Leonardo, 492 - Massa



## Local organizers

Simona Celi

Emanuele Vignali

Katia Capellini

Benigno Marco Fanni

Emanuele Gasparotti

## ESB-ITA Executive Board

Diana **Massai** Politecnico di Torino

Simona **Celi** Fondazione Toscana G. Monasterio

Alessio **Gizzi** Università Campus Bio-Medico di Roma

Michele **Conti** Università degli studi di Pavia

Enrico **Dall'Ara** University of Sheffield

Bernardo **Innocenti** Université Libre de Bruxelles

## Scientific committee

Arti Ahluwalia, Valerio Caleffi, Manuele Carniel, Federica Caselli, Simona Celi, Claudio Chiastra, Michele Conconi, Michele Conti, Luca Cristofolini, Enrico Dall'Ara, Diego Gallo, Chiara Giulia Fontanella, Alessio Gizzi, Bernardo Innocenti, Luigi La Barbera, Nicola Lopomo, Stefania Marconi, Michele Marino, Saulo Martelli, Diana Massai, Francesco Migliavacca, Umberto Morbiducci, Marco Palanca, Salvatore Pasta, Lorenza Petrini, Alberto Redaelli, Rita Stagni, Simone Tassani, Mara Terzini, Silvia Todros, Giuseppe Vairo, Matteo Zago, Elisabetta Zanetti

## Patronage



Fondazione  
Monasterio  
la ricerca che cura



European Society  
of Biomechanics

## With the support of

INTESA



SNPAOLO

Rotary



Fondazione  
Cassa di Risparmio  
di Carrara

## Sponsors of the event

BETA  
SIMULATION SOLUTIONS

CAETECH  
PERFORMANCE EXPERIENCE

Bio3DModel  
Computer Aided Surgery  
a SolidWorks Group company

materialise  
innovators you can count on

3DZ  
Print the Future

# Links between cell mechanobiology and tissue mechanics in human thoracic aortic aneurysms

Stéphane Avril<sup>1</sup>

<sup>1</sup> *Mines Saint-Etienne, Université de Lyon, INSERM, SaInBioSE U1059, Saint-Étienne, France*

## ABSTRACT

Ascending thoracic aortic aneurysm (ATAA) is a life-threatening cardiovascular disease, leading to weakening of the aortic wall and permanent dilation. ATAA affects approximately 10 out of 100,000 persons per year in the general population, and this disease is associated to high risk of mortality and morbidity. The degeneration of the arterial wall at the basis of ATAA is a complex multifactorial process. Individual genetic, biological or hemodynamic factors are inadequate to explain the heterogeneity of ATAA development/progression mechanisms, thus stimulating the analysis of their complex interplay. We established a methodology to quantify non-invasively local stiffness properties of ATAAs using electrocardiographic-gated computed tomography (ECG-gated CT) scans. We showed strong relationship between the extensional stiffness and the rupture stretch of the aortic tissue, supported by biomechanical explanations. Then we discovered the interrelationship between the obtained local stiffness with other established markers of aortic function such as intravascular flow structures. The observed interrelationship corroborates computational predictions of ATAA progression coupling hemodynamics with mechanobiology after hemodynamic insult. Recently, we eventually related these results to the existence of a specific smooth muscle cell phenotype found in ATAA, exhibiting stronger traction forces and thicker morphologies. We will present all these results at the conference and show how they open new perspectives for the development of a digital twin of aortic aneurysms.

Stephane Avril is Professor at Mines Saint-Etienne, France.

He holds a Bachelor in Mathematics (University of Saint-Etienne), a Master (University of Clermont-Ferrand) and PhD (Mines Saint-Etienne) in mechanical and civil engineering.



He served several times as visiting professorship, such as at Technical University Graz (2022), Technical University Vienna (2021), Yale University (2018, 2019).

Dr. Avril's research interest covers the mechanics of soft biological tissues, inverse problems and mechanobiology of the thoracic aorta. The goal of his research is to improve the treatment of cardiovascular diseases by assisting physicians and surgeons with biomechanical numerical simulations

# The science behind *Wonder*

Silvia Schievano

<sup>1</sup> UCL Great Ormond Street Institute of Child Health, London, United Kingdom

## ABSTRACT

Craniosynostosis is a group of congenital craniofacial abnormalities consisting in premature fusion (ossification) of one or more cranial sutures during infancy. This results in growth restriction perpendicular to the axis of the suture and promotes growth parallel to it, causing physical deformation of the cranial and facial skeleton, as well as distortion of the underlying brain, with potential detrimental effects on its function: visual loss, sleep apnoea, feeding and breathing difficulties, and neurodevelopment delay. Conventional management of craniosynostosis involves craniofacial surgery delivered by excision of the prematurely ossified sutures, multiple bone cuts and remodelling of the skull deformities, with the primary goal of improving patient function, while normalising their appearance. Cranial vault remodelling surgical procedures, aided by internal and external devices, have proven functionally and aesthetically effective in correcting skull deformities, but final results remain unpredictable and often suboptimal because of an incomplete understanding of the biomechanical interaction between the device and the skull.

The overall aim of our work is to create a validated and robust computational framework that integrates patient information and device design to deliver personalised care in paediatric craniofacial surgery in order to improve clinical outcomes. Virtual models of the infant skull with craniosynostosis, including viscoelastic properties and mechano-biology regulation, are developed to simulate device implantation and performance over time, and are validated using clinical data from patient populations treated with current devices. Bespoke new devices can be designed allowing for pre-programmed 3D shapes to be delivered with continuous force during the implantation period. Patient specific skull models can be used to virtually test and optimise the personalised devices, and to tailor the surgical approach for each individual case.

Silvia Schievano is Professor of Biomedical Engineering at UCL & Great Ormond Street Hospital for Children, London. She graduated in Engineering from Politecnico of Milan and pursued her PhD degree in clinical cardiovascular engineering at GOSH. Since then, Silvia has been leading on translational engineering research in congenital diseases, predominantly cardiovascular and craniofacial. Her main research activities focus on application of engineering methodologies to clinical practice, in particular 3D printing, VR clinical assessments of complex congenital disease cases, statistical shape modelling and population analyses, and computational simulations to support design of new devices and personalised treatments.



# A numerical framework to model the Thoracic Endovascular Aortic Repair procedure

Anna Ramella<sup>1</sup>, Francesco Migliavacca<sup>1</sup>, Jose Felix Rodriguez Matas<sup>1</sup>, Frederic Heim<sup>2</sup>, Francesca Dedola<sup>3</sup>, Tim Mandigers<sup>3</sup>, Stefania Marconi<sup>4</sup>, Michele Conti<sup>4</sup>, Sara Allievi<sup>3</sup>, Daniele Bisacco<sup>3</sup>, Maurizio Domanin<sup>3</sup>, Santi Trimarchi<sup>3</sup>, Giulia Luraghi<sup>1</sup>

<sup>1</sup>Dipartimento di Chimica, Materiali e Ingegneria Chimica “G. Natta”, Politecnico di Milano, Italy

<sup>2</sup>Laboratoire de Physique et Mécanique des Textiles, Université de Haute Alsace, France

<sup>3</sup>Dipartimento di Scienze Cliniche e di Comunità, Università degli Studi di Milano, Italy

<sup>4</sup>Dipartimento di Ingegneria Civile e Architettura (DICAr), Università degli Studi di Pavia, Italy

**Abstract**—Computational models can be used in understanding common TEVAR complications and therefore must be reliable. In this work, high-fidelity FEA simulations to model the TEVAR clinical procedure are developed and validated. Also, a FSI methodology for replicating the blood fluiddynamic in the post-implantation scenario is proposed.

**Keywords**—high-fidelity, stent-graft, FEA, FSI

## I. INTRODUCTION

Thoracic Endovascular Aortic Repair (TEVAR) is a minimally invasive technique to treat thoracic aorta pathologies, such as aneurysms or dissections [1]. Despite its increasing use, many stent-graft related factors are still to be understood requiring a continuous investigation. In this context, computational models play a significant role and must be reliable if used for procedural planning [2].

This work develops high-fidelity numerical simulations to model the stent-graft and replicate the clinical procedure using the Finite Element Analysis (FEA). Then, a methodology for reproducing the post-implantation hemodynamics is proposed adopting the Fluid-Structure Interaction (FSI) technique.

## II. MATERIALS AND METHODS

Models of the commercial Valiant Captivia stent-graft (Medtronic Inc.) were generated in SolidWorks (Dassault Systèmes). Using ANSA (BETA CAE), the stent is discretized with beam elements and the graft with triangular membrane elements. Experimental crimping/release tests were performed on the device to calibrate the Nitinol (stent) and PET (graft) material parameters and to validate the stent-graft model (Fig. 1.1). The stent pre-stress was included in the assembled model. Then, a novel tracking methodology for replicating the TEVAR procedure in an idealized aorta was set up by carrying out explicit FEA simulations using Ls-Dyna (ANSYS) (Fig. 1.2). For a validation purpose, the same stent-graft was experimentally implanted in a 3D-printed rigid aortic phantom and subjected to CT scanning during deployment. Qualitative and quantitative comparisons between the numerical and experimental results were performed [3].

To study the post-TEVAR hemodynamics, a strongly coupled, 2-way, boundary fitted FSI simulation was performed with the implicit ICFD solver in Ls-Dyna. A physiological velocity waveform was imposed to the inlet of the ascending aorta, while 3-elements Windkessel circuits were assigned to each outlet to account for the downstream resistances [4] (Fig. 1.3). The device and aorta configurations and stress/strain distributions were imported from the FEA simulation.

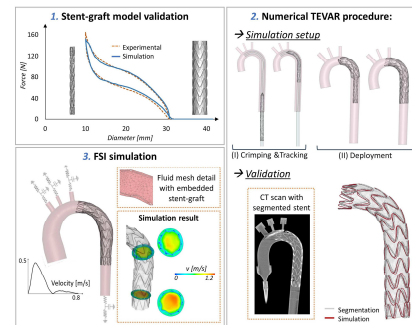


**Figure 1.** (1) Stent-graft model validation with experimental data; (2) stent-graft tracking FEA simulation to model TEVAR: setup and validation; (3) FSI simulation setup and result.

## III. RESULTS AND CONCLUSIONS

The result of the TEVAR procedure validation (Fig. 1.2) shows a good agreement between simulation and experimental stent-graft configurations, with the error - evaluated on the stent strut opening area - being below 3%. Innovative aspects are here proposed regarding the stent-graft model, such as the graft material modelled as a fabric material, the deployment tracking simulation method and the quantitative validation.

The developed strong FSI simulation (Fig. 1.3) is a promising tool amenable to model coupled structures and fluid. It can be useful to deeper investigate the TEVAR procedure. In fact, the methodology takes into account the presence of the device and the stress/strain distribution arising from the FEA simulation.

In conclusion, high-fidelity stent-graft simulations can help designing and optimizing new devices. These analyses will be also applied to patient-specific geometries. In fact, realistic and accurate TEVAR patient-specific models can be used as support for clinical decisions before the implantation.

## ACKNOWLEDGEMENT

This project has received funding from the MIUR FISR-FISR2019\_03221 CECOMES.

## REFERENCES

- [1] D. Nation, “TEVAR: Endovascular Repair of the Thoracic Aorta”, in *Seminars in Interventional Radiology*, 2015. Vol.32(3), pp. 265-271.
- [2] M. Viceconti, “In silico trials: Verification, validation and uncertainty quantification of predictive models used in the regulatory evaluation of biomedical products.” *Methods*, 2021. Vol. 185, pp. 120–127.
- [3] D. Perrin, “Patient-specific numerical simulation of stent-graft deployment: Validation on three clinical cases”, *Journal of Biomechanics*, 2015. Vol. 48(10), pp. 1868-1875.
- [4] S. Pirola, “On the choice of outlet boundary conditions for patient-specific analysis of aortic flow using computational fluid dynamics”, *Journal of Biomechanics*, 2017. Vol. 60, pp. 15–21.

# A retrospective analysis of the sagittal balance in the distal lumbar junctional pathology

S. Montanari<sup>1</sup>, C. Griffoni<sup>2</sup>, G. Barbanti Brodano<sup>2</sup>, L. Cristofolini<sup>1</sup>

<sup>1</sup> Department of Industrial Engineering, Alma Mater Studiorum – Università di Bologna, Italy

<sup>2</sup> Spine Surgery Unit, IRCCS Istituto Ortopedico Rizzoli, Bologna, Italy

**Abstract**—A total of 324 spine surgeries were retrospectively analysed in order to investigate if the spinopelvic parameters are correlated with mechanical failure in the distal junctional pathology. Pelvic tilt and lumbar lordosis, which relate to the specific deformity seem to be a predictor for the failure of the surgery. After the spine fixation, the mismatch PI-LL seems to indicate the recovery of the sagittal balance.

**Keywords**—Junctional pathology, sagittal balance, spinopelvic parameters, posterior fixation.

## I. INTRODUCTION

Mechanical failure of spinal posterior instrumented arthrodesis in the lumbar region is suspected to occur more frequently when sagittal balance is not adequately restored [1]. In the literature, the lumbar distal junctional pathology has received limited attention [2], and is not clear if the spinopelvic parameters of asymptomatic population are suitable to prevent the failure. The aim of this work was to investigate if the spinopelvic parameters which characterize the sagittal balance are predictors of mechanical failure.

## II. METHODS

All lumbar posterior fixations performed in 2017-2019 at Rizzoli Institute were retrospectively analysed to extract all cases of junctional pathology. A total of 83 cases were included in the junctional group (JUNCT) if the revision was required due to distal fixation failure caused by: (i) pedicle screws pullout and/or (ii) breakage of rods or screws and/or (iii) vertebral fracture and/or (iiii) degenerative disc disease in the last instrumented level, or immediately below. All the 241 lumbar fixation surgeries which to date have not failed were identified as a control group (CONTROL). Demographic and clinical data were extracted. The software Surgimap (Nemaris) was used to assess the pelvic incidence (PI), pelvic tilt (PT), T1 pelvic angle (TPA), lumbar lordosis (LL), and sacral slope (SS) from the pre-operative (Pre-op) and post-operative (Post-op) standing lateral X-rays.

## III. RESULTS

Distal lumbar junctional pathology onset was caused by screw pullout in 45% of cases. Junctional pathology was also observed within two years of the first vertebral fixation in 51.8% of failures. Arthrodesis with 7 or more levels were the most common in JUNCT (51.8%) in contrast to CONTROL (14.1%). In the CONTROL group, TPA, PT, and PI-LL showed statistically significant differences between Pre-op and Post-op values ( $p=0.01$ ,  $p<0.0001$  and  $p=0.005$  respectively, *Wilcoxon test*). All the Post-op values were in the recommended range of good balance [3], [4]. In JUNCT,

the worsening of sagittal balance was confirmed by the increase in PT, TPA, SVA, PI-LL and by the decrease of LL ( $p=0.002$ ,  $p=0.003$ ,  $p<0.0001$ ,  $p=0.001$  and  $p=0.001$  respectively, *Paired t-test*) before the revision surgery. The parameters in the JUNCT and CONTROL groups in the Pre-op differed significantly (TPA:  $p=0.03$ , *Kolmogorov-Smirnov test*, SS:  $p=0.03$ , *Unpaired t-test*). In Post-op, PI-LL was significantly different between JUNCT and CONTROL ( $p=0.04$ , *Unpaired t-test*). The regression models of PT and LL vs. PI (Fig.1) were significantly different between JUNCT and CONTROL in Pre-op ( $p=0.01$  and  $p=0.02$ , *Z-test*), but not in Post-op ( $p=0.57$  and  $p=0.35$ , *Z-test*).

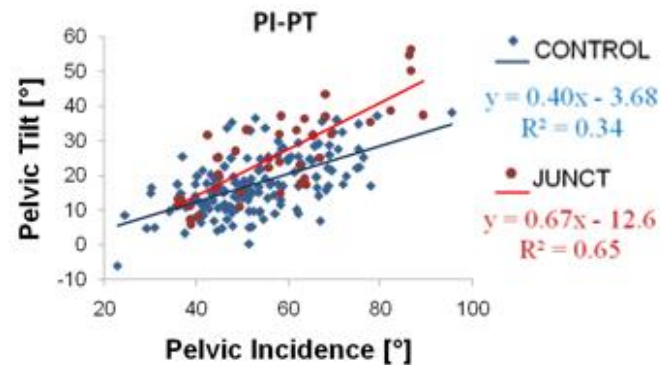


Fig. 1: Regression models of PT vs. PI from Pre-op X-rays for the JUNCT and CONTROL groups.

## IV. DISCUSSION

These results showed that failure is most common in long fused segments, likely due to long lever arms leading to screws pullout or implant failure. This effect was confirmed by the worsening of all the extracted spinopelvic parameters before the revision surgery in JUNCT: if the sagittal balance is not properly restored, after the surgery the balance is expected to worsen, eventually leading to failure. Conversely, as we can see in CONTROL, a good sagittal balance seems to avoid a revision surgery. The mismatch PI-LL after the surgery seems to confirm a good sagittal balance and predict a good correction. The linear regression of PT and LL vs. PI is important in the surgical planning to restore the sagittal balance, but it does not seem to prevent mechanical failure; however, it suggests that the spine deformity and pelvic conformation could be a predictor for the failure after a fixation.

## REFERENCES

- [1] Lau et al, *Spine*, 39:2093-2102, 2014
- [2] Berjano et al, *Eur. Spine J*, 29:86-102, 2020
- [3] Schwab et al, *Eur. Spine J*, 37:1077-1082, 2012
- [4] Li et al, *Global Spine J*, 2021

# CFD simulations and uncertainty quantification to investigate aorta coarctations

A. Mariotti<sup>1</sup>, M.N. Antonuccio<sup>2</sup>, B.M. Fanni<sup>2</sup>, M. Morello<sup>1</sup>, M.V. Salvetti<sup>1</sup>, and S. Celi<sup>2</sup>

<sup>1</sup> Dipartimento di Ingegneria Civile e Industriale, Università di Pisa

<sup>2</sup> BioCardioLab - Bioengineering Unit, Ospedale del Cuore, Fondazione CNR - Regione Toscana G. Monasterio

**Abstract**—Computational Fluid Dynamics (CFD) is widely used to quantify many hemodynamic indicators such as wall shear stress, velocity field, and pressure drops in blood vessels. The present work focuses on coarctation, which is a narrowing of the aorta. Different grades of severity are investigated by varying the diameter of the coarctation. A key issue for the reliability of numerical results is the use of appropriate outflow boundary conditions. We use the 3-element Windkessel model together with a fine-tuning parameter  $\alpha$ . The combined effect of uncertainties in  $\alpha$  and in the grade of severity of the coarctation is investigated through a stochastic approach based on the generalized Polynomial Chaos. This allows a systematic investigation of the effects of the considered parameters starting from a few simulations. The grade of severity has a major impact on the repartition of the flow rate waveform between the descending aorta and the branches and on the pressure drop across coarctation. The interplay between the diameter of the coarctation and  $\alpha$  is important to match the patient-specific physiological conditions.

**Keywords**—hemodynamic simulations, aortic coarctation, uncertainty quantification, stochastic sensitivity analysis.

## I. INTRODUCTION

The Aortic Coarctation (CoA) is a congenital defect consisting of an alteration in the shape of the aorta that appears narrowed in the thoracic district. This defect leads to a pressure gradient ( $\Delta P$ ) across the coarctation, it increases afterload and reduces peripheral perfusion pressures. Indication to invasive treatment is based on values of maximal (systolic) trans-coarctation  $\Delta P$ . Personalized CFD models can be used as a tool to improve the understanding and the clinical outcome of cardiovascular disorders. The reliability of the hemodynamic simulations directly depends on the accuracy of the computational model and of the input parameters and settings [1]. State-of-the-art outflow boundary conditions implies using the 3-element Windkessel model and, in case of coarctation of the aorta, an additional parameter,  $\alpha$ , is proposed [2] to calibrate the model. We carry out herein a systematic analysis of the combined effect of uncertainties in the parameter  $\alpha$  and in the grade of severity of the aortic coarctation, i.e., for different diameters,  $d$ , of the stricture section. A methodology based on the generalized Polynomial Chaos (gPC) is adopted.

## II. PROBLEM DEFINITION AND NUMERICAL METHODOLOGY

The numerical simulations have been performed using the open-source software SimVascular, based on stabilized finite-element method. Starting from the MRI-acquired patient-specific geometry different grades of severity of the CoA are obtained by changing the diameter,  $d$ , of the narrowest section,

sketched in Fig.1. MRI-measured flow rate waveform is imposed at the inlet section. Rigid walls are considered, and 3-element Windkessel model is used at the outlet sections. For the fine-tuning of the model, a non-dimensional splitting value  $\alpha$  was introduced as proposed in [2]. We performed stochastic sensitivity analysis on  $d$  and  $\alpha$  using the gPC method.

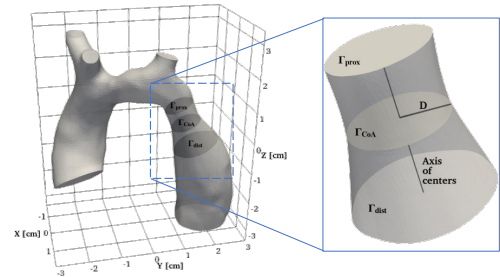


Figure 1: parametric model of the coarctated aorta

## III. RESULTS AND CONCLUSIONS

The stochastic PDFs for the flow rate waveform at the descending aorta and for the pressure drop across coarctation are shown in Figs.2(a,b), respectively. Significant variability of the quantities of interest is evident in the systolic part of the cardiac cycle. The related Sobol indices, shown in Figs.2(c,d), highlight that the parameter  $d$  has a major impact on the repartition of the flow rate waveform between the descending aorta and the branches and on the pressure drop across CoA. The interaction effect between the degree of severity of the coarctation and the parameter  $\alpha$  is also important and should be considered to calibrate the Windkessel model and match the patient-specific physiological conditions.

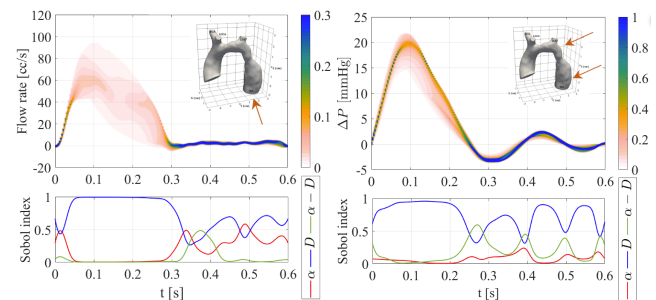


FIGURE 2: flow rate in the descending aorta (left) trans-coarctation  $\Delta P$  (right)

## REFERENCES

- [1] A. Mariotti, A. et al, *Computers and Fluids*, 2021, vol. 230: 105123
- [2] M.N. Antonuccio, et al, *Annals of Biomedical Engineering*, 2021, vol. 42(12) pp. 3497–3507.

# Blood flow rotational energy predicts coronary lesions culprit for future myocardial infarction

M. Lodi Rizzini<sup>1</sup>, V. Mazzi<sup>1</sup>, A. Candreva<sup>1,2</sup>, C. Chiastra<sup>1</sup>, B. De Bruyne<sup>3</sup>, C. Collet<sup>3</sup>, D. Gallo<sup>1</sup>, and U. Morbiducci<sup>1</sup>

<sup>1</sup> Dept. of Mechanical and Aerospace Engineering, Polito<sup>BIO</sup> Med Lab, Politecnico di Torino, Torino, Italy

<sup>2</sup> Dept. of Cardiology, Universitäts Spital Zurich, Zurich, Switzerland

<sup>3</sup> Cardiovascular Center Aalst, OLV-Clinic, Aalst, Belgium

**Abstract**— The capability of coronary blood flow vorticity and rotational energy to predict future myocardial infarction is explored adopting angiography-based computational hemodynamics. As main finding of the study we report that blood flow vorticity and enstrophy overperform the standard clinical predictors of coronary lesion culprit of myocardial infarction.

**Keywords**—Coronary arteries, myocardial infarction, computational hemodynamics, vorticity, rotational energy.

## I. INTRODUCTION

CORONARY artery lesions experience a variety of hemodynamic stimuli promoting their progression and destabilization [1]. Recently, the variability of the wall shear stress (WSS) contraction/expansion action on the endothelium along the cardiac cycle has emerged as a strong predictor of myocardial infarction (MI) [2]. Since the WSS profile is the fingerprint of intravascular hemodynamics on the coronary wall, the present study aims to explore the predictive capacity for future coronary MI of inherent intravascular flow patterns. On the same angiography-based computational hemodynamics dataset analyzed in [2], we test here the hypothesis that vorticity and blood flow rotational energy may dictate detrimental near-wall flow disturbances [2] and then predict MI in stenosed coronary arteries.

## II. METHODS

Coronary vessels retrospectively selected from patients presenting with acute MI and a coronary angiography performed between 1 month and 5 years before the event were considered. The selection resulted in 80 future culprit (FC) vessels and 108 non-future culprit (NFC) vessels [2]. The three-dimensional geometry of each vessel was reconstructed from two angiographic projections. Then, transient computational fluid dynamics (CFD) simulations were performed as detailed elsewhere [2].

The capability of future MI prediction of the clinical markers: percent area stenosis (%AS) and virtual fractional flow reserve (vFFR) was tested against CFD-derived near-wall quantities (time average WSS, TAWSS; topological shear variation index, TSVI [2]) and intravascular flow quantities evaluating vortex structures, the expected dominant type of fluid structures in stenosed coronary arteries. In detail, the considered intravascular flow quantities were the magnitude of the vorticity vector field (a measure of the local rotation of fluid elements), expressed by:

$$\boldsymbol{\omega} = \nabla \times \mathbf{v} \quad (1)$$

where  $\mathbf{v}$  and  $\boldsymbol{\omega}$  are the velocity and vorticity vectors, respectively, and enstrophy, a scalar measure of the rotational energy of blood flow:

$$\varepsilon = \frac{1}{2} |\boldsymbol{\omega}|^2 \quad (2)$$

Vorticity and enstrophy were time-averaged along the cardiac cycle and volume-averaged over anatomically defined segments [2]. For each vessel, the ratio between vorticity or

enstrophy values on the mid segment (i.e., the segment containing the minimum lumen area) and on the segment upstream of the lesion (**Figure 1A**) was adopted to measure the hemodynamic deviation in healthy vs. diseased condition [3]. Classification performances were evaluated by means of receiver operating characteristic (ROC) curves.

## III. RESULTS AND DISCUSSION

An explanatory example of the vorticity profiles establishing within NFC and FC vessels is presented in **Figure 1A** by visualizing Q-criterion isosurfaces colored by local enstrophy values. The analysis of the ROC curves (**Figure 1B**) highlighted that both vorticity (AUC=0.70,  $p<0.0001$ ) and enstrophy (AUC=0.72,  $p<0.0001$ ) ratios are strong predictors of future MI, outperforming the markers currently adopted in the clinical practice %AS (AUC=0.65,  $p=0.0004$ ) and vFFR (AUC=0.63,  $p=0.0017$ ) [2]. Vorticity and enstrophy overperform TAWSS (AUC=0.61,  $p=0.0112$ ) but not TSVI (AUC=0.77,  $p<0.0001$ ) [2]. An intravascular-based prediction of future MI in coronary arteries opens to the possibility of a direct *in vivo* application, thanks to technology advancement in the field of intravascular flow imaging and the increasing resolution of phase-contrast magnetic resonance imaging [4].

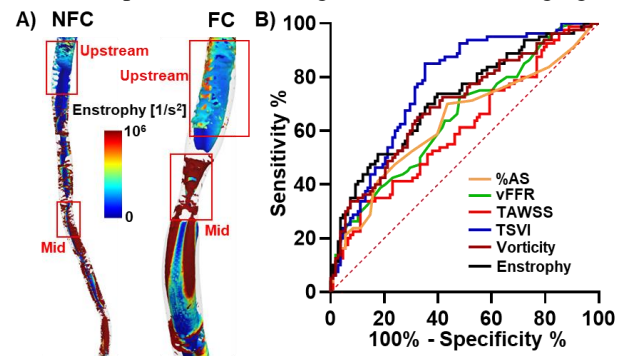


**Figure 1.** A) Q-criterion isosurfaces color-coded with enstrophy values for two explanatory cases, i.e., one NFC and one FC. B) ROC curves for %AS, vFFR, TAWSS, TSVI, vorticity, and enstrophy.

## IV. CONCLUSION

Blood flow rotational energy performs better than currently adopted clinical markers and candidates to future *in vivo* applications.

## REFERENCES

- [1] Lee JM et al., “Identification of High-Risk Plaques Destined to Cause Acute Coronary Syndrome Using Coronary Computed Tomographic Angiography and Computational Fluid Dynamics”, *JACC Cardiovasc Imag*, 12:1032-43, 2019.
- [2] Candreva et al., “Risk of myocardial infarction based on endothelial shear stress analysis using coronary angiography”, *Atherosclerosis*, 342:28-35, 2022.
- [3] Chu et al., “Quantification of disturbed coronary flow by disturbed vorticity index and relation with fractional flow reserve”, *Atherosclerosis*, 273:136-144, 2018.
- [4] Zhuang et al., “The role of 4D flow MRI for clinical applications in cardiovascular disease: current status and future perspectives”, *Quant Imaging Med Surg*, 11(9): 4193–4210, 2021.

# A synergy-based approach to track foot bones motion using different gait analysis protocols

A. Pompili<sup>1</sup>, M. Conconi<sup>1</sup>, N. Sancisi<sup>1</sup>, A. Leardini<sup>2</sup>, and C. Belvedere<sup>2</sup>

<sup>1</sup> Department of Industrial Engineering, University of Bologna, Italy

<sup>2</sup> Movement Analysis Laboratory, IRCCS Istituto Ortopedico Rizzoli, Bologna, Italy

**Abstract**— This study shows a novel synergy-based **Multibody Kinematics Optimization (MKO)** approach for the reconstruction of foot-ankle complex motion from skin marker measures. The complex is considered as a 4 DOF system in which the motion of each bone is the linear combination of 4 synergies, determined from in-vitro experiments through weight-bearing CT. The motion of all bones in the complex is obtained by computing the synergies' linear combination coefficients that minimize the residual error on marker positions. To test the approach, the variation of the Medial Longitudinal Arch (MLA) during gait is computed using different gait analysis (GA) protocols, featuring different number of foot markers, from 2 to 10. The results show the approach estimates the MLA using 3 markers only, with an accuracy similar to that of more complicate GA protocols. Moreover, indentation and separation of foot bones are avoided.

**Keywords**—Multi-segment Foot Model, Multibody kinematics optimization, Soft-tissue artefact, Foot synergies.

## I. INTRODUCTION

Lower limb kinematics is traditionally measured via optoelectronics systems and skin markers, arranged according to established protocols [1]. To improve the estimation of bone pose during inverse kinematics analysis, multibody kinematics optimization (MKO) is generally employed. In this context, the foot is generally considered as a single rigid body, coupled to the tibia with a hinge or spherical joint, making it impossible to estimate the motion of the tarsal bones. To cope with that, estimation of overall foot motion is performed through Multi-Segment Foot Models (MSFM), in which the foot is divided into rigid groups of bones with no constraints between the groups [2]. This approach provides information on the foot mobility, but it requires numerous markers, no bone motion is quantifiable within the segments, and anatomically flimsy indentations or separations among the segments occurred.

In a previous in-vitro study performed using Weight-Bearing CT, we showed that the foot-ankle complex bones motion can be described as the linear combination of four main mobility patterns similar over all specimens (hereinafter synergies) [3]. Synergies can thus be used to represent the foot as a four DOF mechanism within MKO. This novel MKO technique is here applied to the most common marker protocols in gait analysis (GA). Sensitivity to the adopted protocol is evaluated by measuring the Medial Longitudinal Arch (MLA), also comparing the results with those from MSFM.

## II. METHODS

GA data were collected from one subject following the Rizzoli Foot Protocol (RFP) [4]. Foot synergies were scaled isotropically based on the length of the subject foot. A virtual foot, also featuring different sets of virtual markers, was scaled similarly. During the inverse kinematics analysis, the synergies' linear combination coefficients were obtained by minimizing the residual error between experimental and virtual markers. We tested four different GA protocols: RFP

with 10 markers [4], Cast Protocol with 4 markers, T3Dg Protocol with 3 markers and Davis Protocol with 2 markers [1]. To compare the results with the literature, we also applied the MSFM [4]. We evaluated the MLA during GA as the spatial angle between the calcaneal and first metatarsal antero-posterior axis, defined according to [5].

## III. RESULTS

MLA estimation through synergy-based MKO is almost insensitive to the marker protocol, comparing well with MSFM (Fig.1), except the Davis' which resulted in unphysiological values. To discriminate between MSFM and synergy-based MKO, foot postures were visually compared at the largest MLA difference (75% of gait cycle, fig. 1). MSFM led in considerable indentation among the segments (fig. 2).

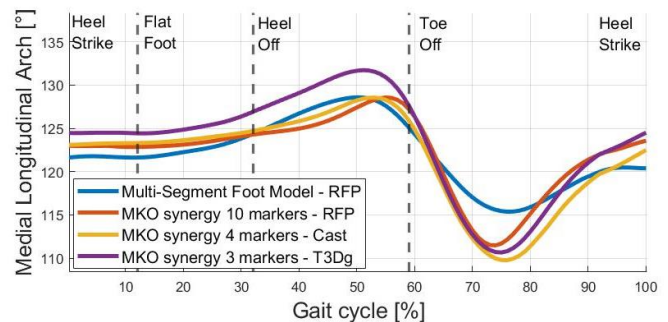


Fig. 1: the MLA for different marker protocols

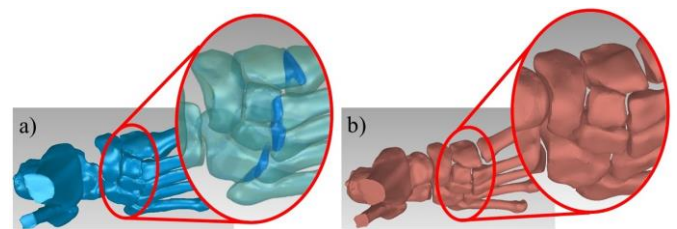


Fig. 2: 3D bone model reconstruction (75% GA cycle) shows the indentation with a) Multi-Segment Foot Model respect to b) MKO synergy 10 markers (RFP)

## IV. CONCLUSION

Synergy-based MKO provides a solid approach to track the foot-ankle complex motion, requiring only 3 foot markers. The approach can be applied retrospectively to previous studies, being compatible with different GA protocols. Future studies will investigate the optimal marker distribution to optimize Synergy-based MKO results.

## REFERENCES

- [1] Ferrari A. et al, 2008. *Gait&Posture*, **28**: 207-216.
- [2] Leardini A. et al. 2017. *J. of Biomech*, **62**: 77-86.
- [3] Conconi M. et al., 2021. *Proc. XXVIII ISB Congress*.
- [4] Leardini A. et al., 2007. *Gait & Posture*, **25**: 453-462.
- [5] Conconi M. et al., 2021. *J. of Foot&Ank Res*, **14**:66.

# Bench to bedside: in-silico and in-vitro evaluation of shocked patients under the ECMO support

E. Gasparotti<sup>1</sup>, E. Vignali<sup>1</sup>, D. Haxhiademi<sup>2</sup>, F. Bardi<sup>1</sup>, M. Scolaro<sup>2</sup>, P.A. Del Sarto<sup>2</sup> and S.Celi<sup>1</sup>

<sup>1</sup> BioCardioLab - Bioengineering Unit, Ospedale del Cuore, Fondazione Monasterio, Italy

<sup>2</sup> Anesthesiology and Intensive Care Unit, Ospedale del Cuore, Fondazione Monasterio, Italy

**Abstract**— Extracorporeal membrane oxygenation is widely used in the support of circulatory failure although its complex interactions with the failing heart and its effects on haemodynamics and perfusion are not yet understood.

In this work the in-silico and in-vitro approaches were investigated and compared to estimate the effects of the ECMO procedure on cardiogenic shocked patients.

**Keywords**—ECMO, cardiogenic shock, mechanical circulatory support, mock circulatory loop, CFD.

## I. INTRODUCTION

EXTRACORPOREAL Membrane Oxygenation (ECMO) is a mechanical circulatory support. It is used to support cardiac function in patients with heart failure. The complex interaction between ECMO and native cardiac function is poorly understood [1]. The use of in-vitro and in-silico simulations can help to measure fluid mechanics parameters that are essential for a personalized ECMO support. The aim of this study is to investigate the ECMO procedure using in-silico and in-vitro methods to evaluate the changes in hemodynamic parameters with different levels of retrograde ECMO support at different cardiogenic shock conditions.

## II. MATERIALS AND METHODS

Anatomic and functional flow data were extracted from MRI acquisitions of healthy human aorta. The in-silico and in-silico approaches were performed with the same boundary conditions and geometry.

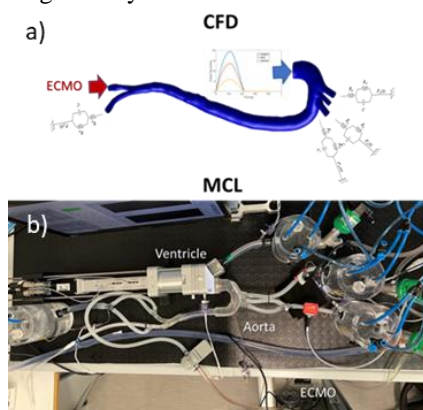


Figure 1. ECMO simulative environments: (a) in-silico boundary conditions and (b) experimental setup

The inlet boundary condition was set to reproduce the aortic flow waveform during both healthy and failure conditions. Two different failure conditions were imposed by reducing the healthy patient stroke volume (70 ml) of 70% (SVR) and 30% (MLD). For each condition, six different constant flows (1-2-3-4-5-6 l/min) were imposed at the left iliac branch (IL) to

reproduce the ECMO support. For all simulations, lumped RCR model outlet boundary conditions were imposed at epiaortics (EP) and right IL branches. The in-silico approach consists in a Computational Fluid Dynamics (CFD) simulation (Fig. 1a). The in-vitro approach was based on Mock Circulatory Loop (MCL) (Fig. 1b) and consists of i) a piston pump [2], to reproduce the aortic inlet flow waveforms; ii) a centrifugal pump, to impose the ECMO support; iii) a 3D printed phantom of aorta and iv) hybrid units to impose outlets conditions. The in-silico and in-vitro results were compared.

## III. RESULTS

Fig. 2 shows the results of the CFD and MCL simulations. The CFD and MCL simulations exhibit similar values and trends of the results with the ECMO support for both MLD and SVR shocks. The Epiaortic flow increases linearly with the increasing of ECMO support, up to reach the healthy pre-shock values (Fig. 2a). The Ventricular work increases linearly in both SVR and MLD shock (Fig. 2b).

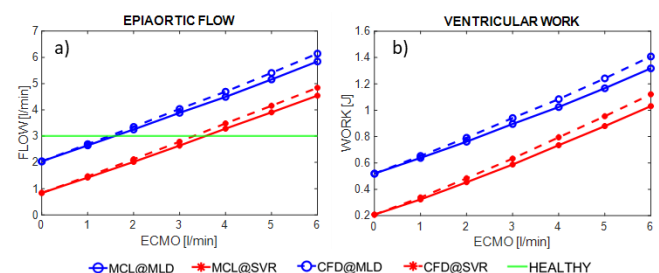


Figure 2. CFD and MCL results: Epiaortic flow (a) and Ventricular work (b)

## IV. DISCUSSION AND CONCLUSION

The computational and experimental systems were successfully developed for the analysis of ECMO device in cases of cardiogenic shock. It was possible to assess that: i) the flows in the aortic vessels are a combination of the severity of the shock combined with the degree of ECMO support and ii) the healthy flow conditions can be re-established in both simulated shock degrees. ECMO leads to an overload of the left ventricle, which impairs the cardiac recovery process [3].

## ACKNOWLEDGEMENT

MeDiTaTe Project has received funding from the European Union's Horizon 2020 under Grant Agreement 859836.

## REFERENCES

- [1] D. Abrams et al, J. Am. Coll. Cardiol., 2014
- [2] E. Vignali et al, ASAIO Journal, 2022
- [3] L. Truby et al, ASAIO Journal, 2017

# A classification model for predictions of thrombectomy outcomes

S. Bridio<sup>1</sup>, G. Luraghi<sup>1</sup>, F. Migliavacca<sup>1</sup>, D. González<sup>2</sup>, P. Díez<sup>3,4</sup>,  
J.F. Rodríguez Matas<sup>1</sup> and A. García-González<sup>3</sup>

<sup>1</sup> Department of Chemistry, Materials and Chemical Engineering “Giulio Natta”, Politecnico di Milano, Italy

<sup>2</sup> Aragon Institute of Engineering Research, Universidad de Zaragoza, Spain

<sup>3</sup> Laboratori de Càlcul Numèric, E.T.S. de Ingenieria de Caminos, Universitat Politècnica de Catalunya-BarcelonaTech, Spain

<sup>4</sup> International Center for Numerical Methods in Engineering, CIMNE, Barcelona, Spain

**Abstract**—Endovascular thrombectomy (EVT) is a treatment for acute ischemic stroke. In this work, a classification model, trained on high-fidelity simulations of the EVT procedure, is proposed to provide a tool for fast estimations of the chances of success or failure of EVT procedures on stroke patients.

**Keywords**—Classification model, kernel optimization, thrombectomy, stroke.

## I. INTRODUCTION

ENDOVASCULAR thrombectomy (EVT) is the main treatment for acute ischemic stroke, aiming at removing the thrombus from the cerebral arteries with a stent-retriever. The treatment must be performed in the first few hours from symptoms onset, allowing a short time window for pre-operative planning. High-fidelity computational simulations of EVT can predict the treatment outcome but require a long computational time [1]. In this work, a classification model is proposed, trained on high-fidelity EVT simulations, for providing fast estimates on the success of the procedure.

## II. MATERIALS AND METHODS

Ninety-four patient-specific cerebrovascular anatomies are reconstructed from images of stroke patients. A thrombus is placed in each vascular model, with lengths and compositions varied in ranges derived from the literature [2]. High-fidelity finite-element simulations of the EVT procedure with a Trevo ProVue stent-retriever (Stryker, USA) are run, using the settings reported in [1]. A total of 81 out of 94 simulations have a positive outcome, i.e. thrombus is successfully removed from the vasculature, and 13 have a negative outcome (Fig.1).

The results of the simulations are used to train the classification model: based on vascular anatomy and thrombus characteristics, the model is intended to cluster samples with positive and negative outcome, and to predict the class where new test samples lie. The method used for classification relies on two successive kernel Principal Component Analyses (kPCA). The first, applied to the anatomic description using a Gaussian kernel [3], the second, including the thrombus characteristics, using a kernel optimized with a Semidefinite Programming (SDP) kernel optimization algorithm [4]. The kernel function is optimized such that, in the principal components space, the distance between samples belonging to different clusters (positive and negative outcome) is maximized. The same kernel function is then used to project new test cases (defined by vascular anatomy and thrombus characteristics) to the principal components space. The

distances of the projected test sample to the barycentre of each of the two clusters are calculated to assign the test sample to either the positive EVT outcome cluster, or the negative one.

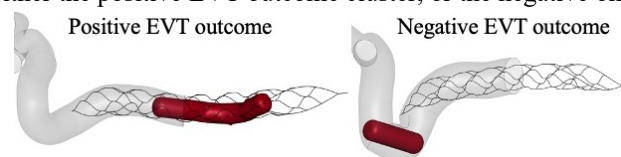


Fig1: Examples of EVT simulations with positive and negative outcome.

## III. RESULTS AND DISCUSSION

A total of 81 samples are used to train the model (71 with positive and 10 with negative EVT outcome), whereas 13 samples are used for testing the model (10 with positive and 3 with negative EVT outcome). To evaluate the results, bootstrapping with 20 repetitions is performed, selecting at each iteration a different group of test samples. In all the bootstraps, the two clusters are successfully described (Fig.2). The classification of the test samples provides an average of 77% correct predictions, 18% false positives and 5% false negatives. The performance of the model is limited by the small number of samples belonging to the negative outcome class. Despite this limitation, the proposed method is promising and it is seen as a valuable tool for performing a fast pre-operative evaluation of the chances of success of an EVT procedure.

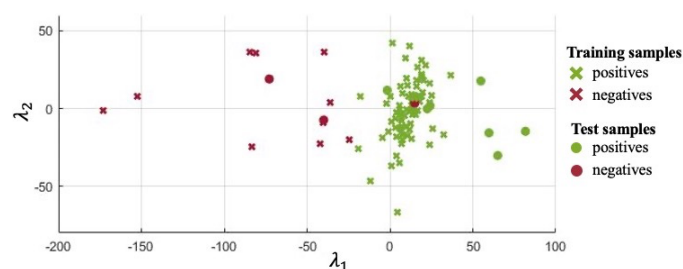


Fig2: Classification model results from one of the bootstraps, shown in the first two dimensions ( $\lambda_1$ ,  $\lambda_2$ ) of the principal components space.

## REFERENCES

- [1] G. Luraghi et al, “The first virtual patient-specific thrombectomy procedure”, *J. Biomechanics*, 2021, 126:110622.
- [2] B.G. Dutra et al, “Thrombus imaging characteristics and outcomes in acute ischemic stroke patients undergoing endovascular treatment”, *Stroke*, 2019, 50:2057–2064.
- [3] A. García-González et al, “A kernel Principal Component Analysis (kPCA) digest with a new backward mapping (pre-image reconstruction) strategy”, *ArXiv*, 2020.
- [4] K.Q. Weinberger et al, “Learning a kernel matrix for nonlinear dimensionality reduction”, *21<sup>st</sup> int. conf. on Machine learning*, 2004, 106.

# Experimental and computational simulation of a non-invasive closed-loop breathing circuit

A. Formaggio<sup>1,2</sup>, M. De Luca<sup>1,2</sup>, G. Putame<sup>1,2</sup>, S. Borrelli<sup>1,2</sup>, A. L. Audenino<sup>1,2</sup> and M. Terzini<sup>1,2</sup>

<sup>1</sup> Department of Mechanical and Aerospace Engineering, Politecnico di Torino, Torino (Italy)

<sup>2</sup> Polito<sup>BIO</sup>Med Lab, Politecnico di Torino, Torino (Italy)

**Abstract**—A lumped circuit model of a closed-loop ventilation system is here proposed and validated with experimental measurements performed on a simulated patient.

**Keywords**—CPAP, closed breathing circuit, lumped model.

## I. INTRODUCTION

CPAP (continuous positive airway pressure) therapy, widely used during the COVID-19 pandemic to treat patients with hypoxemic respiratory failure, is traditionally delivered in an open-configuration. A new non-invasive ventilation system was proposed [1] able to deliver CPAP through a closed-loop breathing circuit. The closed-loop circuit aims to improve the working pressure control and to reduce the oxygen consumption and the noise to the patient.

## II. MATERIALS AND METHODS

### A. Experimental simulation

The closed-loop ventilation circuit [1] was assembled using commercial components and connected to a simulated patient (TestChest® V3, Organix GmbH, CH). Both the healthy [2] and the COVID-19 patient conditions [3] were simulated at three different CPAP pressures (5, 10 and 15 cmH<sub>2</sub>O).

### B. Computational model

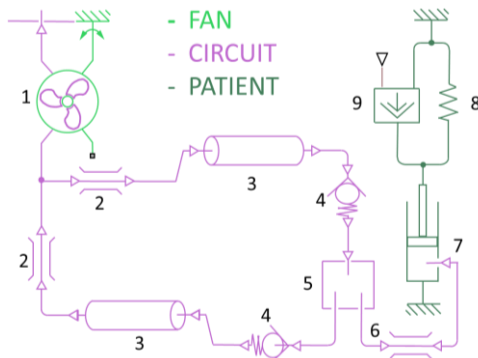


Figure 1. Schematics of the closed-loop circuit with its building blocks: 1) Blower; 2) Localized load losses; 3) Friction load losses; 4) Unidirectional valves; 5) Patient's interface; 6) Patient's airway; 7) Lung; 8) Lung and rib cage total compliance; 9) Respiratory muscles

A lumped circuit model (Figure 1) of the closed-loop system was designed in Simscape (Mathworks), in order to build an *in silico* testbench for future optimization of the design parameters (e.g., components layout, working pressure regulation). The commercial components resistances were determined by measuring the pressure drop as function of the stream flowing through each component, while the patient's blocks were set reproducing the simulated patient. The fan block, based on the provided characteristic curves, is driven by

implementing the same PID controller tested experimentally. The muscle activation curve was derived from the simulator and then imposed as input to the computational model.

## III. RESULTS

To compare the experimental and computational results, the flow through the patient's airway and the pressure at the patient's interface were analysed. A representative result for an imposed pressure of 10 cmH<sub>2</sub>O is reported in Figure 2. The computational model captures extremely different breathing patterns, even when high variations occur during patient's respiration, as with COVID-19 condition where the respiration rate increases from 12 up to 36 breaths per minute.

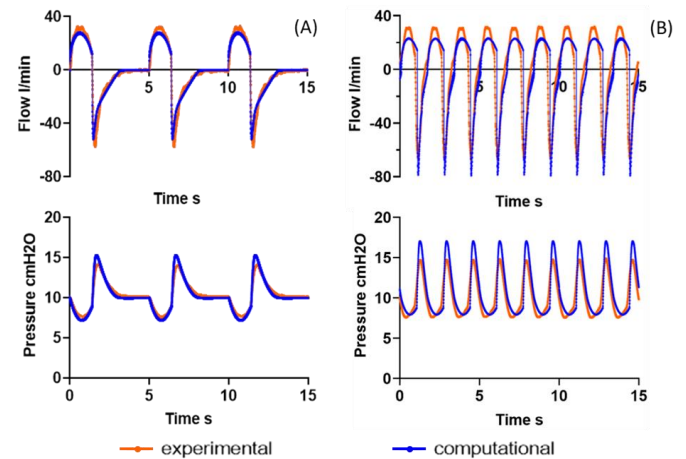


Figure 2. Flow and pressure curves as a function of time for the healthy (A) and COVID-19 (B) conditions.

## IV. Conclusion

The developed lumped model succeeded in reproducing simulated patients, ranging from healthy to pathologic, and concurrently monitoring the effects of CPAP on their airways. Finally, this tool constitutes an *in silico* testbench able to simulate and optimize different types of ventilation circuits.

## ACKNOWLEDGEMENT

This work was supported by DIVOC (INFRA-P2, Linea B).

## REFERENCES

- [1] M. Cavaglia et al. "Noninvasive mechanical ventilation in the COVID-19 era: Proposal for a continuous positive airway pressure closed-loop circuit minimizing air contamination, oxygen consumption, and noise", in *Artificial Organs*, 2021, 45(7), pp.754-761,
- [2] J.M. Arnal et al. "Parameters for Simulation of Adult Patients During Mechanical Ventilation", in *Respiratory Care*, 2018, 63(2):158-168.
- [3] L. Gattinoni et al. "Covid-19 Does Not Lead to a "Typical" Acute Respiratory Distress Syndrome", in *American Journal of Respiratory and Critical Care Medicine*, 2020, 201(10), pp. 1299-1300

# Deploying digital twins of the cardiovascular system in clinics: a deep learning-based automatized framework

M.A. Scarpolini<sup>1,2</sup>, M. Mazzoli<sup>1</sup>, S. Garzia<sup>1,3</sup>, A. Clemente<sup>4</sup>, A. Monteleone<sup>4</sup>, K. Capellini<sup>1</sup> and S. Celi<sup>1</sup>

<sup>1</sup> BioCardioLab, Fondazione Toscana G. Monasterio, Massa, Italy

<sup>2</sup> Department of Industrial Engineering, University of Rome "Tor Vergata", Roma, Italy

<sup>3</sup> Department of Information Engineering, University of Pisa, Pisa, Italy

<sup>4</sup> Department of Radiology, Fondazione Toscana G. Monasterio, Massa, Italy

**Abstract**—Digital twins represent a new powerful numerical tool to give personalized treatment for cardiovascular diseases, however their translation in a clinical environment is still limited mainly due to long computational times. This work shows an automatized workflow to build a real-time digital twin using deep learning algorithms and computational fluid dynamics simulations. Results show that the computation time can be reduced from hours to a few seconds.

**Keywords**—Unet, ROM, CFD, SSM.

## I. INTRODUCTION

CARDIOVASCULAR diseases (CVDs) are accounted for 45% of all deaths in Europe [1]. In the last years the ever-growing available computational power and the developed numerical tools have paved the way to give a structured, reproducible, and predictive framework (digital twins) for developing personalized strategies for CVDs treatment. Despite this, their high computational demand in terms of cost and time, still limits their adoption in a clinical environment. In this work we show a fully automatized workflow to build a high-fidelity digital twin of the thoracic aorta by combining deep learning (DL) algorithms, DL-based reduced order models (ROM) and computational fluid dynamics (CFD).

## II. MATERIALS AND METHODS

### A. Aorta segmentation

The first step of this framework is the segmentation of thoracic CT scans to obtain a 3D model of the patient's thoracic aorta. The segmentation starts from the aortic root and includes the whole visible aorta and supra-aortic vessels. A UNet-based [2] neural network was trained on a dataset of 50 aortas manually segmented from patient-specific CT scans.

### B. Morphological features extraction

A specific statistical shape model (SSM) was built from the dataset of 50 aortas to extract morphological features of each geometry. With respect to the literature, the developed tool is able to cope with supra-aortic vessels shape changes. The SSM is used to assess the geometrical similarity between each new segmented aorta coming from the presented patient and the ones of the dataset.

### C. Hemodynamic simulation

Steady CFD simulations were performed to compute hemodynamic indices. Constant pressure boundary conditions

are imposed at each outlet and a systolic peak velocity value was chosen as inlet condition. To speed up CFD simulations, a specific DL-based ROM was developed. The ROM is based on graph neural networks [3] and was trained on a large-scale dataset of CFD simulations of 500 different geometries computed on the bases of the SSMs results. When a new patient-specific aorta, representable by the SSM, is presented, this approach allows to estimate hemodynamic indices in real-time, otherwise a new CFD simulation is run. All CFD simulations were performed on a volumetric mesh automatically generated in ANSA through a specific python script developed in-house.

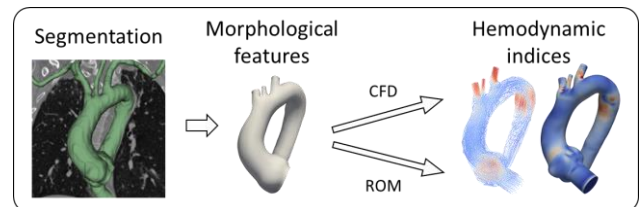


Figure 1: Entire workflow.

## III. RESULTS

The automatic segmentation reaches a mean dice score of 0.93 compared to the manual one, while the DL-based ROM have a mean absolute error of 5% for the WSS, compared to CFD. This workflow allows to extract patient-specific information about the thoracic aorta from a CT scan of a patient almost real-time (~30 sec.).

## IV. CONCLUSIONS

A completely automatized workflow for the construction of a digital twin of the thoracic aorta has been developed with a significant speed improvement that enables the potential application in clinical environments.

## ACKNOWLEDGEMENT

This project has received funding from the Marie Skłodowska-Curie grant agreement No 859836.

## REFERENCES

- [1] A.W. Group et al, Eur. Heart J. 39(7), 508–579 (2017).
- [2] O. Ronneberger et al, MICCAI 234-241 (2015).
- [3] B. Thamsen et al, IEEE Trans Med Im 40.5 1438-1449 (2021).
- [4] N. Verma et al, Proceedings of the CVPR 2598-2606 (2018).

# Failure location and failure mode in human vertebrae with metastases

Giulia Cavazzoni<sup>1,2</sup>, Enrico Dall'Ara<sup>2</sup>, Luca Cristofolini<sup>1</sup>, Marco Palanca<sup>1</sup>

1. Dept of Industrial Engineering, Alma Mater Studiorum – University of Bologna, Bologna, IT

2. Dept of Oncology and Metabolism, and INSIGNEO, The University of Sheffield, Sheffield, UK

**Abstract**—The aim of the study is to identify the failure location and mode in human metastatic vertebrae. 12 spine segments with different types of metastases were used. A global Digital Volume Correlation (DVC) approach was used to quantify the internal strain field. Different failure location and mode were found for lytic and blastic metastases.

**Keywords**—Spinal metastases, in situ mechanical test, digital volume correlation, failure mode.

## I. INTRODUCTION

Bone metastases affect the spine by reducing the load-bearing capacity of the vertebrae and possibly, triggering fractures. In case of vertebrae with lytic metastases, which radiologically appear as regions with low bone mineral density, lesions size and position are fundamental predictors of the bone strength [1]. By contrast, it is unclear how blastic metastases, which radiologically appear as regions with high bone mineral density, affect the vertebral strength. Indeed, while blastic metastases are expected to provide a higher bone strength, fractures frequently occur in patients with these metastases. The aim of the study was to evaluate if the radiographical images reflect the mechanical behaviour of human vertebrae with different types of metastases through the experimental identification of the failure location and mode.

## II. MATERIAL AND METHODS

12 thoraco-lumbar cadaveric spine segments were obtained through an ethically approved donation program. Each segment consisted in one vertebra with radiologically observable lytic (n=8) or blastic metastases (n=4), and one adjacent vertebra without visible lesions, as a control. Each specimen was  $\mu$ CT scanned (Scanco VivaCT80, isotropic voxel size=39 $\mu$ m) in unloaded condition. Then, each specimen was compressed until failure and scanned again. A global Digital Volume Correlation approach (BoneDVC [2]) was used to quantify the strains distribution at fracture within the vertebral bodies, with a measurement spatial resolution of 1.95mm. The failure load was recorded for each spine segment. The three-dimensional strain distributions were compared between the metastatic and the control vertebrae (Kolmogorov-Smirnov test). Compressive strains were averaged on each metastatic and control vertebra to identify the vertebra undergoing the largest deformations, which are indicators of tissue failure.

## III. RESULTS

The failure load of the specimens with lytic and blastic metastases was 1859 $\pm$ 929N and 2903 $\pm$ 2180N (mean $\pm$ SD), respectively. These failure loads correspond to the lower range

of the typical healthy thoracic and lumbar vertebrae [3], [4]. The strain distributions of the metastatic and control vertebrae were significantly different ( $p < 0.05$ ). The failed bone tissue was localized in the metastatic vertebra for specimens with lytic (6/8) and blastic (1/4) lesions (Fig. 1a, 1b). Two different failure location and mode were identified. In case of vertebrae with lytic metastases, the failure occurs between the endplate and the lesion where the larger strains were measured (Fig. 1c). By contrast, in case of vertebrae with blastic metastases the failure occurred in the over-deformed regions around the metastases (Fig. 1d).

## IV. CONCLUSION

Size and position of lytic metastases are confirmed as fundamental predictors of the bone strength. Blastic metastases showed, instead, a more complex mechanical behaviour which cannot be predicted with only lesions size and position. In fact, in some specimens, the radiographically dense regions seem to be weaker than the healthy trabecular tissue. This could be due to the different local mechanical behaviour of the blastic tissue [5], as highlighted for the first time by the unexpected deformation pattern within the vertebrae.

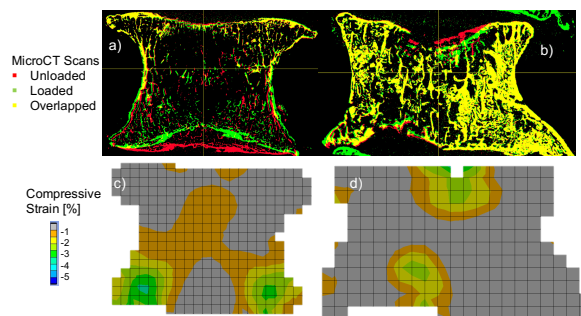


Fig.1:  $\mu$ CT scans of the vertebra with lytic (a) and blastic (b) metastases in unloaded condition (red) and at failure (green). DVC 3D strain map at failure of the vertebra with lytic (c) and blastic (d) metastases.

## ACKNOWLEDGEMENT

The study was partially funded by AOSpine (AOSDIA\_2019\_063), Marie Skłodowska-Curie Actions (MSCA-IF-EF-ST,832430/2018) and EPSRC Multisim Grant (EP/K03877X/1,EP/S032940/1).

## REFERENCES

- [1] M. Palanca *et al.* (2021), *Bone*; 151:116028
- [2] E. Dall'Ara *et al.* (2017), *FrontiersInMaterials*; 4:31
- [3] Moro *et al.*, (1995), *CalcTissuelnter*; 56:206-209
- [4] Perilli *et al.*, (2012), *Bone*; 50:1416-25
- [5] Stadelmann *et al.*, (2020), *Bone*; 141:115598

# 0D hemodynamic model to assess coronary flow at different effort conditions in AAOCA

V. Ceserani<sup>1</sup>, G. M. Formato<sup>2</sup>, M. Lo Rito<sup>3</sup>, G. Zuniga<sup>3</sup>, M. Agnifili<sup>4</sup>, A. Rosato<sup>1</sup>, F. Secchi<sup>5,6</sup> and M. Conti<sup>1</sup>

<sup>1</sup> DICAr, University of Pavia, Italy

<sup>2</sup> 3D and Computer Simulation Laboratory, IRCCS Policlinico San Donato, San Donato Milanese, Italy

<sup>3</sup> Department of Congenital Cardiac Surgery, IRCCS Policlinico San Donato, San Donato Milanese, Italy

<sup>4</sup> Department of Clinical and Interventional Cardiology, IRCCS Policlinico San Donato, San Donato Milanese, Italy

<sup>5</sup> Department of Biomedical Sciences for Health, University of Milan, Italy

<sup>6</sup> Department of Radiology, IRCCS Policlinico San Donato, San Donato Milanese, Italy

**Abstract**— Anomalous aortic origin of the coronary artery (AAOCA) can be associated with sudden cardiac death (SCD), usually related to physical effort. Our aim is to develop a patient-specific (PS) hemodynamic model based on clinical data to assess the coronary blood flow (CBF) in AAOCA, to understand how the disease and its hemodynamical consequences during effort affects myocardial perfusion and the related risk of ischaemia.

**Keywords**—AAOCA, coronary flow, lumped-parameter model.

## I. INTRODUCTION

AAOCA is a rare congenital disease that can cause SCD during physical effort. Structural modeling has already shown a limited intramural expansion of the anomalous coronary artery (CA) during effort [1]. Given such a premise, the goal of the present study is to understand how this phenomenon affects myocardial perfusion developing a PS hemodynamic model to assess the CBF in AAOCA.

## II. MATERIALS AND METHODS

### A. Clinical data and model definition.

Multimodal diagnostic data are integrated to define a PS lumped-parameter model to evaluate CBF under different hemodynamic conditions. The model describes each arterial segment as an electrical circuit whose components depend on the geometry of the vessel, its wall material properties and blood hemodynamics [2] (Fig. I A). The parameters related to the CAs radial expansion can be fixed or vary in time according to the CA lumen dynamics, recorded during IntraVascular UltraSound (IVUS).

### B. Boundary conditions (BCs).

A PS pressure waveform is used as inlet condition. The aorta outlet is modeled with a Windkessel circuit, whereas the CA outlet is defined by 6-elements circuit with an intramyocardial pressure source (ventricular pressure) [2] (Fig. I A). The total resistance of each outlet is split among circuit resistive parameters following the algorithm proposed by Sankaran et al. [3]. The total aortic resistance is evaluated with the patient's cardiac output (CO) and mean arterial pressure [3]. The total coronary resistance is defined during catheterization measurements under resting and hyperemic condition. The left ventricular pressure (LVP) waveform is rescaled based on the PS data, the right one is evaluated as 20% of LVP [3].

## III. RESULTS

The results of simulated CBF are shown in Table I and Figure I B. Resting and hyperemic *in-vivo* measurements are used.

## IV. CONCLUSION

Although physical effort is not yet simulated, the present results suggest that our computational model could be a valuable tool to quantify myocardial perfusion in AAOCA subjects, allowing to replicate conditions that cannot be reproduced even using invasive diagnostic tools such as catheterization.

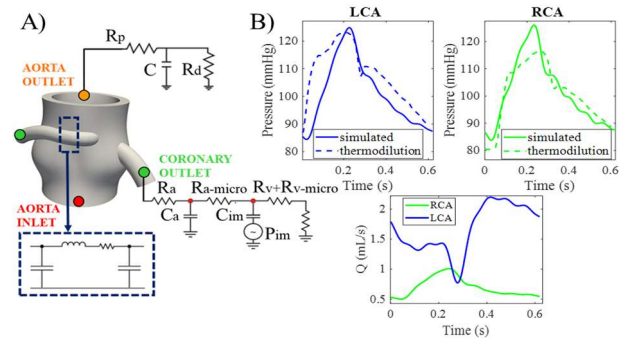


FIGURE I. A) Schematic representation of the OD-model. B) Patient's results: on the top pressure simulated vs *in-vivo* measurements, on the bottom computed CBF for right and left CA (RCA, LCA).

TABLE I

PATIENT	CBF SIMULATED		CBF MEASURED	
	Rest	Hyperemia	Rest	Hyperemia
1 Anomalous RCA	0.7	6.5	0.75	6.25
	1.5	6.8	1.72	7.75
2 Normal RCA	1.7	5.22	1.73	5.53
	1.02	5.24	1.02	5.05
3 Anomalous RCA	2.17	3.55	2.67	4.77
	0.82	3.16	0.96	3.47

Simulated and measured CBF [mL/s] are reported for three patients.

## ACKNOWLEDGEMENT

Funding by Italian Ministry of Health (GR-2019-12369166).

## REFERENCES

- [1] M. Lo Rito, R. M. Romarowski, A. Rosato, S. Pica, F. Secchi, A. Giamberti, F. Auricchio, A. Frigiola and M. Conti, "Anomalous aortic origin of coronary artery biomechanical modeling: Toward clinical application," *Journal of Thoracic and Cardiovascular Surgery*, vol. 161, no. 1, pp. 191-201, 2021.
- [2] N. Westerhof, F. Bosman, C. J. De Vries and A. Noordergraaf, "Analog studies of the human systemic arterial tree," *Journal of Biomechanics*, vol. 2, no. 2, pp. 121-143, 1969.
- [3] S. Sankaran, M. E. Moghadam, A. M. Kahn, E. E. Tseng, J. M. Guccione and A. L. Marsden, "Patient-specific multiscale modeling of blood flow for coronary artery bypass graft surgery," *Annals of Biomedical Engineering*, vol. 40, no. 10, pp. 2228-2242, 2012.

# A comprehensive study to develop a numerical model of the left atrial appendage occlusion

F. Danielli<sup>1</sup>, F. Berti<sup>1</sup>, B.M. Fanni<sup>2,3</sup>, E. Gasparotti<sup>2,3</sup>, G. Pennati<sup>1</sup>, L. Petrini<sup>4</sup> and S. Celi<sup>2</sup>

<sup>1</sup> *LaBS, Department of Chemistry, Materials and Chemical Engineering, Politecnico di Milano, Milan, Italy*

<sup>2</sup> *BioCardioLab, Fondazione Toscana “Gabriele Monasterio”, Massa, Italy*

<sup>3</sup> *Department of Information Engineering, University of Pisa, Pisa, Italy*

<sup>4</sup> *Department of Civil and Environmental Engineering, Politecnico di Milano, Milan, Italy*

**Abstract**—Left Atrial Appendage Occlusion (LAAO) is a well-established treatment for the closure of the LAA in patients affected by atrial fibrillation. Nevertheless, the morphological complexity of the anatomical site hinders the clinical procedure, resulting in possible drawbacks. In this scenario, FE modeling of the implant could optimize the preoperative planning, resulting in an increased success rate. This work aims to propose a comprehensive study to develop a reliable numerical model of the LAAO, discussing the influence of model uncertainties.

**Keywords**—Atrial fibrillation treatment, Finite element analysis, Occlusion device, Patient-specific anatomy.

## I. INTRODUCTION

LEFT Atrial Appendage Occlusion (LAAO) with self-expandable Nitinol devices is a percutaneous procedure used to prevent thrombus formation generating over 90% in left atriums affected by atrial fibrillation. Real-world clinical outcomes proved how LAAO is a non-inferior alternative to pharmacological treatment based on oral anticoagulants. Despite the demonstrated safety and efficacy of LAAO, the intra-subject complexity and the inter-subject heterogeneity of the LAA hinder the device sizing and positioning, resulting in eventual postprocedural drawbacks, such as peri-device leakage [1]. In this regard, Finite Element (FE) modeling is a robust tool in guiding clinical decisions among the available strategies (e.g. 3D imaging modalities, 3D printing of anatomical phantoms). To date, the works available in the literature on the FE modeling of LAAO [2] define the optimal device positioning without providing evidence about a thorough investigation of crucial features affecting the outcome of the procedure. The objective of the current study is to propose a comprehensive study to build a FE model of LAAO, including virtual models of the device and patient-specific LAAs (Figure 1). Model uncertainties and implant variability will be discussed.

## II. MATERIAL AND METHODS

### A. Device Model

A physical sample of the Watchman device (Boston Scientific) was available. CT images were used to ensure a high-fidelity reconstruction, and the built CAD model was discretized with 1D elements. In-vitro tests were designed to characterize the thermo-mechanical behavior of the Nitinol frame and to validate the FE model. Finally, the device model was scaled to obtain several sizes fitting different anatomies.

### B. Anatomy Model

Based on CT images, a number of patient-specific anatomies were reconstructed at ten equally-spaced phases of the cardiac cycle and discretized with 2D elements. Time-dependent behavior of the anatomical site was analyzed to evaluate the constraints given by the surrounding structures (e.g. pulmonary veins and mitral valve). Then, LAA wall properties were investigated: FE simulations were performed to calibrate a normalized stiffness, assuming from the literature both the atrial pressure gradient and the wall thickness [3].

### C. LAAO Model

Several deployments of the device were simulated. As input, the following parameters were varied: (i) LAA wall thickness and elastic modulus while maintaining constant the calibrated normalized stiffness; (ii) positioning of the device to be deployed within the LAA. As output, the level of compression of the device and the wall-device distance were evaluated.

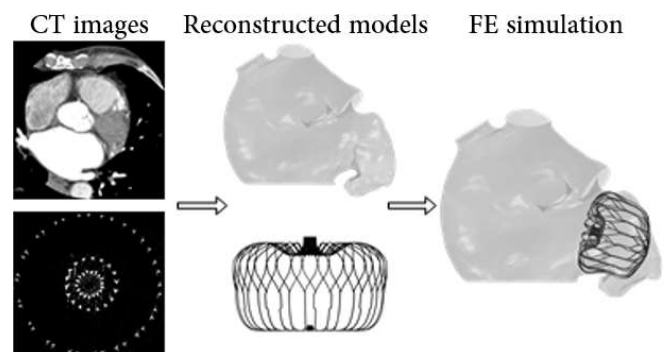


Figure 1 Workflow to develop a reliable FE model of LAAO: CT image acquisition of the anatomy and the device (left), reconstruction of the corresponding models (middle), and FE simulation of the implant (right).

## III. RESULTS AND CONCLUSION

The validation of the device FE model (A) and an exhaustive characterization of patient-specific anatomies (B) led to develop a numerical tool for investigating the influence of anatomical features (wall thickness and elastic modulus) and procedural variability (positioning of the crimped device) on the implant outcome (LAA occlusion). The proposed approach could be extended to different devices.

## REFERENCES

- [1] D. Hong *et al*, *Sci.Rep.* 1–11 (2022).
- [2] A. M. Bavo *et al*, *J.Cardiovasc.Comput.Tomogr.* 14,149-154 (2020).
- [3] K. Słodowska *et al*, *J.Cardiovasc.Electrophysiol.* 32,2262-2268 (2021).

# Patient-specific Fluid Structure Interaction simulations of Non Contact Tonometry

E. Redaelli<sup>1</sup>, J. Grasa<sup>1,2</sup>, B. Calvo<sup>1,2</sup>, J. F. Rodriguez Matas<sup>3</sup> and G. Luraghi<sup>3</sup>

<sup>1</sup> Aragón Institute of Engineering Research (I3A), University of Zaragoza, Spain.

<sup>2</sup> Centro de Investigación Biomecánica en Red en Bioingeniería, Biomateriales y Nanomedicina (CIBER-BBN), Spain.

<sup>3</sup> LaBS, Department of Chemistry, Materials and Chemical Engineering “Giulio Natta”, Politecnico di Milano, Italy.

**Abstract**— Non-Contact Tonometry (NCT) is a diagnostic tool intended to characterize corneal biomechanics in vivo. This work aims to validate an in-silico NCT by comparing the clinical biomarkers of four patients to the numerical results of the same patient-specific simulations.

**Keywords**—Fluid-Structure Interaction simulations, corneal biomechanics, keratoconus, patient-specific models.

## I. INTRODUCTION

Keratoconus (KC) is a corneal disease characterized by a region of high curvature and reduced thickness [1]. Understanding the biomechanical properties of the healthy and diseased region is crucial to diagnose the pathology in time. Non-contact tonometry (NCT) (Corvis ST®) is a diagnostic tool in which a defined air pulse is applied to the eye. The cornea deforms depending on the interaction between the air pressure, the intraocular pressure (IOP), the thickness, and the biomechanical properties of the tissues involved. To detect the mechanical properties, a Fluid-Structure Interaction (FSI) simulation is necessary [2]. This work presents four patient-specific simulations of two healthy and two keratoconus corneas subjected to Corvis ST. The clinical biomarkers are compared with the numerical outputs to validate the procedure.

## II. MATERIALS AND METHODS

The finite element corneal models are constructed based on data retrieved by Pentacam®, a tomographer which creates an elevation map (point cloud describing the anterior surface of the cornea) and a pachymetry map (corneal thickness measured in microns). Through the software ANSA (BETA CAE Systems) a surface fitting is performed, and the corneal geometry is obtained. Each geometry is then linked to an idealized limbo and sclera [2]. The cornea and the limbus are modelled as anisotropic nearly incompressible hyperelastic materials while the sclera is modelled as isotropic. The humours are modelled as incompressible fluids pressurized at a spatially homogenous intraocular pressure (IOP). Initially, the zero-pressure configuration of each eye is computed following an iterative algorithm. Then, a positive input flow rate is imposed on the fluid cavities to reach the patient-specific IOP. The inlet Gaussian air puff velocity of the Corvis ST® (maximum of 120 m/s during a period of 20 ms) is imposed at a nozzle 11 mm distant from the corneal apex. Zero pressure is imposed as an outlet boundary condition. The air is modelled as an incompressible fluid whose density and dynamic viscosity are  $\rho=1.25 \text{ kg/m}^3$  and  $\mu=1.8 \cdot 10^{-5} \text{ Pa}\cdot\text{s}$ . A turbulence model based on a variational multiscale approach is assumed.

## III. RESULTS AND DISCUSSION

The air puff velocity for one healthy and one keratoconus patient are depicted in Fig. 1.a,b. The main biomarkers inferred from Corvis ST are compared in the four cases, two examples are shown in Fig 1.b,c where the comparison between the clinical and numerical peak distance and deflection amplitude is shown. The congruability of three biomarkers in the four cases demonstrates that the simulations proposed can be used for further analysis regarding the corneal biomechanics.

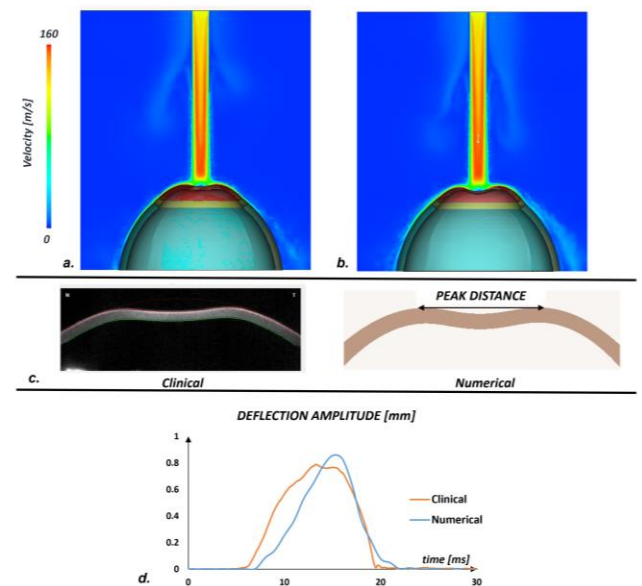


Figure 1: Air velocity contour in the instant of highest concavity for one healthy (a) and one keratoconus (b) patient. Comparison between the clinical and numerical peak distance (c) and deflection amplitude (d).

## IV. CONCLUSION

The validation of patient-specific FSI simulations to model NCT have shown very promising results and constitutes a fundamental step to find accurately the corneal tissue properties of both healthy and pathological eyes.

## ACKNOWLEDGEMENT

This project has received funding from the European Union’s Horizon 2020 research and innovation program under the Marie Skłodowska-Curie grant agreement No 956720. Clinical data were kindly provided by Professor Jos Rozema (University of Antwerp).

## REFERENCES

- [1] J. Santodomingo-Rubido et al, *Contact Lens Anterior Eye*, p. 101559, 2022
- [2] M. Á. Ariza-Gracia et al., *Comput. Methods Appl. Mech. Eng.*, vol. 340, pp. 202–215, 2018

# An experimental/computational approach for fluid dynamic characterization of AAA

M.N. Antonuccio<sup>1,2</sup>, E. Gasparotti<sup>1</sup>, L. Giuggioli<sup>1,3</sup>, E. Vignali<sup>1</sup>, S. Avril<sup>2</sup>, A. This<sup>4</sup>, L. Rouet<sup>4</sup>, S. Celi<sup>1</sup>

<sup>1</sup> BioCardioLab - Bioengineering Unit, Ospedale del Cuore, Fondazione CNR - Regione Toscana "G. Monasterio", Italy

<sup>2</sup> MINES Saint-Étienne, Univ Lyon, Univ Jean Monnet, France

<sup>3</sup> University of Pisa, Information Engineering Department, Italy

<sup>4</sup> Philips Research Paris, France

**Abstract** — Compliant phantoms and experimental circulatory loops have gathered importance during years as they can reproduce hemodynamics at a patient-specific level in terms of both 3D geometry and inlet/outlet boundary conditions. If combined with medical imaging, such as echography, these tools can deepen the knowledge of cardiovascular pathologies. In this work, flow fields in abdominal aortic aneurysm phantoms are reconstructed from Color-Doppler Ultrasound images. *In-silico* data, obtained from Computational Fluid Dynamics, are used for further comparisons.

**Keywords**— Abdominal Aortic Aneurysm, Color-Doppler Imaging, Mock Circulatory Loop Systems, Velocity Flow Mapping.

## I. INTRODUCTION

HEMODYNAMICS plays a crucial role in many vascular disease such as abdominal aortic aneurysm (AAA) [1]. Flow patterns can be reproduced experimentally by inserting patient-specific phantoms of AAA in mock circulatory loop systems. Moreover, Color-Doppler Ultrasound (CD-US) imaging can partially capture flow patterns by providing a projection of the blood flow on the US beams. The missing flow information can be reconstructed by algorithms based on biomechanical principles [2]. The aim of this work is to quantify the hemodynamics of a patient-specific AAA phantom, inserted in a hybrid mock circulatory loop (HMCL) system, and acquired by means of CD-US, for supporting the characterization of this disease.

## II. MATERIALS AND METHODS

The setup is shown in Fig. 1. A patient-specific AAA phantom was manufactured using Sylgard 184.

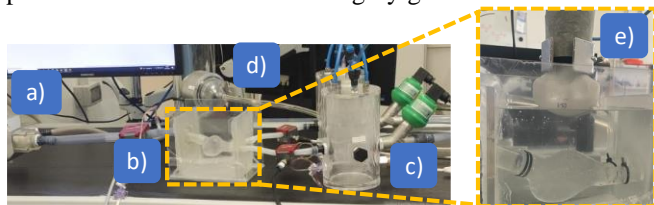


Figure 1 Experimental setup: a) piston pump; b) AAA phantom; c) hybrid chambers; d) centrifugal pump; e) US probe

A HMCL was used to impose the desired flow rate at the inlet of the phantom [3]. A mixture of glycerol and water (60:40) and 100  $\mu\text{m}$  diameter spherical particles were used as blood mimicking fluid. *In-vitro* CD-US images were acquired using an EPIQ 7C US scanner (Philips Healthcare) with a 5 MHz convex array. To reconstruct the velocity flow field in the bi-dimensional domain of interest, an algorithm that takes the CD-US velocity as input was used. Moreover, a Computational Fluid Dynamics (CFD) simulation was carried out, prescribing same boundary conditions (flow and pressure)

as the experiment, to generate *in-silico* CD-US images from the simulated 3D velocity field. *In-vitro* and *in-silico* results were compared, and the *in-silico* average magnitude error was computed.

## III. RESULTS

*In-vitro* CD-US acquisitions at the peak systole and the related reconstructed velocity magnitude and streamlines are shown Fig. 2a-2b, respectively. *In-silico* CD-US image, generated from the CFD simulation, and related reconstructed velocity magnitude and streamlines are reported in Fig. 2b-2e, respectively. The ground truth (GT) velocity, used to compute *in-silico* reconstruction errors, is reported in Fig. 2c. An average magnitude error of  $\sim 10\%$  was computed *in-silico*.

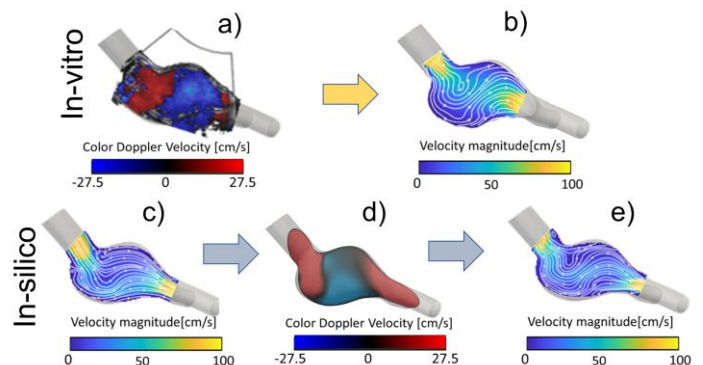


Figure 2 CD-US images and reconstructions at peak systole. First row: *in-vitro*; second row: *in-silico*

## IV. DISCUSSION AND CONCLUSION

Velocities are higher at the inlet/outlet and gradually reduce at the aneurysm in both cases. Velocity streamlines are deflected towards AAA bottom wall with a small vortex close to the aneurysm neck both *in-silico* and *in-vivo*, in agreement with GT velocity. Reconstructing flow fields from CD-US allows assessing the hemodynamics of AAA, which could be very useful in clinics to complement the diagnosis of this disease. Moreover, AAA phantoms inserted in the HMCL system, can be beneficially used to investigate a variety of geometries and flow conditions.

## ACKNOWLEDGEMENT

MeDiTaTe Project has received funding from the European Union's Horizon 2020 research and innovation programme under Grant Agreement 859836.

## REFERENCES

- [1] McLaughlin et al., *Arterioscler*, 2010.
- [2] Assi et al, *Phys. Med. Biol.*, 62:7131–7147, 2017.
- [3] Vignali et al, *ASAIO Journal*, January 12, 2022.

# How does the interconnection mechanism affect the static response of spinal fixators? A validated FE study

L. Ciriello<sup>1</sup>, F. Berti<sup>1</sup>, L. La Barbera<sup>1,2</sup>, T. Villa<sup>1,2</sup>, G. Pennati<sup>1</sup>

<sup>1</sup> Department of Chemistry, Materials and Chemical Engineering "Giulio Natta" - LaBS, Politecnico di Milano (Italy)

<sup>2</sup> IRCCS Istituto Ortopedico Galeazzi (Italy)

**Abstract**—Posterior spinal fixation is a well-established treatment for column disorders. Although various numerical studies are present in the literature on the topic, many simplifications are still affecting the reliability of the results, especially regarding the interconnection mechanism (IM). In particular, the effect of its tightening is often neglected, even if it plays an important role in the system's stiffness and local stress distribution. This work aims to develop a detailed and validated model of the IM.

**Keywords**— Finite Element Analysis, elastic-plastic material, model credibility

## I. INTRODUCTION

Posterior spinal fixation is the gold standard to treat different column disorders. It consists of the secure assembly of rods and pedicle screws, which is guaranteed by the application of a tightening torque at the Interconnection Mechanism (IM). In turn, it consists of different subcomponents (Figure 1a). The global stiffness of the device and the rod local damage due to the screw tightening are known to be significantly important to describe overall behavior under external loads. Nevertheless, the literature computational models are becoming increasingly anatomically complex but still approximated in describing the interactions among the subcomponents [1-3]. The present study aims at increasing awareness in the field of spinal fixation modeling by investigating the mechanical response of the IM in terms of (i) stiffness and (ii) magnitude and distribution of residual stresses due to the tightening.

## II. MATERIALS AND METHODS

A Detailed Model (DM) of the IM was built using Abaqus 2020 environment (Dassault Systemes, SIMULIA Corp., USA). Given that all the IM components are made from the same material, elastic-plastic material properties were globally assigned ( $E=110\text{GPa}$ ,  $\sigma_Y=885\text{MPa}$ ). A general contact interaction property was set among all the components with a friction coefficient equal to 0.35 to account for the tightening effect (Figure 1a). For the safe of comparison, a Simplified Model (SM), was considered, in which the assembly step was neglected and all the subcomponents were modeled as welded, as described in literature [1-3].

### A. Tightening of the IM

The manufacturer specified a value of 8 Nm for the tightening torque associated with the correct functioning of the IM. The anterior part of the tulip was gripped in a clamp and, through the use of a torque wrench, it was possible to tight and measure the total angle of rotation of the nut. The same boundary conditions were applied in the DM and a comparison with experimental tests was performed. The DM was used to evaluate the internal state of residual stresses arising in the IM after tightening. Particular attention was posed to the nut-rod

contact in terms of the Von Mises stresses.

### B. Spinal fixation system stiffness evaluation

To quantify the static properties of the IM, the ASTM F1798 standard [4] was used (Figure 1c): this test provides an indirect verification of the macroscopic mechanical behavior of the IM after tightening and comparison among SM, DM, and experimental test in terms of stiffness (K).

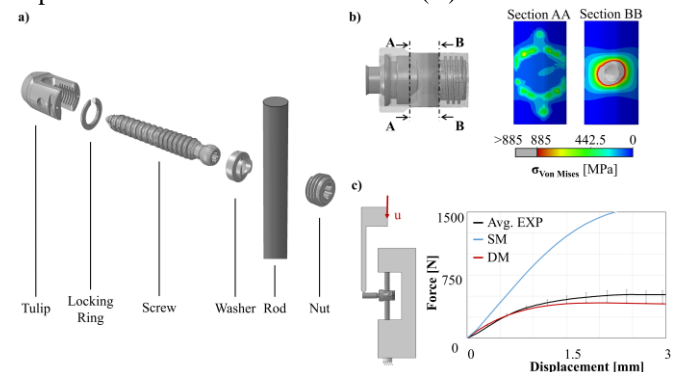


Figure 1: a) The components of the IM; b) residual stresses due to IM tightening on the rod in two different sections; c) the setup according to the ASTM F1798 standard (left) and the force-displacement curves (right).

## III. RESULTS AND CONCLUSION

### A. Tightening of the IM

The average experimental screw rotation angle value is  $155.5^\circ \pm 6.4^\circ$ , reasonably close to  $159.4^\circ$  of the DM. This suggests the good mimicking of the complex behavior of the IM. The simulation indicated important residual stresses in the rod due to the tightening (Figure 1b).

### B. Spinal fixation system stiffness evaluation

The results of the static test according to the ASTM F1798 standard and corresponding simulations for both SM and DM were reported in Table 1 and Figure 1c. DM good matches the experiment, whereas the SM has a totally different behaviour.

Table 1 Value of the stiffness (K) for the experimental and numerical curves.

	K [N/mm]	% diff. (Model vs. Exp)
Exp. Avg±St.Dev.	467.2±34.3	-
Simplified Model	904.5	93.6 %
Detailed Model	488.7	4.6%

In conclusion, this study highlights the importance of a detailed modeling of the IM, which affects the results in terms of system's stiffness, and local residual stresses due to tightening.

## REFERENCES

- [1] La Barbera et al, Proc Inst M E H, 228(10):1014-26, 2014.
- [2] La Barbera et al, Proc Inst M E H, 231(2):176-185, 2017.
- [3] Chu et al, PLoS One, 14(11): e0224699, 2019.
- [4] ASTM F1798, 2019.

# Impact of wall distensibility on prominent features of carotid bifurcation hemodynamics

S. Zambon<sup>1</sup>, M. Arminio<sup>1</sup>, U. Morbiducci<sup>1</sup>, C. Chiastra<sup>1</sup> and D. Gallo<sup>1</sup>

<sup>1</sup> PoliTo<sup>BIO</sup>Med Lab, Department of Mechanical and Aerospace Engineering, Politecnico di Torino, Turin, Italy

**Abstract**— The effect of wall distensibility is evaluated on intravascular and near-wall hemodynamics in healthy carotid bifurcation computational models. The comparison between two-way fluid-structure interaction (FSI) simulations and the corresponding rigid wall simulations revealed that hemodynamic features are comparable qualitatively, but not quantitatively.

**Keywords**— Fluid-structure interaction, computational fluid dynamics, topological skeleton, helical flow, atherosclerosis.

## I. INTRODUCTION

THE hemodynamic environment at the carotid artery bifurcation plays a relevant role in the origin and progression of atherosclerosis [1]. Recently, the variability of the wall shear stress (WSS) contraction/expansion action on the endothelium along the cardiac cycle has been associated with clinical markers of atherosclerosis [2]. Moreover, specific intravascular helical flow features in the bifurcation have been proven to play an atheroprotective role [1]. To obtain local hemodynamic features, those studies relied on computational fluid dynamics (CFD) models under the rigid wall assumption. In this work, the effect of wall distensibility on these emerging hemodynamic features is explored by implementing a fully coupled two-way fluid-structure interaction (FSI) simulation accounting for prestress of the arterial wall, external tissue support, and arterial wall anisotropic material properties.

## II. METHODS

The volumetric fluid domain of healthy carotid bifurcations was obtained from magnetic resonance (MR) angiography [1]. The wall structural domain was generated by extruding the lumen wall with subject-specific thickness. The fully coupled two-way FSI approach, based on the arbitrary Lagrangian-Eulerian formulation, was adopted and implemented in SimVascular [3]. Subject-specific inlet flow rate waveforms were extracted from phase-contrast MR measurements [1] and imposed at the inlet section. Three-element Windkessel boundary conditions were tuned to match the subject-specific measured flow rate split and imposed at the outlets. For the solid domain, the anisotropic nonlinear HGO model was adopted accounting for the presence of the collagen fibrillar component, whose direction was determined by the principal stress directions at the initial loading state [4]. Such state was obtained by calculating iteratively the so-called prestress tensor under diastolic flow conditions [3]. Viscoelastic support of the tissue surrounding the carotid outer wall was accounted for by imposing a Robin-type boundary condition [3]. For the purpose of comparison, CFD simulations were carried out under a rigid wall assumption adopting the same fluid computational grid and simulation settings. Intravascular flow was characterized in terms of helicity intensity [1]. The

variability of the WSS contraction/expansion action along the cardiac cycle was quantified by the topological shear variation index (TSVI) [2], defined as the root mean square deviation of the divergence of the normalized WSS with respect to its average over the cardiac cycle.

## III. RESULTS AND DISCUSSION

For the sake of brevity, the findings obtained on one paradigmatic model are reported. In the FSI simulation, the diameter of the common carotid artery (CCA) varies between 6.6 mm and 7.2 mm along the cardiac cycle. Contour maps of TSVI in distensible and rigid wall simulations indicate qualitatively similar results (Figure 1). Quantitatively, surface-averaged TSVI values are higher in the distensible model (294.3 vs. 245.8  $m^{-1}$ ), although maximum TSVI values are lower (2262.9 vs. 2377.9  $m^{-1}$ ). The peculiar bi-helical patterns characterizing the bifurcation flow field are observed in both distensible and rigid models, although larger helical structures develop in the CCA of the distensible model, and in the bifurcation region of the rigid model. Lower helicity intensity values are found in the distensible model (7.4 vs. 11.2  $m/s^2$ ).

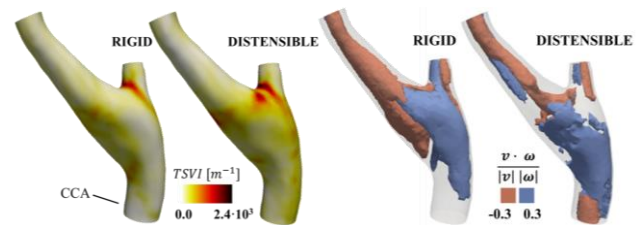


Figure 1- TSVI contour maps (left panel). Helical flow patterns visualized using isosurfaces of the normalized internal product of velocity and vorticity vectors (right panel).

## IV. CONCLUSION

Using the developed FSI numerical framework, it emerged that hemodynamic features are comparable in terms of localization and topology when modelling wall distensibility or under the rigid wall assumption. However, quantitative differences emerge, deserving further consideration. Their influence on the association between hemodynamics and atherosclerosis will be subject to future investigations.

## REFERENCES

- [1] Gallo et al., "Segment-specific associations between local haemodynamic and imaging markers of early atherosclerosis at the carotid artery: an *in vivo* human study," *J R Soc Interface*, 15(147):20180352, 2018.
- [2] Morbiducci et al., "Wall shear stress topological skeleton independently predicts long-term restenosis after carotid bifurcation endarterectomy," *Ann Biomed Eng*, 48(12):2936–2949, 2020.
- [3] Updegrove et al., "SimVascular: an open source pipeline for cardiovascular simulation," *Ann Biomed Eng*, 45(3):525–541, 2017.
- [4] Hariton et al. "Stress-modulated collagen fiber remodeling in a human carotid bifurcation," *J Theor Biol*, 248(3):460–470, 2007.

# A method to calibrate the mechanical boundary conditions of a high-fidelity thoracic aorta model

L. Geronzi<sup>1,2</sup>, M. Sensale<sup>2</sup>, A. Martinez<sup>1,2</sup>, M. Rochette<sup>2</sup>, P.P. Valentini<sup>1</sup> and M.E. Biancolini<sup>1</sup>

<sup>1</sup>Department of Enterprise Engineering “Mario Lucertini”, University of Rome Tor Vergata, Via del Politecnico,1, 00133 Rome, Italy  
<sup>2</sup>Ansys France, 69100, Villeurbanne, France

**Abstract**—We performed a calibration of the mechanical boundary conditions for a thoracic aorta model including the effect of the soft tissue, the interaction of the vessel with the spine and the motion due to the heart. We minimised the discrepancy between the splines derived from the segmented boundaries of cine magnetic resonance imaging (cine-MRI) data and the respective splines built from the deformed computational model.

**Keywords**— Aorta, Soft Tissue, Biomechanics, Heart Motion

## I. INTRODUCTION

CARDIOVASCULAR patient-specific modelling aims to recreate vascular anatomies with the goal of improving diagnosis and optimizing clinical treatments. A strong effort to build high-fidelity patient-specific aortic models concerns the inclusion of the annulus motion, the surrounding soft tissue and the relationship of the aorta with the spine [1].

## II. MATERIAL AND METHODS

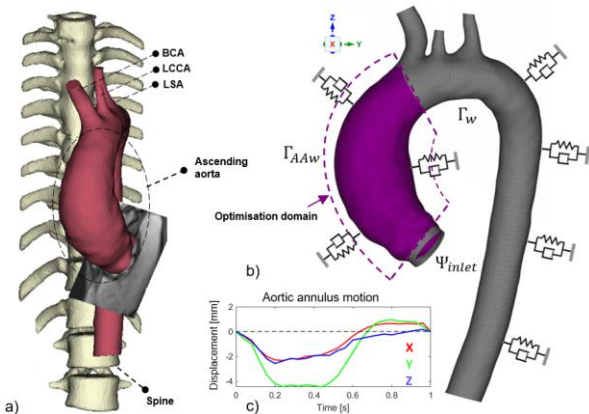


Fig. 1: a) The segmented aorta and spine. b) The structural model. c) The displacements imposed on the inlet boundary.

The procedure, here applied for a single thoracic aorta (TA) geometry, consists of two steps: in the first one, we segmented the anatomies (Fig. 1a) to build the finite element (FE) model (Fig. 1b) with the Robin boundary conditions (BCs) defined in [2]. We run then a fluid-dynamic simulation coupled with a 0D closed loop to extract the wall pressure  $P_w(t)$  and we tracked the motion of the annulus deriving its displacement in space:  $Dx(t)$ ,  $Dy(t)$  and  $Dz(t)$  (Fig. 1c). In particular, concerning the BCs, we connected each  $i$ -node of the wall  $\Gamma_w$  to three dampers and springs, each for a  $j$ -direction of the space. The stiffness of each spring was modelled as:

$$K_{j_i} = K_{ST} + W_{d_i} W_j K_{SPINE} \quad (1)$$

where  $K_{ST}$  was the first sought parameter representing the stiffness of the soft tissue,  $W_j$  the weight to be optimised for each  $j$ -direction of the space,  $K_{SPINE} = 10^6$  Pa/m the stiffness linking the aorta to the spine [3] and  $W_{d_i}$  the scaling factor to represent the distance to the vertebrae:

$$W_{d_i} = 1 - \alpha \frac{d_i}{d_{\max}} \quad (2)$$

with  $\alpha=0.95$ ,  $\mathbf{d}$  the vector containing the minimum Euclidean distance of each node to the spine and  $d_{\max}=\max(\mathbf{d})=142$  mm. In the second step, we performed an iterative procedure taking into account the zero-pressure model and running a structural simulation applying  $P_w(t)$  and  $Dx(t)$ ,  $Dy(t)$  and  $Dz(t)$  at the inlet boundary  $\Psi_{\text{inlet}}$ . Starting with  $\mathbf{p}^0=[W_x^0, W_y^0, W_z^0, K_{ST}]=[1, 1, 1, 10^5$  Pa/m] and using Levenberg-Marquardt, we minimised the following loss function:

$$f(\mathbf{p}) = \sqrt{\sum_{\varphi} \sum_{l=1}^m \sum_{k=1}^{n_l} |d_{l,k}^{\varphi}(\mathbf{p})|^2} \quad (3)$$

where  $\varphi=25$  was the number of cine-MRI frames from which we retrieved the motion of the ascending aorta wall  $\Gamma_{AAW}$ ,  $m=11$  the number of splines from the full 2D dataset,  $n_l$  the number of points for the  $l$ -spline and  $d_{l,k}^{\varphi}(\mathbf{p})$  the nearest neighbour distance of each  $k$ -point belonging to the  $l$ -spline and all the points of the spline derived from the intersection between the cine-MRI plane and the deformed aortic model.

## III. RESULTS AND CONCLUSION

The loss function  $f(\mathbf{p})$  was reduced by 34% after 19 iterations. The value of the calibrated parameters was  $\bar{\mathbf{p}} = [0.6, 0.02, 0.04, 1.5 \times 10^4$  Pa/m]. The effect of the calibration on the model are shown in Fig. 2. With our method we improved the matching between the simulated model and the 2D sequence.

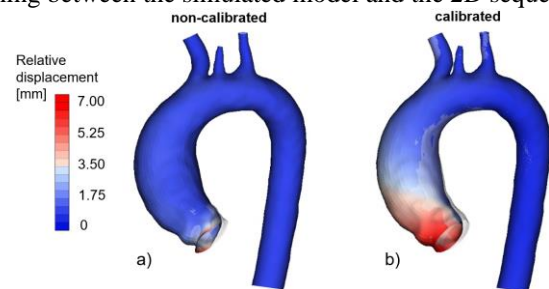


Fig. 2: Contours of the relative systolic-diastolic displacement for a) the model with non-calibrated parameters and b) the tuned model.

## ACKNOWLEDGEMENT

The research has received funding from the European Union’s Horizon 2020 research and innovation programme under the Marie Skłodowska-Curie grant agreement No 859836, MeDiTATe: “The Medical Digital Twin for Aneurysm Prevention and Treatment”.

## REFERENCES

- [1] Taylor and Figueroa, *Annu. Rev. Biomed. Eng.* 11:109–134, 2009.
- [2] Moireau et al., *Biomech. Model. Mechanobiol.*, 11(1), 1–18, 2012.
- [3] Gindre et al., *IEEE. Trans. Biomed. Eng.*, 64(5), 1057–1066.

# Investigating the impact of wall distensibility on aortic flow using a network-based approach

K. Calò<sup>1</sup>, K. Capellini<sup>2</sup>, G. De Nisco<sup>1</sup>, D. Gallo<sup>1</sup>, S. Celi<sup>2</sup>, and U. Morbiducci<sup>1</sup>

<sup>1</sup> PoliTo<sup>BIO</sup>Med Lab, Politecnico di Torino, Torino, Italy

<sup>2</sup> BioCardioLab, Fondazione Toscana Gabriele Monasterio, Massa, Italy

**Abstract**— The impact of aortic wall distensibility on spatiotemporal coherence of large-scale flow patterns was investigated by applying a network-based approach to CFD models under the rigid-wall assumption and to distensible models based on a Radial Basis Functions (RBF) mesh morphing technique. The findings of the study suggest that the similarity of velocity time-histories along the cardiac cycle is only moderately affected by the aortic wall distensibility.

**Keywords**—Aorta, Computational fluid dynamics, Radial basis functions, Mesh morphing, Network science.

## I. INTRODUCTION

TO contribute to the assessment of the impact of uncertainties associated with the rigid-wall assumption in computational hemodynamics models of the aorta, this study aims at investigating the effects of wall distensibility on the spatiotemporal coherence of the aortic flow on a dataset of three personalized CFD models of healthy human thoracic aorta. To do so, a network-based approach [1] was applied to CFD data from the rigid-wall simulation and from the distensible simulation where the patient-specific aortic wall motion was reproduced using a recently proposed RBF mesh morphing technique [2]. For each model, the correlation between the patient-specific inlet flow rate waveform and the axial velocity waveforms obtained from the simulations at each node of the computational grid was used to build a “one-to-all” network [1].

## II. METHODS

Using ECG-gated CT images, aortic geometries were reconstructed at different phases of cardiac cycle. The shape deformation of the ascending aorta (AAo) geometry along the cardiac cycle was obtained following three steps [2]: (1) calculation of the RBF solution targeting the position of the aorta geometry with respect to its baseline configuration (at 0% phase of cardiac cycle), for each of the selected phases, (2) calculation of the RBF incremental solution to reshape the aorta geometry over the cardiac cycle, and (3) coupling of the transient RBF solution with the CFD simulation. Simulations for the rigid and deformable cases were performed using the finite volume method to solve the discretized Navier-Stokes equations on tetrahedral meshes, assuming blood as Newtonian. Further details on the simulation setup are reported elsewhere [2].

The flow rate waveform  $Q(t)$  at the AAO inlet (Figure 1) and the axial velocity component waveforms  $V_{ax}(t)$  calculated at each node of the computational grid were used to build networks. Pearson correlation coefficients  $R_i^{V_{ax}}$  were computed between  $V_{ax}(t)$  waveforms in the rigid and deformable geometries, for each node  $i$ . The spatiotemporal

similarity of  $Q(t)$  waveform with the large-scale aortic flow was evaluated building a “one-to-all” network [1] for the rigid and deformable case, respectively. The network nodes corresponded to the center of mass of the AAO inlet section (where  $Q(t)$  is defined) and to all the nodes of the computational grid. The link between the inlet node and each node  $i$  was weighted by the correlation coefficient  $R_i^{Q-V_{ax}}$  between  $Q(t)$  and  $V_{ax}(t)$  at that node.

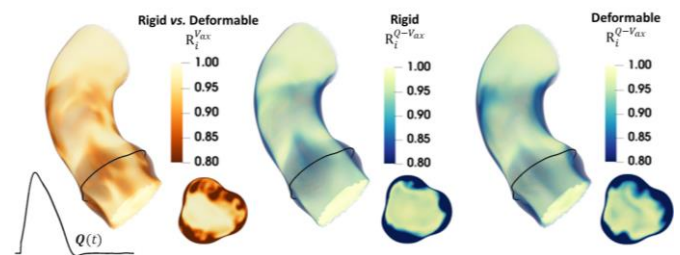


Fig. 1.  $R_i^{V_{ax}}$  and  $R_i^{Q-V_{ax}}$  volumetric maps for one representative aortic model. The patient-specific inlet flow rate waveform  $Q(t)$  is also displayed, as well as a cross-sectional view of the aortic root.

## III. RESULTS AND DISCUSSION

The  $R_i^{V_{ax}}$  volumetric map (an explanatory case is presented in Figure 1) highlighted a very high similarity in the intravascular axial flow waveforms between the rigid and distensible case (median=0.97, IQR=0.07). A moderate loss in similarity ( $R_i^{V_{ax}} < 0.80$ , Figure 1) was bounded in the near-wall regions of the aortic root and of the mid AAO. Consistently, the degree of dynamical similarity between  $Q(t)$  and  $V_{ax}(t)$  waveforms in the deformable aorta is comparable to that in the rigid model, as emerged from the  $R_i^{Q-V_{ax}}$  maps (Figure 1): in both rigid and deformable models,  $Q(t)$  waveform markedly shapes the dynamics of axial flow in the bulk of the vessel, while it has a minor impact on the aortic root and AAO inner wall hemodynamics.

## IV. CONCLUSION

The presented results suggest that, compared to the distensible models, the rigid-wall assumption preserves the large-scale aortic flow patterns in terms of similarity between  $Q(t)$  and  $V_{ax}(t)$  waveform shapes.

## REFERENCES

- [1] K. Calò, et al., “Spatiotemporal Hemodynamic Complexity in Carotid Arteries: An Integrated Computational Hemodynamics and Complex Networks-Based Approach”, *IEEE Transactions on Biomedical Engineering*, 2020, 67(7):1841-53.
- [2] K. Capellini, et al., “A novel formulation for the study of the ascending aortic fluid dynamics with in vivo data”, *Medical Engineering & Physics*, 2021, 91:68-78.

# LED illuminated PIV velocity field characterization in a patient specific aortic aneurysm phantom

F. Bardi<sup>1,2,3</sup>, M.N. Antonuccio<sup>1,2</sup>, E. Gasparotti<sup>1</sup>, M. Aguirre<sup>2</sup>, S. Avril<sup>2</sup>, E. Vignali<sup>1</sup>, and S. Celi<sup>1</sup>

<sup>1</sup> BioCardioLab - Bioengineering Unit, Ospedale del Cuore, Fondazione CNR - Regione Toscana "G. Monasterio", Italy

<sup>2</sup> MINES Saint-Étienne, Univ Lyon, Univ Jean Monnet, France

<sup>3</sup> PrediSurge, Saint-Étienne, France

**Abstract**—The Abdominal Aortic Aneurysm (AAA) is a highly diffused life-threatening condition. In recent years, experimental and numerical techniques were demonstrated to be reliable tools for AAA investigation. Given this, a Hybrid Mock Circulatory Loop and a cost-effective LED Particle Image Velocimetry (PIV) setup were used to characterize the fluid dynamic behaviour in a compliant AAA phantom. Several boundary conditions have been tested, and the instantaneous velocity field was measured in lower part of the aneurysm.

**Keywords**—Abdominal Aortic Aneurysm, Hybrid Mock Circulatory Loop, Particle Image Velocimetry, Fluid Structure Interaction.

## I. INTRODUCTION

HEMODYNAMICS play a crucial role in the progression of Abdominal Aortic Aneurysms (AAAs). Research efforts are still required to better understand the pathology progression and formation. For this purpose, *in-vitro* experiments and *in-silico* numerical approaches can allow to analyse the AAA hemodynamics in controlled and reproducible environments. The aim of this work is to reproduce physiological conditions in a patient specific AAA by both using a Hybrid Mock Circulatory Loop (HMCL) embedded with 2D Particle Image Velocimetry (PIV) and numerical FSI simulations.

## II. MATERIALS AND METHODS

The experimental HMCL-PIV setup is shown in Figure 1. A patient specific AAA phantom was manufactured by means of 3D printing and Sylgard 184 casting. The model was inserted into a HMCL, and piston pump [1] was used to impose a pulsatile flow rate at the inlet. The pressure at the iliac outlets was dynamically regulated according to a 3-element Windkessel model.

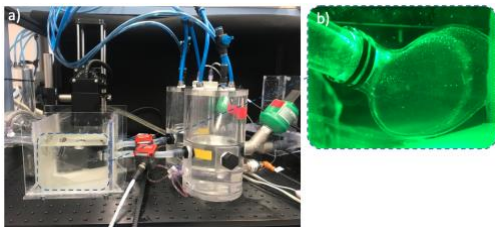


Figure 1: a) Experimental setup with focus on b) AAA phantom

A mixture of glycerol and water (61:39%) was used as working fluid together with 10  $\mu\text{m}$  – diameter hollow spherical particles. A pulsed high-power LED, supplied with pulses with 10  $\mu\text{s}$  width of and a pulse 200  $\mu\text{s}$  of separation, and a line light were used to create a light sheet [2]. The illumination system

was synchronized with a high-speed camera and with the movement of the piston pump, via an FPGA routine embedded in the control software of the HMCL. Nineteen flow field measurements were acquired per cardiac cycle and seven different conditions, varying the flow rate and the Windkessel parameters, were analyzed. The same fluid dynamic conditions were simulated on the same geometry by setting up FSI simulations to allow for experimental-numerical comparison. The Sylgard 184 material properties were obtained by performing a mechanical test with a specific testing setup [3].

## III. RESULTS

The numerical-experimental velocity magnitude maps in the AAA region of interest for the baseline are shown in Figure 2. It is possible to notice the swirling behaviour at the AAA level both in systole and diastole. The numerical and experimental approaches have demonstrated a good agreement in terms of velocity maps.

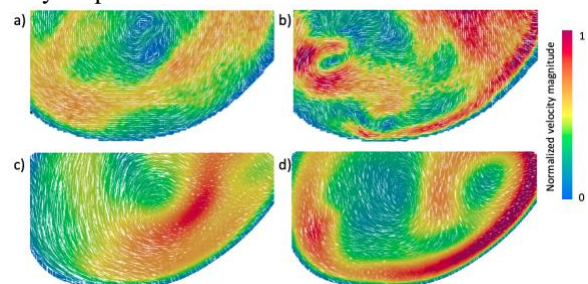


Figure 2: velocity magnitudes according to experimental (a,b) and numerical methods (c,d) at systolic (a,c) and diastolic (b,d) phases.

## IV. DISCUSSION AND CONCLUSION

The proposed HMCL-PIV setup was successfully adopted to characterize a phantom. The velocity distribution maps were in good agreement with the FSI numerical results, confirming the potential of the approach. With the current work, a method for the experimental-numerical evaluation of patient specific AAA hemodynamics was assessed.

## ACKNOWLEDGEMENT

This work was supported by the MeDiTaTe Project from the European Union's Horizon 2020 research and innovation programme under Grant Agreement 859836.

## REFERENCES

- [1] Vignali et al, ASAIO, 12, 2022.
- [2] Willert et al, Meas. Sci. Technol., 21 075402, 2010.
- [3] Vignali et al, MDPI, 10(4):386, 2021.

# Deployment Simulations of Coronary Stents: Digital Analysis of "What if" Scenarios

L. Antonini<sup>1</sup>, G. Poletti<sup>1</sup>, G.S. Karanasiou<sup>2</sup>, D.I. Fotiadis<sup>2</sup>, L. Petrini<sup>3</sup> and G. Pennati<sup>1</sup>

<sup>1</sup> LaBS, Dept. of Chemistry, Materials and Chemical Engineering "Giulio Natta", Politecnico di Milano, Milan, Italy

<sup>2</sup> Dept. of Biomedical Research Institute–FORTH, University Campus of Ioannina, Ioannina, Greece

<sup>3</sup> Dept. of Civil and Environmental Engineering, Politecnico di Milano, Milan, Italy

**Abstract**—The increasing accuracy of the deployment simulations of coronary stents plays a key role in the attempt to refine, reduce and replace clinical trials. Furthermore, the computational approach allows assessing several "What if" scenarios. In this work it is intended to present the potential of a computational tool in evaluating the following scenarios: variations in stent design, compare existing stents, compare anatomy configurations, and compare different procedures.

**Keywords**—BVS, stent deployment simulations, scenarios.

## I. INTRODUCTION

DEVELOPMENTS in the computational capabilities and the increasing reliability of simulations of coronary stent deployment are intended to serve the principle of the 3Rs (Refine, Reduce and Replace) supporting standard pre-clinical and clinical device assessment activities [1]. The potential of an *in silico* approach also allows undertaking investigations that would not be feasible *in vivo*. Within the InSilc project [2], based on literature reviews and a survey with possible stakeholders, four "What if" scenarios were defined: 1) compare variations in the design of the same stent; 2) compare existing stents when implanted in the same artery; 3) compare the response of different arteries when treated with the same device; 4) observe how changes in the procedures may lead to different outcomes. This work presents a selection of examples to show the potential of the four scenarios.

## II. MATERIALS AND METHODS

The stent models were developed based on manufacturer information, literature and device analysis to ensure model reliability. The arteries, derived from 3D reconstructions of clinical images, were modelled considering a diverticula, media, generic plaque, lipid pools and calcifications.

### A. Detail variation in stent design

Two PLLA prototypes of bioresorbable vascular scaffold (BVS) were compared. The aim was to assess whether the presence of holes in the V-struts could limit the concentration of high stresses without compromising the radial strength.

### B. Compare existing stents

The performance of a BVS was compared with that of a metallic stent. To enhance the device characteristics, an artery without significant curvature and with an evenly distributed atherosclerotic plaque was selected.

### C. Compare anatomy configurations

The ability of a novel BVS to re-establish the physiological lumen of a vessel was tested in two different arteries observing the stress exerted on the vessel and any malapposition.

### D. Compare different clinical procedures

A metal stent was used to treat a bifurcated artery following two procedures inspired by clinical practice. The latter differs from the former by the presence of two additional steps: side branch opening and post optimisation technique (POT).

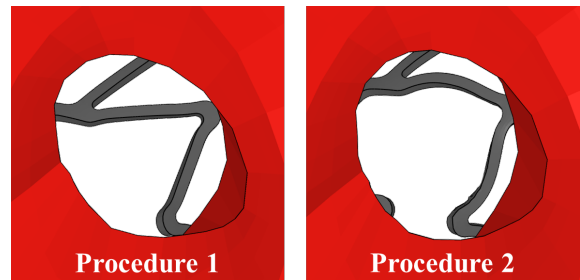


Figure 1 - Detail of the stent struts in the side branch lumen.

## III. CONCLUSION

The results obtained in the first scenario demonstrated the positive effects of the presence of the holes in the stent design. A lower concentration of high stresses was found with a substantial equivalence in terms of the ability to restore the vessel lumen. The second scenario demonstrated the superior capacity of the metallic stent in reopening the lumen compared to its polymeric counterpart. The analysis performed with the third scenario showed that in one anatomy the stent was subjected to significantly higher stress due to a concentrated stenosis. Moreover, in the same artery a clear malapposition of the device was observed. Finally, the last scenario, showed that the branch opening reduced the area of access to the side vessel occupied by the stent struts with potential beneficial effects on fluid dynamics. Furthermore, the final POT reduced the presence of malapposition in the proximal part of the vessel.

## ACKNOWLEDGEMENT

This project has received funding from the European Union's Horizon 2020 research and innovation programme under grant agreement no 777119. This article reflects only the authors' view and the Commission is not responsible for any use that may be made of the information it contains.

## REFERENCES

- [1] Antonini et al., "Validation of the computational model of a coronary stent: a fundamental step towards *in silico* trials", in *Journal of the Mechanical Behavior of Biomedical Materials*, 122 (2021) 104644.
- [2] Karanasiou et al., "An *in silico* trials platform for the evaluation of effect of the arterial anatomy configuration on stent implantation", in *IEEE Eng. In Medicine & Biology Society (EMBC)*, 2021.

# Smartphone-based *in vitro* approach for PIV and PTV analyses in coronary arteries

E. Torta<sup>1</sup>, G.C.A. Caridi<sup>1</sup>, C. Chiastra<sup>1</sup>, U. Morbiducci<sup>1</sup>, D. Gallo<sup>1</sup>

<sup>1</sup> PoliTo<sup>BIO</sup>Med Lab, Department of Mechanical and Aerospace Engineering, Politecnico di Torino, Turin, Italy

**Abstract**— This work proposes a low cost and safe test bench adopting a smartphone camera system and a low-power laser for the *in vitro* quantitative evaluation of local hemodynamics within realistic coronary artery phantoms. Smartphone-based Particle Tracking Velocimetry (PTV) and Particle Image Velocimetry (PIV) measurements are compared to conventional PIV measurements to define their range of applicability.

**Keywords**—Coronary hemodynamic, Particle Image Velocimetry, Particle Tracking Velocimetry, Smartphone.

## I. INTRODUCTION

PARTICLE Image Velocimetry (PIV) and Particle Tracking Velocimetry (PTV) are *in vitro* measurement techniques relying on a Eulerian and Lagrangian reconstruction of the flow field, respectively. Currently, their adoption is hampered by the cost of the *in vitro* set-up components, the high energy consumption, burdensome maintenance and the strict safety requirements related to the high-power lasers. Alternative test benches have adopted more convenient and less hazardous solutions based on cameras embedded in commercial smartphones and low-power light sources [1], but their use for the investigation of cardiovascular flows is still unexplored. The present study aims to demonstrate the feasibility of PIV and PTV measurements based on smartphone cameras and low-power light source in realistic phantoms of healthy and stenotic left anterior descending (LAD) coronary arteries. The performance of the proposed approach, its requirements and range of applicability are evaluated against conventional PIV measurements.

## II. METHODS

The study was conducted using two silicone phantoms (Elastrat, Switzerland) in scale 1:1 representing a patient-specific replica of a healthy LAD reconstructed from angiographic images and its artificially generated stenotic condition. Measurements were carried out under steady-state flow conditions with inlet Reynolds number  $Re$  in the range 21-210, according to *in vivo* measurements [2]. A 40:60 glycerin-water solution was seeded with polyamide particles (density 1030 kg/m<sup>3</sup>, diameter 60  $\mu$ m). In the smartphone-based set-up, the camera of the Samsung Galaxy S9+ (12800x720 pixels, 960 Hz) and a low-power continuous wave laser were used for time-resolved image acquisitions. In the conventional PIV set-up (Dantec Dynamics A/S, Denmark), one HiSense Zyla camera (CMOS, 2560x2160 pixels) and a dual pulsed Nd:YAG laser were adopted. Both Eulerian and Lagrangian flow analyses were performed in MATLAB (MathWorks, USA).

## III. RESULTS

The smartphone-based approach properly captures the main

flow features identified by the conventional PIV measurements in both healthy and stenotic vessel phantoms. In the stenosed LAD phantom, particle traces visualizations highlight the presence of a post-stenotic recirculation region which becomes larger as  $Re$  increases (Figure 1). For the purpose of comparison with conventional and smartphone-based PIV measurements, PTV measurements underwent a Lagrangian-Eulerian transformation of the velocity magnitude ( $|\mathbf{v}|$ ). While in the healthy phantom smartphone-based and conventional measurements are in very good agreement (data not shown), in the stenosed LAD phantom smartphone-based measurements underestimate  $|\mathbf{v}|$  in the stenotic region when the inlet  $Re$  is higher than 64 (Figure 1), due to the high flow velocity (up to 40 cm/s) and the fixed acquisition frame rate (960 Hz) of the smartphone camera. However, the former limitation can be circumvented by using scaled-up phantoms.

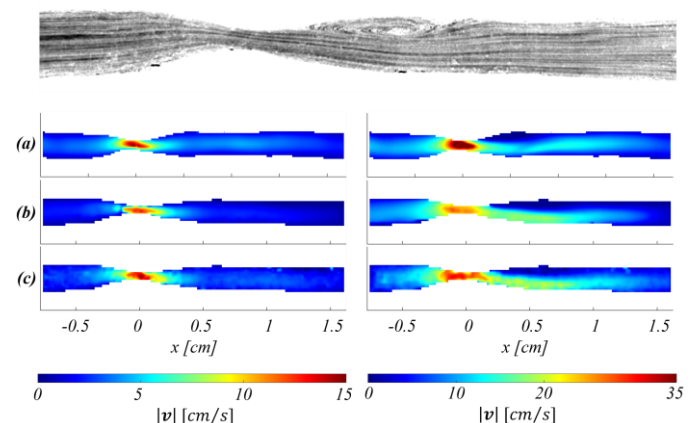


Figure 1- Particle traces from smartphone-based PIV at  $Re=64$  (top panel). Eulerian velocity fields obtained from (a) conventional PIV, (b) smartphone-based PIV, (c) smartphone-based PTV at  $Re=21$  (bottom left panel) and  $Re=64$  (bottom right panel).

## IV. CONCLUSION

These findings demonstrated that the proposed system provides affordable flow measurements and visualizations of the flow field in coronary artery phantoms, enabling its use for educational and research purposes for low-cost, practical investigations. Advancements related to smartphone technologies in the near future will increase the accuracy and reliability of the proposed approach, enabling its extension to a wide variety of biomedical applications.

## REFERENCES

- [1] Cierpka et al., "Flow visualization by mobile phone cameras". *Exp Fluids*, 2016, 57:108.
- [2] Kessler et al., "Assessment of coronary blood flow in humans using phase difference MR imaging. Comparison with intracoronary Doppler flow measurement". *Int J Card Imaging*, 1998, 14(3):179-86.

# Bioreactor design to burst *in-vitro* skeletal muscle differentiation of 3D bioprinted constructs

G. Loi<sup>1</sup>, F. Scocozza<sup>1</sup>, F. L. Ronzoni<sup>2</sup>, G. Cusella<sup>2</sup>, F. Auricchio<sup>1</sup>, G. Ceccarelli<sup>2</sup>, and M. Conti<sup>1</sup>

<sup>1</sup>Department of Civil Engineering and Architecture, University of Pavia, Pavia, Italy

<sup>2</sup>Department of Public Health, Experimental Medicine and Forensic, Human Anatomy Unit, University of Pavia, Pavia, Italy

**Abstract**— This study proposes an engineered platform composed by 1) PDMS stretchable rectilinear structures with a central channel in which fibrin-based hydrogel loaded with murine myoblasts (C2C12 cells) will be bioprinted, and 2) a bioreactor capable of mechanically stimulating structures in order to burst *in-vitro* skeletal muscle differentiation.

**Keywords**— **Bioprinting, Skeletal muscle regeneration, Mechanical stimulation bioreactor, Computational simulations.**

## I. INTRODUCTION

Skeletal muscle diseases have a high social and economic impact as they affect annually a total of about 107.5 million people in US with treatment costs exceeding \$980.1 billion per year [1]. Drugs development for these diseases is difficult because preclinical platforms commonly used (animal models and 2D *in-vitro* cultures) are unsuitable [2]. However, it has been seen that 3D engineered platforms are able to replicate the structural and functional complexity of tissues [2]. In this context, we propose a protocol to create an engineered platform to replicate skeletal muscle complexity. The proposed platform is composed by: 1) PDMS rectilinear structures with a central channel in which fibrin-based hydrogel loaded with murine myoblasts (C2C12 cells) will be bioprinted (figure 1A) [3], and 2) a bioreactor capable of mechanically stimulating structures and improve tissue maturation.

## II. MATERIALS AND METHODS

PDMS Sylgard 184 (1:10) was used to fabricate the structures. In order to investigate the mechanical properties of our PDMS and of our stretchable structures, customizable molds were designed with Autodesk Inventor® and 3D printed. PDMS was cast inside the mold and left to crosslink for about 1 hour at 60°C. PDMS tensile tests were performed in accordance with the standard ASTM D412 for tensile testing of rubber and elastomeric materials. From the fitting of the resulting curves, we obtained the coefficients of the hyperelastic constitutive model of our material used for the subsequent computational simulations. To optimize the mechanical stimulus apply by the bioreactor, *in-silico* and experimental tensile tests of our structures were carried out. Finally, we worked on the bioreactor cell chamber; its prototypes were designed on Autodesk Inventor and then printed in PA12 using the HP MultiJet Fusion 580 Color. In order to reduce trial-and-error, the bioreactor geometry optimization was carried out using *in-silico* simulations. All the mechanical tests were performed using a MTS Insight 30 Instrument equipped with a 10 kN load cell while computational simulation were performed using Abaqus software.

## III. RESULTS AND DISCUSSION

PDMS tensile tests produced stress-strain curves which were fitted in order to obtain the constitutive parameters used for the subsequent computational simulations. About tensile tests of stretchable constructs, force-displacement curves were obtained and the average curve was compared with the computational model results. As shown in figure 1B, the computational model has been validated; in fact, experimental data are very close to the computational one. Finally, to design the bioreactor cell chamber, we started by simulating a first configuration which showed the flexion of the mobile part during the stretching application (figure 1C). As this behavior was undesirable for our application, the configuration has been optimized until all the samples are stretched equally (figure 1D).

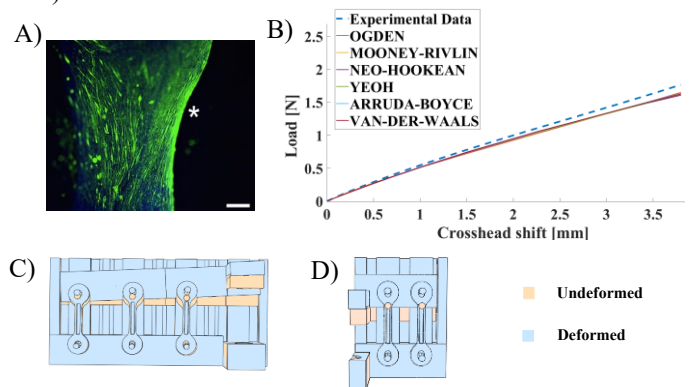


Fig. 1. A) Bioprinted cell viability after 21 days of culture [3]. B) Stress-strain curves: comparison between experimental (dot line) and computational data; Computational simulations for the bioreactor design: C) first and D) optimal configuration.

## IV. CONCLUSION

The choice of the optimal cell chamber geometry and the validation of the computational models, performed in this study, are the first step to obtain a suitable mechanical stimulation bioreactor with well-defined characteristics for skeletal muscle tissue engineering. The next step will be the bioprinting and the biological tests.

## REFERENCES

- [1] E., Yelin, “The burden of musculoskeletal diseases in the United States” in *Seminars in arthritis and rheumatism*, vol. 46, no. 3, 2016, pp. 259-260.
- [2] H. Mohammadi, Mohammad, “Engineered muscle tissues for disease modelling and drug screening applications” in *Current pharmaceutical design*, vol. 23, no. 20, 2017, pp. 2991-3004
- [3] F.L. Ronzoni, “Myoblast 3D bioprinting to burst *in-vitro* skeletal muscle differentiation.” in *Journal of Tissue Engineering and Regenerative Medicine*, vol. 16, no. 5, 2022, pp. 484-495.

# Computational modelling of tissue growth in bioprinted scaffolds

P. Gaziano, G. Vairo, and M. Marino

*Department of Civil Engineering and Computer Science, University of Rome Tor Vergata*

**Abstract**—The present work addresses the development of a computational model for tissue growth in bioprinted scaffolds. Transport equations are introduced to model the different mechano-chemo-biological mechanisms involved in the process, starting from intercellular molecular pathways, up to cell mobility and production of extracellular constituents, through scaffold degradation.

**Keywords**—Tissue growth, Bioprinting, Cell biology, Culture optimization.

## I. INTRODUCTION

TISSUE growth within bioprinted scaffolds is the result of a multi-factorial process made up by: *i*) cell differentiation; *ii*) cell proliferation and/or migration; *iii*) extracellular matrix (ECM) production; *iv*) production and assembly of ECM and cells in a functional form. Cells in bioprinting receive a 3D stimulus since fully embedded in a matrix material. The interaction between cells and, e.g., hydrogels might significantly alter cell biology. Moreover, growth factors, oxygen, nutrients, and waste should be properly transported in/out of the constructs since cells are embedded in the middle. Furthermore, tissue growth is successful only if properly tuned with scaffold degradation. All these factors reveal a complex mechanobiological stimulus applied to cells in bioprinting applications. Unfortunately, the spatiotemporal changes of mechanobiological stimuli and the coupled spatiotemporal changes in tissue growth are both difficult to measure experimentally. Accordingly, *in silico* approaches might be of great advantage for optimizing neotissue formation for tissue engineering applications.

## II. MATERIALS AND METHODS

The mathematical description of the afore-introduced mechano-chemo-biological mechanisms involves chemical reactions and diffusive/advection processes. This is obviously true for molecular transport in cell-cell signalling pathways, but it applies also for the description of cell proliferation and motility. Moreover, modelling frameworks shall account for a multi-physics description, since transport equations should be coupled with an analysis of the mechanical response of constructs, affected for instance by the synthesis of tissue constituents but also scaffold degradation over time. Finally, cells mobility/proliferation within the scaffold determines a significant change of cells domain within the simulation, in the framework of moving boundary problems.

These challenges are tackled here by introducing a phase-field model of the problem. In fact, phase-field models allow to straightforwardly account for moving domains and how evolution equations of internal mechanisms affect moving

volumes and surfaces without the need of remeshing procedures. In addition, the phase-field method opens for a simple treatment of the coupling between the intra- and extra-cellular elements that modulate cell compaction/proliferation. This coupling enables the simulation of the internal cell-cell communications that drive tissue growth in the scaffold, including crucial mechanisms for bioprinted scaffolds such as chemotaxis, haptotaxis, and durotaxis.

## III. RESULTS

Numerical results highlight the role of the interplay between scaffold degradation and tissue growth. The developed simulation tool allows to investigate: *i*) how scaffolds are degraded by enzymes produced by cells; *ii*) the increased cell mobility and proliferative activities associated with local scaffold degradation; *iii*) the dependency of enzymes production and cell activity as function of the availability of nutrients at different locations within the 3D scaffolds.

## IV. CONCLUSION

The developed computational framework is a first step towards a predictive tool for tissue growth in bioprinted scaffolds. The digital twin of the process will be coupled with a sensor platform based on optic fibers that allows to gain detailed information on the heterogeneous properties of scaffolds as produced during bioprinting. The integrated *in-vitro/in-silico* models will be employed to develop an optimization strategy for the culture of bioprinted constructs in bioreactors, with the aim of maximizing neotissue formation and minimizing the waste of culture bath nutrients.

## ACKNOWLEDGEMENT

M. Marino acknowledge the funding of the Italian Ministry of Education, University and Research MIUR (Programma per Giovani Ricercatori - anno 2017 Rita Levi Montalcini) and of Regione Lazio (POR FESR LAZIO 2014; Progetti di Gruppi di Ricerca 2020; project: BIOPMEAT, n. A0375-2020-36756).

## REFERENCES

- [1] M. Conti, G. Santesarti, F. Scocozza, M. Marino, "Models and simulations as enabling technologies for bioprinting process design". In: M. Conti, M. Marino (Eds.), *Bioprinting*, Academic Press, ISBN 9780323854306, 2022, chapter 6, pp. 137-206.
- [2] A. Moure, H. Gomez, "Phase-Field Modeling of Individual and Collective Cell Migration". *Arch Computat Methods Eng* 28, 2021, pp. 311-344.
- [3] U. Akalp, and S.J. Bryant, F.J. Vernerey, "Tuning tissue growth with scaffold degradation in enzyme-sensitive hydrogels: a mathematical model", *Soft Matter* 12(36), 2016, pp. 7505-7520.

# A customized flexible substrate for investigating cell response to controlled uniaxial stretch

B. Masante<sup>1,2</sup>, G. Putame<sup>1</sup>, A.T. Lugas<sup>1</sup>, M. Tosini<sup>1</sup>, I. Roato<sup>2</sup>, F. Mussano<sup>2</sup>, M. Terzini<sup>1</sup>, A. Audenino<sup>1</sup>, D. Massai<sup>1</sup>

<sup>1</sup> *Polito<sup>BIO</sup>Med Lab, Department of Mechanical and Aerospace Engineering, Politecnico di Torino, Italy*

<sup>2</sup> *Bone and Dental Bioengineering Lab, CIR-Dental School, Department of Surgical Sciences, University of Torino, Italy*

**Abstract**—*In vitro* mechanical cues are extremely important for mimicking the native tissue and for investigating the cellular behaviour when exposed to defined stimuli. Here, we designed and characterized a flexible substrate, intended to be used within an existing bioreactor, for exposing the cultured cells to controlled uniaxial stretch.

**Keywords**—Flexible substrates, mechanotransduction, bioreactor, digital image correlation.

## I. INTRODUCTION

MECHANICAL forces play a crucial role in multicellular organisms, with consequences in cell differentiation, tissue renewal and homeostasis, as well as in pathogenesis [1]. In view of mechanotransduction studies, dynamic culture devices (i.e., bioreactors) replicating *in vitro* defined native-like mechanical stimuli represent powerful investigation tools. Here, we developed, characterized, and tested a customized flexible substrate, to be used in combination with a tunable stretch bioreactor [2], for culturing adherent cells under controlled uniaxial stretch, with the final aim of elucidating the role played by mechanical stretch on different cell types.

## II. MATERIALS AND METHODS

The flexible substrate, to be clamped in a stretch bioreactor [2], was designed with two parallel rectangular wells (Fig. 1A) for allowing experiment parallelization. In order to guarantee planar and uniform uniaxial strain, the substrate shape and size were optimized by finite element analyses (FEA, Abaqus), imposing a uniaxial displacement of 3 mm (15% of strain) to one side of the substrate while fixing the opposite one. Once the optimized design was defined, the corresponding mould was designed and 3D-printed, and polydimethylsiloxane (PDMS, Sylgard 184) was poured in it (60 °C for 6 h). The digital image correlation (DIC, isi-sys GmbH) method was adopted to characterize the mechanical behaviour of the substrate under uniaxial stretch and to validate the simulation outcomes. For the preliminary cell experiments, after autoclave sterilization, the substrates were functionalized with collagen I (Sigma Aldrich) and seeded with human adipose-derived stem cells (ASC52-telo hTERT, ATCC) or with human primary periodontal ligament staminal cells (PDLSCs) from healthy donors. After 4 h in incubator (37°C, 5% CO<sub>2</sub>), the cell-seeded substrates were clamped in the bioreactor (Fig. 1B) and were exposed to cyclic uniaxial stretch (8% pre-strain combined with cycles of additional 7% strain for 90 s, at 1 Hz, every 6 h [3]) for 3 days (n=3). As control, cell-seeded substrates were cultured statically for 3 days (n=3). At the end of day 3, the expression of osteogenic markers (e.g., osteocalcin (OCN) and RUNX2) was assessed.

## III. RESULTS

FEA analyses demonstrated that, when uniaxially stretched, the substrate design guarantees a deformation of  $0.133 \pm 4.2\%$  at the bottom of both wells, as partially confirmed by the DIC

analysis ( $0.147 \pm 9.1\%$  left well and  $0.154 \pm 10.9\%$  right well) (Fig. 1C). Preliminary biological tests revealed that ASCs and PDLSCs respond differently to cyclic uniaxial stretch. In detail, stretched PDLSCs showed an increasing trend of OCN and RUNX2 expression, while ASCs were characterized by a slightly decreasing trend for both markers (Fig. 1D).

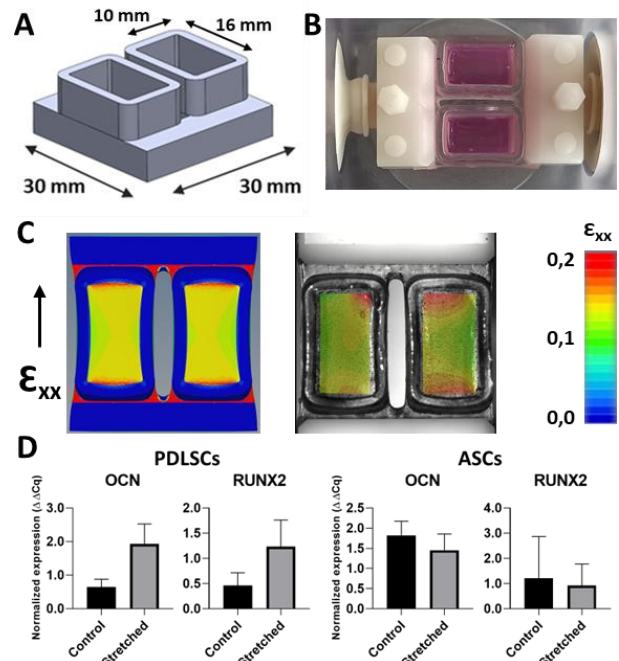


Fig. 1. (A) Technical drawing of the flexible substrate; (B) PDMS substrate clamped in the bioreactor; (C) FEA (left) and DIC (right) results; (D) Gene expression of PDLSCs (left) and ASCs (right).

## IV. CONCLUSION

The developed flexible substrate, to be used in combination with a stretch bioreactor, allows providing controlled uniaxial stretch to cells adherent to two parallel wells. Preliminary biological tests revealed that PDLSCs and ASCs respond differently when exposed to uniaxial stretch, with PDLSCs showing an increasing trend of osteogenic marker expression. Further DIC analyses are in progress for assessing the reasons of the slight substrate strain inhomogeneity, in comparison to the FEA results. Finally, biological tests imposing different stretch patterns and using different cell types are ongoing, with the final aim to understand the cause-effect relationships between mechanical stretch and cellular behaviour.

## REFERENCES

- [1] T. Mammoto, "Mechanobiology and developmental control," *Annual review of cell and developmental biology*, vol. 29, pp 27-61, 2013
- [2] G. Putame, "Compact and tunable stretch bioreactor advancing tissue engineering implementation. Application to engineered cardiac constructs," *Medical Engineering and Physics*, vol. 84, pp. 1-9, 2020
- [3] T. de Jong, "Adipose-Derived-Stem-Cell-Seeded Fibrin Matrices for Periodontal Ligament Engineering: The Need for Dynamic Strain," *Journal of Biomaterials and Tissue Engineering*, vol. 7(12), pp 1303-1312, 2017

# Integrated Strategies for the Design of Core-Shell Structures as Advanced Barrier Models

Nicole Guazzelli<sup>1,2</sup>, Ludovica Cacopardo<sup>2</sup>, Antony Ieva<sup>3</sup>, Alessandro Corti<sup>3</sup> and Arti Ahluwalia<sup>1,2</sup>

<sup>1</sup>Department of Information Engineering, University of Pisa, Italy

<sup>2</sup>Research Centre 'E. Piaggio', Pisa, Italy

<sup>3</sup>Department of Translational research and new technologies in medicine and surgery, Pisa, Italy

**Abstract**—Despite recent advances in in-vitro technologies, to date a reproducible and controllable method for the fabrication of 3D dynamic biological barriers which respect the curvature of physiological systems is lacking. Here we present a new integrated in-silico/in-vitro strategy for fabricating 3D core-shell structures, which can be embedded in magneto-responsive agarose hydrogels able to mimic dynamic contraction of tissues.

**Keywords**— in-vitro/in-silico approach, human barrier models, core-shell beads, magneto-responsive hydrogels.

## I. INTRODUCTION

The 3D architecture of the physiological environment profoundly influences cell behaviour. To date, in-vitro models of biological barriers do not couple the typical 3D curvature of many tissues with the dynamic conditions found in vivo [1,2]. Self-assembled spheroids and organoids are now emerging as powerful tools to replicate 3D structures. However, the spontaneous formation of an internal lumen is difficult to standardise and can be time-consuming. Here, we present an in-vitro/in-silico strategy (Fig. 1) to obtain cell-laden core-shell structures with predictable and controlled geometry, which can be encapsulated in magneto-responsive hydrogels for mimicking physiological deformations.

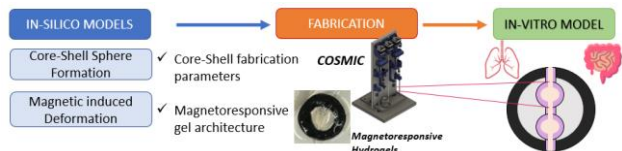


Figure 1: Workflow for generating in-silico/in-vitro models of biological barriers.

## II. METHOD

Controlled formation of core-shell alginate drops was obtained using a Core-Shell Microbead Creator (COSMIC) equipped with a commercial coaxial needle (16-26 G). The drops were crosslinked in CaCl<sub>2</sub>. Biphasic magneto-responsive (MR) gels (Fig. 2D) were obtained by casting a solution of 1% w/v agarose (A9539, Sigma Aldrich), 0.1% w/v Pluronic-127 (Creative PEGWorks), and 5% - 10% - 15% w/v iron (II,III) oxide nanoparticles (637106, Sigma Aldrich) for the active domain, and 0.5% w/v agarose solution for the passive domain in custom moulds. The core-shell spheroids were embedded in the passive domain of the MR hydrogels. Preliminary tests with permanent magnets were performed to analyse the MR gels deformation.

In-silico models were implemented in Comsol Multiphysics and Matlab. Considering the equilibrium between inertial, viscous, and surface tension forces and the hindered Ca<sup>2+</sup> ion transport through porous media, the core-shell sphere geometry was predicted as a function of the extruded material and of the crosslinking time [3]. Then the deformation of MR hydrogels was estimated as a function of the magnet distance and the magnetic field amplitude.

Preliminary tests were performed encapsulating Caco-2 (1.5 million/mL) cells in the shell, which was composed of 20

mg/mL alginate (A0682, Sigma Aldrich) and rat tail collagen (1 mg/mL, A10483-01, Gibco). The core was made of 10 mg/mL Pluronic-127. A 0.1 M calcium chloride (CaCl<sub>2</sub>) solution was placed under the needle to allow alginate crosslinking. Cell viability and permeability tests were performed using the Alamar Blue assay.

## III. RESULTS

The in-silico model of core-shell sphere formation highlighted that the best results in terms of shell thickness were obtained with a core extrusion speed of 10 μL/s, shell extrusion speed 20 μL/s, and crosslinking time 10 min (Fig. 2C). The predicted shell thickness (Fig. 2A) was also confirmed by the experimental results.

The magnetic deformation model provided the optimal composition of the cylindrical biphasic MR agarose hydrogels to obtain physiological deformations of both domains: a) active domain: 1% w/v agarose, 1% w/v pluronic-127, 15% w/v iron NPs; b) passive domain: 0.5% agarose. The optimal active domain thickness was also identified as 3 mm. Moreover, the experimental tests with permanent magnets confirmed the MR gel deformation range predicted by the model (Fig. 2B).

Cell tests show that the encapsulation procedure is cytocompatible (Fig 2E).

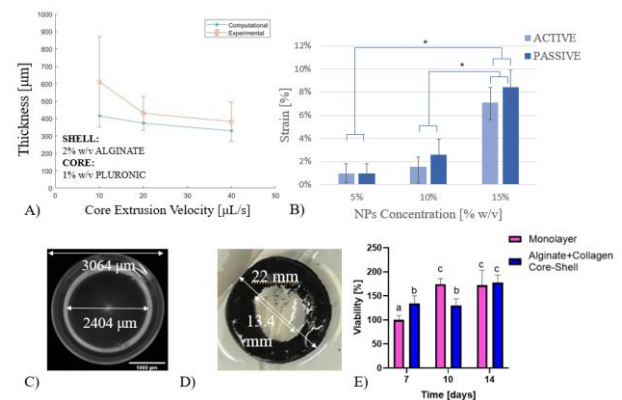


Figure 2: A) Predicted shell thickness compared to experimental measurements; B) MR 1% w/v agarose gels experimental deformation ( $p < 0.05$ ); C) 10s20 core-shell bead - 1.25X; D) MR gels; E) Caco-2 Cell viability (different letters indicate significant differences,  $p < 0.05$ ).

## IV. CONCLUSION

This in-vitro/in-silico approach represents a promising strategy for the fabrication of core-shell spheroids with defined geometry. In particular, the in-silico tools can be used to predict the effects of different core-shell material combinations, reducing experimental time and costs. Further investigations are currently ongoing to improve the model's physiological relevance.

## REFERENCES

- [1] S. Callens et al., *Biomater.* 119739, 2020
- [2] N. Arumugasaamy et al., *Ann. Biomed. Eng.* 1–21, 2019
- [3] A. Hajikhani et al., *J. Mech. Phys. Solids* 104476, 2021

# Impedance-based microfluidic device for erythrocyte deformability analysis

R. Reale<sup>1,§</sup>, A. De Ninno<sup>2,§</sup>, P. Bisegna<sup>3</sup>, and F. Caselli<sup>3,\*</sup>

<sup>1</sup> Center for Life Nano Science@Sapienza, Italian Institute of Technology (IIT), Rome, Italy

<sup>2</sup> Institute for Photonics and Nanotechnology, Italian National Research Council, Rome, Italy

<sup>3</sup> Department of Civil Engineering and Computer Science, University of Rome Tor Vergata, Rome, Italy  
(§ equal contribution, \* corresponding author)

**Abstract**—We present an original microfluidic device for contactless and optics-free erythrocyte deformability analysis. The system comprises a hyperbolic channel with integrated microelectrodes in a cross-shaped configuration. Deformation of red blood cells (RBCs) under extensional flow is achieved, and the deformed cell shape is quantified by an electrical anisotropy index, at a throughput of 300 cell/s. Due to its simplicity and potential for integration, the proposed approach holds promises for fast and low-cost erythrocyte deformability assays.

**Keywords**—Hyperbolic microchannel, Microfluidic impedance cytometry, Cell shape, Erythrocyte deformability

## I. INTRODUCTION

THE biophysical properties of cells have emerged as useful label-free biomarkers. For example, quantitative measurements of RBC deformability are crucial to understanding and diagnosing RBC-related diseases, such as various forms of hereditary anaemia, diabetes, and malaria infection. This raises the need for accurate, robust, and sensitive methods for cell mechanical characterization. Here, we present an original microfluidic platform combining extensional-flow deformability cytometry [1] with impedance cytometry [2].

## II. EXPERIMENTAL

The microfluidic chip consists of a glass microscope slide with integrated gold microelectrodes, bonded to a PDMS-embedded microchannel (Figure 1(a)). The microchannel has a hyperbolic profile and hence generates an extensional flow which induces cell elongation in the flow direction (total Hencky strain  $\epsilon_H \cong 3$ ). The electrodes are arranged in a cross-shaped configuration [3]. This configuration allows to acquire two current signals,  $I_F$  and  $I_T$ , respectively, probing cell electrical impedance along two orthogonal directions, namely the flow direction (“F” subscript) and the transverse-to-flow direction (“T” subscript). An impedance spectroscopy (HF2IS, Zurich Instruments) is used to acquire these electrical current signals. For validation purposes, the sample flow through the detection area is simultaneously acquired using a high-speed camera (frame rate 12500 fps, shutter time 3.9  $\mu$ s) connected to an inverted microscope.

## III. RESULTS

When a spherical cell (i.e., with an isotropic shape) is in the centre of the cross, the two signals  $I_F$  and  $I_T$  are identical by symmetry. On the contrary, they differ in the case of a cell with an anisotropic shape (Figure 1(b)). Therefore, an anisotropy

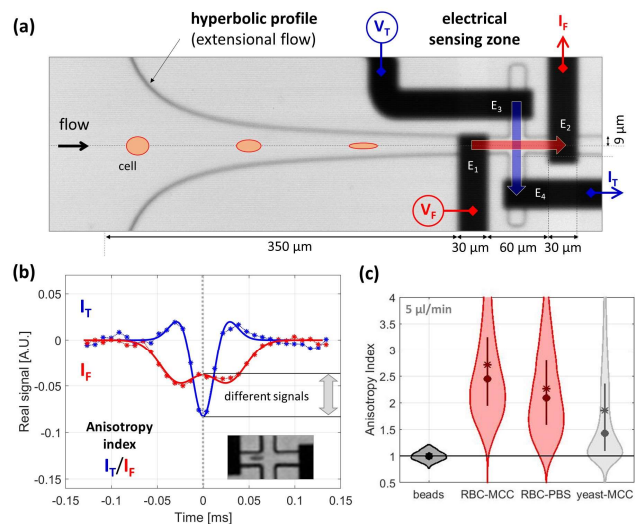


Figure 1: a) Microscopy image of the hyperbolic microchannel with the integrated electrical sensing zone composed by four coplanar electrodes ( $E_1$ – $E_4$ ) in cross configuration. AC voltages  $V_F$  and  $V_T$  are applied to  $E_1$  and to  $E_3$ , respectively. b) Example of the recorded electrical current signals  $I_F$  and  $I_T$  along with a snapshot of the flowing RBC. c) Violin plots of the anisotropy index obtained for polystyrene beads, RBCs in MCC, RBCs in PBS and yeasts in MCC.

index  $AI$  can be defined as  $AI = I_T(t_c)/I_F(t_c)$ , where  $t_c$  denotes the time instant when the cell is in the centre of the cross. As shown in Figure 1(c), at a flow rate of 5  $\mu$ l/min, the median anisotropy index of healthy RBCs in a viscous buffer containing methylcellulose (MCC) is 2.5, which translates the elongated cell shape under extensional stress. By comparison, median  $AI$  values of 2, 1.5, and 1 are measured for RBCs in a less viscous buffer (phosphate buffered saline, PBS), yeast cells in MCC (due to their rigid cell wall), and polystyrene beads, respectively.

## ACKNOWLEDGEMENT

This work was supported by Regione Lazio under grant E85F21002390002 (MicroSystemQ, “Research Groups 2020 Programme”).

## REFERENCES

- [1] T. Yaginuma *et al.*, “Human red blood cell behavior under homogeneous extensional flow in a hyperbolic-shaped microchannel,” *Biomicrofluidics*, vol. 7(5), 2013.
- [2] A. Salahi *et al.*, “Modified Red Blood Cells as Multimodal Standards for Benchmarking Single-Cell Cytometry and Separation Based on Electrical Physiology,” *Anal. Chem.*, vol. 94(6), 2022.
- [3] M. Shaker *et al.*, “An impedance-based flow micro-cytometer for single cell morphology discrimination,” *Lab Chip*, vol. 14(14), 2014.

# A Novel Method for Characterizing Retinal Biomechanics

B. Belgio<sup>1</sup>, F. Berti<sup>1</sup>, F. Potere<sup>1</sup>, S. Mantero<sup>1</sup> and F. Boschetti<sup>1</sup>

<sup>1</sup> Dept. of Chemistry, Materials, and Chemical Engineering “Giulio Natta”, Politecnico di Milano, Italy

**Abstract**—In this study, we present a novel technique to evaluate retina mechanical response to multiaxial loadings, which are more representative of the *in vivo* condition. To this end, we first designed and fabricated a new easy setup. Then we carried out biomechanical measurements associated with numerical simulations to identify tissue mechanical parameters.

**Keywords**—Retina biomechanics, Ophthalmology.

## I. INTRODUCTION

Mechanical factors are believed to play a key role in the pathogenesis of retinal diseases [1]. Hence, understanding retinal biomechanics is crucial to build suitable *in vitro/in silico* models and to develop new therapies. Currently, the knowledge of retina mechanical properties is still limited and mainly based on uniaxial tensile tests. Despite its extensive use, this test does not replicate retina *in vivo* conditions.

Multiaxial tests seem more representative of the *in vivo* loadings. Here, we present a novel method to assess retina response to multiaxial stresses. We developed an innovative setup to measure the load-displacement response and we investigated tissue elastic properties by using numerical simulations.

## II. MATERIALS AND METHODS

Pig eyes (n=10) were obtained from a local abattoir within 1-hour postmortem. After careful detachment from the posterior wall of the eye, retinal specimens were clamped between two 3D printed discs mounted on an electromechanical testing machine (Bose EnduraTEC ELF 3200) (Figure 1a). The discs had a circular hole of 5 mm in diameter at their center. A hemispherical stainless-steel head punch was pushed through the sample at a displacement rate of 0.1 mm/s (Figure 1b).

Numerical simulations were performed in Abaqus/Standard 2020 mimicking the experimental setup. A linear elastic material ( $E=220$  GPa,  $\nu=0.3$ ) was assigned to the punch, while elastic-plastic properties were assumed for the retina. To identify the actual values, retinal elastic ( $E$ ) and plastic ( $\sigma_y$ ) parameters were varied starting from our previous results of uniaxial tensile tests [3]. The thickness of retina samples was determined using optical coherence tomography (DRI OCT Triton Plus, Topcon) to account for variability in the model geometrical features.

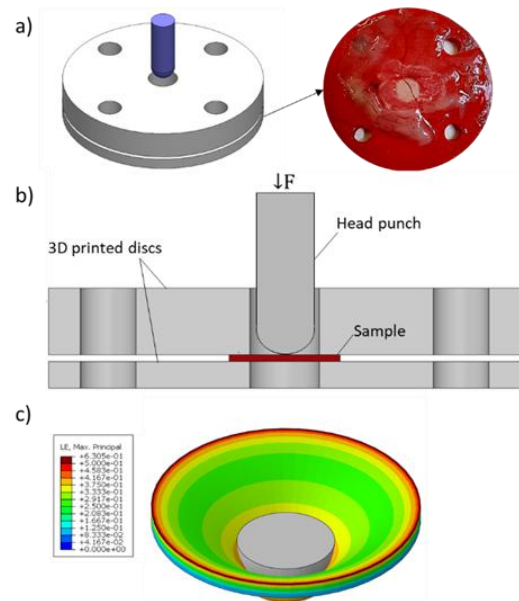


**Figure 1:** a) Top view of the two discs and picture of a sample placed on the lower disc; b) Scheme of the setup developed for multiaxial tests; c) Contour plot of max principal strain in the numerical simulations of retina sample.

## III. RESULTS AND CONCLUSION

The average retina thickness was  $0.35 \text{ mm} \pm 0.04 \text{ mm}$ .

The load-displacement experimental curve shows an initial lower load area followed by a region of increased mechanical response to the applied stresses. The computational data well fit the average experimental behavior with  $E=7$  kPa and  $\sigma_y=1.7$  kPa (Figure 1c).

We developed a novel simple experimental technique for identifying retina biomechanical properties when subjected to multiaxial stresses as *in vivo*. The association of this method with numerical simulations allows the determination of retina elastic modulus and plastic properties. This value could be set as a reference property which scaffolds, meant for retina tissue engineering, and *in vitro/in silico* models must approximate in order to well reproduce retinal tissue.

## ACKNOWLEDGEMENT

We thank Dr. Fumagalli and his Fumagalli Industria Alimentari located in Como for kindly providing the pigs eyes.

## REFERENCES

- [1] I. C. Campbell, “Biomechanics of the posterior eye: A critical role in health and disease”, in *J. Biomech. Eng.*, vol.136 no..2, 2014.
- [2] B. Belgio, “Towards an *in vitro* retinal model to study and develop new therapies for age-related macular degeneration”, in *Bioengineering*, vol. 8 no. 2, 2021.

# Patient-Specific Stomach Models to Mimic Endoscopic Sleeve Gastroplasty

A. Berardo<sup>1,2,3</sup>, I. Toniolo<sup>3,4</sup>, P. Pirini<sup>5</sup>, E. L. Carniel<sup>3,4</sup>

<sup>1</sup> Department of Civil, Environmental and Architectural Engineering, University of Padova, Italy

<sup>2</sup> Department of Biomedical Sciences, University of Padova

<sup>3</sup> Centre for Mechanics of Biological Materials, University of Padova, Italy

<sup>4</sup> Department of Industrial Engineering, University of Padova, Italy

<sup>5</sup> Department of Information Engineering, University of Padova, Italy

**Abstract**— Bariatric surgery is the most effective treatment for severe obesity. Endoscopic procedures are spreading, one above all the Endoscopic Sleeve Gastroplasty (ESG), well tolerated, safe and effective. However, revision or reversal can occur, index of a non-optimal intervention design, that could be achieved by coupling bioengineering and medical competences. Computational tools and patient-specific approach can help medical staff in improving bariatric procedures applicability and reliability, and in individualizing the optimal post-surgical stomach configuration, without an invasive approach.

**Keywords**—Obesity, ESG, finite elements, bariatric surgery.

## I. INTRODUCTION

THE growing burden of obesity as a chronic disease necessitates a multifaceted approach. There has been an increase in the number of available endoscopic therapies for weight management with ESG proving to be one of the best options. It consists in reducing the effective volume of the stomach using lines of full-thickness sutures. ESG appears to be well tolerated, safe and effective [1], however, some patients required revision or reversal during the first year [2]. Computational modelling and the *in-silico* medicine can introduce an innovative point of view, by simulating, modifying and thus improving the surgical procedures. In this work, a patient-specific approach was adopted to predict ESG procedure on patient-specific models of bariatric patients.

## II. METHODS

Starting from pre-surgical stomach models of patients with severe obesity developed in [3], ESG was simulated by introducing 3-points wires features along the corpus region, which connected the anterior and posterior walls with the great curvature, in order to mimic full-thickness sutures (Fig. 1). The constitutive formulation adopted for gastric tissues was an anisotropic hyperelastic model with two families of fibers, (details in [3]). Then the stomach behavior was analyzed when subjected to an increase of intragastric pressure.

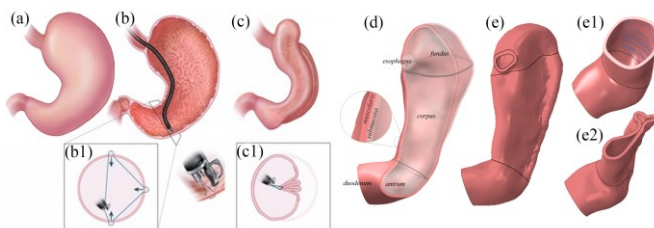


Figure 1: ESG procedure by [4] from pre-surgical (a) to ESG stomach (c). ESG probe (b) selects 3 points (b1); transversal view of the closed sutures (c1). (d) 3D-stomach model. (e) simulated ESG. (e1) wire features and closure (e2).

## III. RESULTS

In Fig. 2 the pressure-volume behaviour of the pre- and post-surgical configurations is reported. Elongation strains were computed and compared, as well. By reducing the stomach volume with ESG, the intragastric pressure increases more rapidly, while stomach average strain decreases. However, ESG appears to be less invasive than LSG, since does not require a removal of a part of the stomach, thus allowing a greater elongation of the gastric wall, which positive reflexes on the gastric mechanoreceptors and satiety.

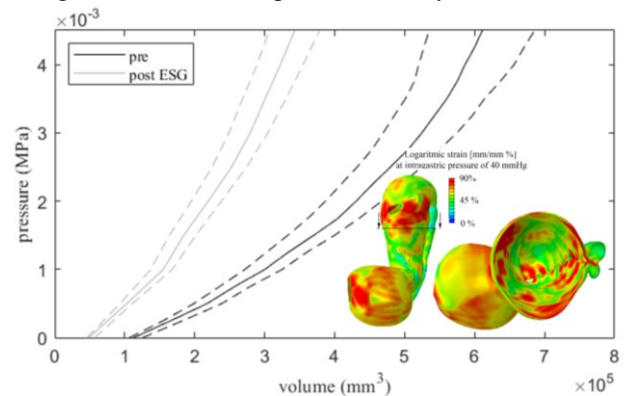


Figure 2: pressure-volume curves of pre-surgical configurations (black curve with first and third quartile in dashed lines) and simulated ESG (grey lines).

## IV. CONCLUSION

The methods of bioengineering can provide *a priori* data that will contribute to the choice of the optimal surgical procedure, tailored on patient's medical needs.

## ACKNOWLEDGEMENTS

Project N° FISR2019\_03221, titled CECOMES: CEntro di studi sperimentali e COMputazionali per la ModelliStica applicata alla chirurgia.

## REFERENCES

- [1] R. Sharaiha, *Five-year outcomes of endoscopic sleeve gastroplasty for the treatment of obesity*, Clinical Gastroenterology and Hepatology 2020, <https://doi.org/10.1016/j.cgh.2020.09.05>
- [2] A. Alqahtani, *Short-term outcomes of endoscopic sleeve gastroplasty in 1000 consecutive patients*, Gastrointestinal Endoscopy 2019, <https://doi.org/10.1016/j.gie.2018.12.012>.
- [3] I. Toniolo, *Patient-specific stomach biomechanics before and after laparoscopic sleeve gastrectomy*. Surgical Endoscopy 2022, <https://doi.org/10.1007/s00464-022-09233-7>.
- [4] G. Lopez-Nava, *Endoscopic Sleeve Gastroplasty for Obesity: a Multicenter Study of 248 Patients with 24 Months Follow-Up*, OBES SURG 2017, [10.1007/s11695-017-2693-7](https://doi.org/10.1007/s11695-017-2693-7).

# Mechanical characterization of pancreatic suture threads and pancreatic tissue

F. De Gaetano<sup>1</sup>, M. Pagnanelli<sup>2,3</sup>, R. Ponce<sup>1</sup>, M. Panico<sup>1</sup>, G. Capretti<sup>2,3</sup>, G. Nappo<sup>2</sup>, A. Zerbi<sup>2,3</sup>, ML Costantino<sup>1</sup>

<sup>1</sup> Politecnico di Milano, Milan (ITALY);

<sup>2</sup> IRCCS Humanitas – Pancreatic Surgery, Milan (ITALY)

<sup>3</sup> Hunimed, Humanitas University, Milan (ITALY)

**Abstract**—Though pancreatic cancer is the fourth cause of death from cancer worldwide, there is a lack of knowledge about the mechanical properties of pancreatic tissue. Moreover, there are no surgical tools specifically developed for the pancreatic surgery but are adapted from other kind of cardiothoracic surgery. In this work, not only the mechanical properties of the physiological pancreatic tissue but also the strength of suture threads were investigated in order to find the best suture wire to use during pancreatic surgery.

**Keywords**—pancreatic surgery, soft tissue, mechanical characterization, suture threads.

## I. INTRODUCTION

Pancreatic cancer is the fourth cause of death from cancer worldwide and surgical resection, when feasible, is the only curative treatment [1]. Pancreatic fistula, that consists of the leakage of pancreatic juice into the abdomen, is a treacherous postoperative complication with a rate of 10-20%. It is strongly related to pancreatic parenchyma consistency and structure, and it is one of the most feared complications [2]. A solution to the leakage of fluids can be handled by the development of new materials, techniques, and devices for this type of surgery, designed specifically for the pancreatic environment. For that reason it is fundamental to investigate the human pancreatic parenchyma characteristics and the evaluation of the mechanical properties of the main suture threads used during the pancreaticoduodenectomy.

## II. METHODS

### A. Suture threads

For this study four different suture materials have been tested: Prolene<sup>®</sup> 4-0 (polypropylene - Ethicon), Monocryl<sup>®</sup> 4-0 (poliglecaprone 25- Ethicon), Vicryl<sup>®</sup> 4-0 (polyglactin 910 - Ethicon), and PDSII<sup>®</sup> 5-0 (polydioxanone – Ethicon). Tensile axial tests were carried out until the rupture of the samples using the MTS Synergie 200H single-axial actuation machine (MTS System Corporation, MN, USA). Six threads of each suture material were tested in addition to the baseline, in the following fluids: saline solution, bile and pancreatic juice, at several immersion time 1, 3 and 7 days. Each sample was stored in a temperature-controlled environment at 37 °C.

### B. Human pancreatic characterization

All the samples tested in this work come from human pancreas collected by the surgeons during the pancreatic resection. The sample were properly cut to obtain rectangular specimen and were tested using the UNHT<sup>3</sup> Bioindenter (Anton Paar, Graz, AU). To obtain a flat surface, samples were dip in 4% agarose. The micro indentation curve was obtained,

and the elastic modulus ( $E_{Hz}$ ) was calculated fitting the experimental curve with the Hertz model (Figure 1).

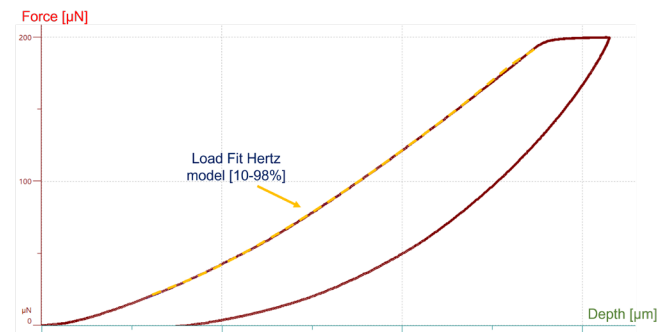


Figure 1: Characteristic test curve of a human pancreas sample in agarose.

## III. RESULTS

Maximum stress and elastic modulus at small deformation ( $\epsilon=0-0.03$ ) were obtained for all the suture threads in all the conditions. All the 4-0 threads show a reduction of the maximum stress moving from the saline solution to pancreatic juice and bile. In particular, the bile seems to be the most critical fluid for the preservation of the mechanical properties of the threads. On the other side, PDSII<sup>®</sup> 5-0 shows good stability to degradation not only in the several fluids but also at the different immersion time ( $E=20.6 \pm 1.7$  MPa), without statistically significant differences.

According to preliminary results, fresh pancreatic tissue shows small elastic modulus  $E_{Hz} = 37.6 \pm 6.8$  kPa.

## IV. DISCUSSION

Pancreas is a viscoelastic soft tissue that is complex to analysed based on the fibrous capsule surrounding it. These tests show huge difference in the mechanical proprieties of the pancreatic tissue compared the thread normally used during the surgery, even if the Monocryl<sup>®</sup> 4-0 resulted the thread with the lowest elastic modulus ( $E=5.85 \pm 0.52$  MPa) thus being close to the elastic modulus values of the pancreas. Moreover, all the threads used in the pancreatic surgery show a degradation of their mechanical properties even after only one day of immersion in biological fluids.

## REFERENCES

- [1] Siegel, R. L et al. Cancer Statistics, 2021. CA. Cancer J. Clin. 71, 7–33 (2021).
- [2] Bassi C. et al. The 2016 update of the International Study Group (ISGPS) definition and grading of postoperative pancreatic fistula: 11 Years After. Surgery 161, 584–591 (2017)

# Experimental and numerical mechanical assessment of patient-specific subperiosteal implants

I. Rota<sup>1</sup>, L. Ciriello<sup>1</sup>, G. Negrini<sup>1</sup>, M. Bonacina<sup>2</sup>, T. Villa<sup>1,3</sup>, and D. Gastaldi<sup>1</sup>

<sup>1</sup> Department of Chemistry, Materials and Chemical Engineering “Giulio Natta” - LaBS, Politecnico di Milano (Italy)

<sup>2</sup> Ars&Technology Srl, Italy

<sup>3</sup> IRCCS Istituto Ortopedico Galeazzi (Italy)

**Abstract**—Subperiosteal implants are patient-specific devices used to treat severe jawbone atrophies. To date, there are no standards to assess the mechanical reliability of custom-made devices. This work proposes a test protocol for the mechanical characterization of subperiosteal implants by applying an integrated numerical and experimental approach.

**Keywords**—Patient-specific, Numerical analysis, Experimental test protocol, Mechanical characterization.

## I. INTRODUCTION

Bone atrophy is the reduction in bone mass due to a resorption process. Severe mandibular or maxillary bone atrophies require a step of bone regeneration before the use of endosseous implants. Subperiosteal implants are an alternative to restore the physiological functions of the jaw in a single surgical session [1]. The new Additive Manufacturing (AM) technologies such as Laser Powder Bed Fusion (LPBF) allow the production of patient-specific devices characterized by complex geometries [2]. A relevant issue regarding patient-specific devices is the lack of standards in Medical Device Regulation 2017/745 to verify their mechanical reliability.

The aim of the work is the identification of a strategy – which integrates both experimental and numerical tests – to support the mechanical characterization of patient-specific implants.

## II. MATERIALS AND METHODS

An experimental setup was designed to test a patient-specific mandibular implant produced in LPBF Ti6Al4V ELI (Figure 1a). The setup is composed of a polymeric resin bone phantom, an aluminium container, spacers in LPBF-titanium to be placed over the abutments and an aluminium superior plate that transfers the load on the abutments.

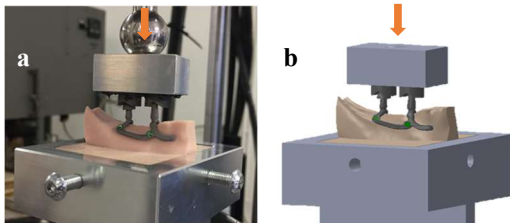


Figure 1. (a) Experimental and (b) FEM setup of mandibular implant

Mechanical characterization of the resin was performed through compression and nanoindentation tests to define the mechanical behavior at macro and micro-scale.

A static assessment of the implant structure was carried out by means of displacement-controlled compression tests

applying the load with a spherical punch.

Finite Element Model (FEM) that simulates the same loading and boundary conditions of the experimental test was created (Figure 1b). Homogeneous and isotropic material properties were set to implants ( $E=107$  GPa,  $\nu=0.34$ ,  $\sigma_y=1025$  MPa), screws ( $E=114$  GPa,  $\nu=0.33$ ), and container and plate ( $E=70$  GPa,  $\nu=0.3$ ). The material properties of the bone phantom ( $E=0.875$  GPa,  $\nu=0.35$ ,  $\sigma_y=12.5$  MPa) were assigned based on the results of the resin mechanical characterization.

## III. RESULTS AND CONCLUSION

Figure 2a shows the Force – Displacement curves obtained from experimental and finite element analysis of the implant.

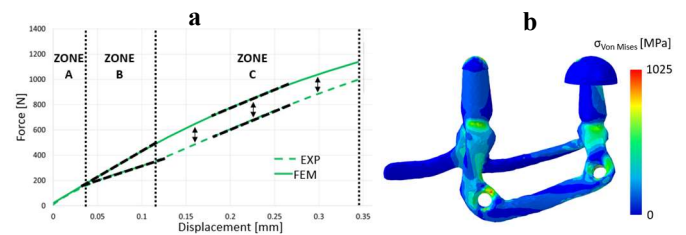


Figure 2. (a) Experimental and FEM Force - Displacement curves (b) Von Mises stress color map of the implant

FEM curve shows a good accuracy in reproducing the experimental results in zones A and C with differences in stiffnesses of 5% and 3%, respectively. Zone B has a difference in stiffnesses of 64% which results in an overestimation of the force. This could be attributed to the initial sliding in the experiment, whereas it is not detect by FEM. Von Mises stress distribution (Figure 2b) proves that the implant has no yielded zones adding significant information to assure the safety of the implant.

The designed setup guarantees to test the device using cost efficient and reusable components easy to assemble. The replicability of the experimental setup allows its use to test patient-specific subperiosteal implants with an effective test protocol. The numerical model effectively reproduces the stiffness of the experimental test in most of the Force – Displacement curve with overall acceptable results.

In conclusion, the integrated experimental and numerical approach of this work is a first step in the investigation of strategies to support the mechanical characterization of patient-specific devices.

## REFERENCES

- [1] C. Mangano et al, 3D Printing in Medicine, 6.1:1-14, 2020.
- [2] M. Cerea et al, BioMed research international, 2018.

# Statistical shape modelling of the femoral canal for the design of osseointegrated prostheses for amputees

V. Betti<sup>1</sup>, M.L. Ruspi<sup>1</sup>, G. Galteri<sup>1</sup>, E.F.A. Ognisanto<sup>1</sup>, and L. Cristofolini<sup>1</sup>  
<sup>1</sup> Department of Industrial Engineering, University of Bologna, Italy

**Abstract**—The aim of this work was to parametrize this variability in the femoral canal. 72 canals were segmented and used to simulate 16 level of osteotomy. Main modes of variation were computed and several parameters were calculated. Results showed that the relevance of these parameters depend on the level of osteotomy considered.

**Keywords**—Statistical shape modelling, femoral canal.

## I. INTRODUCTION

The anatomy of the femur shows a high inter-patient variability, making it challenging to design standard prosthetic devices that perfectly adapt to the geometry of each individual [1]. Over the past decade, Statistical Shape Models (SSMs) have been largely used as a tool to represent an average shape of many three-dimensional objects, as well as their variation in shape [2]. However, no studies of the morphology of the residual femoral canal in patients who have undergone an amputation have been performed.

The aim of this study was therefore to evaluate the main modes of variation in the shape of the canal, therefore simulating and analysing different levels of osteotomy.

## II. MATERIALS AND METHODS

In order to assess the variability of the femoral canal, 72 CT-scans of the lower limb were selected. A segmentation was performed to isolate the region of interest (ROI), ranging from the lesser tip of the trochanter to the 75% of the total length of the femur. The canals were then sized to scale, aligned, and 16 levels of excision were simulated, starting from a section corresponding to 25% of the ROI and up to the distal section. For each level, the main modes of variations of the femoral canal were identified through Principal Component Analysis (PCA), extrapolating Principal Components (PCs) and so defining the variability model [3]. After obtaining the average shape  $\bar{M}$ , the extreme geometries  $M_{i,\pm 2\sigma}$ , associated to these modes were computed as:

$$M_{i,\pm 2\sigma} = \bar{M} \pm \varphi_i \cdot 2\sqrt{\lambda_i} \quad (1)$$

Where  $\varphi_i$  are the eigenvectors representing the PCs, and  $\lambda_i$  are the eigenvalues associated to them, providing the respective variance. The shape of the canal for  $M_{i,\pm 2\sigma}$  was reconstructed every 10 mm and best fitted with an ellipse (Fig.1). The following parameters were then calculated: i) *radius of curvature (ROC)*, by reconstructing the arc of circumference passing through the centroids of the canal; ii) *ellipticity*, as the ratio between the major and the minor axis of the ellipse; iii) *conicity*, obtained as the square root of the ratio between the area in the distal segment and the minimum area; and iv) *diameter*, calculated as the square root of the average area. In order to identify which are the main deformations explained by the main modes, these parameters were compared, for each level of osteotomy, between the two extreme geometries of the main modes of variation, calculating their difference divided by the average of their values [ $\text{var}\%$ ].

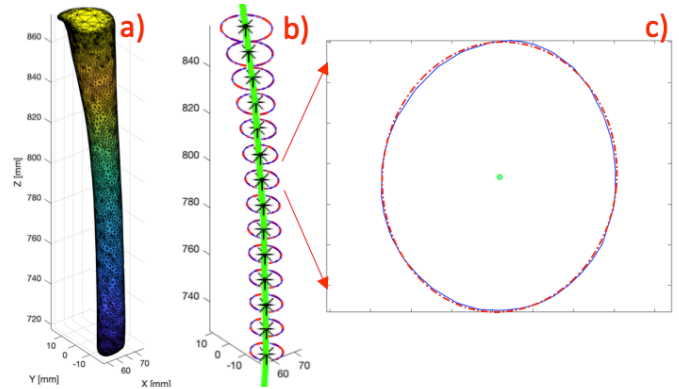


Fig. 1: The procedure to obtain the parameters. a) Geometry of the canal for a level of excision; b) Reconstruction of the shape each 10 mm, with the *radius of curvature* in green; c) Enlarged view of a slice: the real shape of the canal (blue) and the best-fitting with an ellipse (red).

## III. RESULTS

Results from PCA analysis pointed out that the first three PCs explained more than the 87% of the total variance, for each level of simulated osteotomy. By analysing  $M_{i,2\sigma}$  and  $M_{i,-2\sigma}$  for a distal osteotomy (e.g. 80% of the length of the canal), the first PC was associated to a combination of ROC ( $\text{var}\% = 41\%$ ), conicity ( $\text{var}\% = 28\%$ ) and ellipticity ( $\text{var}\% = 7\%$ ). PC<sub>2</sub> was still associated with the ROC ( $\text{var}\% = 16\%$ ), while PC<sub>3</sub> turned out to be associated with the diameter ( $\text{var}\% = 38\%$ ).

## IV. DISCUSSION

Through the SSM presented in this study, a quantitatively evaluation of the deformation of the intramedullary canal has been made possible. By analysing the extreme geometries obtained from the first three modes of variance, it is clear that the first three PCs accounted for the variations in terms of curvature, conicity, ellipticity and diameter of the femoral canal with a different weight, depending on the level of osteotomy. Through this work, it was also possible to parametrize these variations according to the level of excision. The results given for the segment corresponding to the 80% of the length of the canal showed that, at that specified level, the ROC, conicity and ellipticity were the anatomical parameters with the highest range of variability, followed by the variation in terms of diameter. Therefore, the analysis carried out can provide information about the relevance of these parameters depending on the level of osteotomy suffered by the amputee. In this way, optimal strategies for the design and/or customization of osteo-integrated stems can be offered depending on the patient's residual limb.

## REFERENCES

- [1] Christensen et al. In *Forensic Anthropology*, 2014, pp.301-319.
- [2] Ambellan et al, In *Adv Exp Med Biol*, 2019, pp.67-84.
- [3] Pascoletti et al. In *Applied Science*, 2021, 11(11).

# 3D-Mapping of the mechanical properties of the bone tissue via atomic force microscopy

A. Gambardella<sup>1</sup>, M. Bontempi<sup>1</sup>, F. Salamanna<sup>1</sup>, M. Maglio<sup>1</sup>, R. Capozza<sup>2</sup>, A. Visani<sup>1</sup> and M. Fini<sup>1</sup>

<sup>1</sup>C. S. Surgical Science and Technology, IRCCS Rizzoli Orthopaedic Institute, Via di Barbiano 1/10-40136 Bologna, Italy

<sup>2</sup>Institute for Infrastructure and Environment, The University of Edinburgh, Thomas Bayes Road, Edinburgh, EH9 3JL, United Kingdom

**Abstract**— Three-dimensional maps of mechanical properties obtained by atomic force microscopy represent an elegant and exhaustive tool for non-destructive and high spatial resolution analyses of the bone tissue. Here we present some strategies to map the Young's modulus of bone through analysis of the Force-distance curves on samples characterized by strong structural and compositional heterogeneity and provide some examples of application of such methods. In particular, we discuss the experimental setup and the theoretical models suitable to estimate elastic and elastic-plastic deformations for moduli ranging from tens of GPa to a few kPa.

**Keywords**—elastic modulus, bone, atomic force microscopy, 3D mapping.

## I. INTRODUCTION

MAPPING a given chemical, physical or mechanical property of a material via Atomic Force Microscopy (AFM) relies on the combination of high spatial resolution of the AFM measurement (lower to a few nm's) and extreme sensitivity of the instrument's probe in detecting small force variations during its interaction with the surface [1].

Small-scale mechanical characterization of bone tissue is critical in regenerative or degenerative phenomena, as structural or compositional changes often take place at submicrometric distances, thus beyond the reach of traditional nanoindentation experiments. Despite this, AFM-based nanoindentation is not a routine due to a lot of experimental and theoretical issues: 1) high overall complexity and cost of the experimental setup; 2) difficulty in applying the biomechanical models available to intrinsic heterogeneity of bone and 3) possible bias due to the presence of implanted material. The present work shows that when traditional AFM measurement (even with small radius of curvature tips, relatively soft cantilevers, standard environmental conditions) are combined with a solid validation of the experimental protocol, it is possible to obtain 3D mapping of the mechanical properties of bone in a reproducible and reliable fashion. This allows to accurately monitor the gradual change in tissue's mechanical properties due to structural and/or compositional changes, possibly induced by altered state or the presence of implants, biomaterials, etc.

## II. MATERIALS AND METHODS

### A. Experimental setup

Histological sections of bone tissue (thickness  $\sim 100 \mu\text{m}$ ), previously embedded in methacrylate, were characterized both topographically and by acquisition of force-distance (F-d) curves on scales varying between  $100 \mu\text{m}^2$  and  $1 \mu\text{m}^2$ , with

resolution up to  $512 \times 512$  pixels. A stand-alone AFM (NT-MDT, Moscow, Russia) was used in contact mode of operation using tips with a radius of curvature of  $R \sim 10 \text{ nm}$ , mounted on cantilevers with spring constant  $6 < k < 30 \text{ N/m}$ . A Python routine was implemented for processing the experimental curves. Surface deformations were assimilated to a Hertzian-like model for purely elastic deformations, while the Oliver-Pharr model was used for elastic-plastic deformations [2].

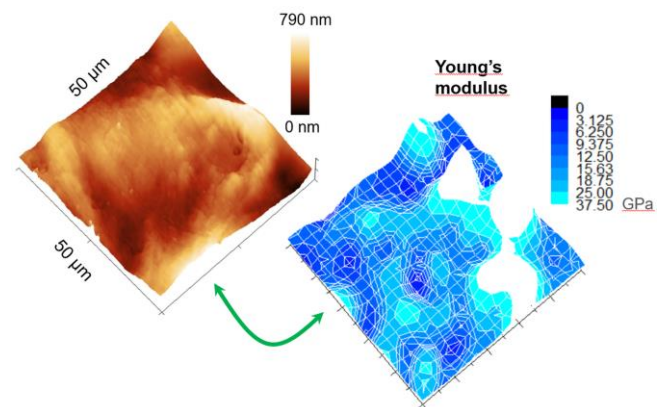


Figure 1-(Left)  $50 \times 50 \mu\text{m}^2$  AFM image of cortical bone and (right) space distribution of the corresponding Elastic modulus (Oliver-Pharr method).

## III. RESULTS

The combination of 3D topographic mapping/surface elasticity modulus made it possible to correlate surface topographic information ( $R_A$  or  $R_s$  roughness, possible spatial anisotropy, etc.) with local variations of the elastic modulus (E), which can be accompanied by a measure of the viscoelasticity of the surface, expressed in terms of adhesion strength ( $F_{Adh}$ ) or its Hardness (H), thus allowing fine characterization of gradients of these properties between different bone regions. The obtained values of E, typically ranging from 2 to 25 GPa are in good agreement with previous findings [3]. The comparison between 3D maps taken on the same region also allows to discriminate between elastic and/or elastic-plastic deformation of the tissue which can be, in principle, associated to a structural and/or compositional origin. Thus, AFM-based nanoindentation, along with the experimental protocol developed in this work, is capable to describe, by means of a fast and relatively inexpensive measurement, the gradients of the mechanical properties of bone tissue, possibly in relation to its topography. The AFM measurement represents, for bone, a natural complement to

traditional histology and histomorphometry measurements; indeed, these latter can help in qualitative identification of the various surface components, which might be highlighted only after appropriate histological stainings.

#### ACKNOWLEDGEMENT

We acknowledge the Italian Ministry of Health 5x1000 2018 (redditi 2017) “Ottimizzazione di innesti massivi in chirurgia vertebrale e nella chirurgia di ricostruzione articolare” project for the financial support.

#### REFERENCES

- [1] O. H. Olubowale et al., “May the Force Be with You! Force–Volume Mapping with Atomic Force Microscopy” in *ACS Omega*, 6, pp. 25860–25875.
- [2] S. V. Kontomaris et al., “A novel approximate method to calculate the force applied on an elastic half space by a rigid sphere” in *European Journal of Physics*, 42, pp. 025010–025026.
- [3] P. J. Turner, “Atomic force microscopy and indentation force measurement of bone” in *Nanomedicine: Nanotechnology, Biology and Medicine*, 1, pp. 624–649.

# Patient-specific Biomechanical Assessment of Carotid Plaque Vulnerability

N. Curcio<sup>1</sup>, A. Rosato<sup>2</sup>, D. Mazzaccaro<sup>3</sup>, G. Matrone<sup>1</sup>, M. Conti<sup>2</sup>

<sup>1</sup>Dept. of Electrical, Computer and Biomedical Engineering, University of Pavia, Pavia, Italy

<sup>2</sup>Dept. of Civil Engineering and Architecture, University of Pavia, Pavia, Italy

<sup>3</sup>IRCCS Policlinico San Donato, San Donato Milanese, Italy

**Abstract**— The assessment of carotid plaque rupture risk is a valuable clinical information that can help preventing adverse cardiovascular events. Our aim is to develop a patient-specific workflow for quantifying the risk of rupture connected to plaque composition by means of biomechanical simulations.

**Keywords**—Vulnerable carotid plaque, patient-specific model, finite element analysis

## I. INTRODUCTION

Carotid plaque rupture is the main trigger of acute cardiovascular events and it depends on plaque composition, morphology and biomechanics [1]. Computational analyses have the potential to characterize the three-dimensional stress/strain distributions in patient-specific models of the carotid with plaque, and to estimate the risk of plaque rupture [2]. In this context, we propose a workflow based on clinical data that allows to develop a patient-specific geometric model of atherosclerotic carotid artery and to perform three-dimensional finite element analysis (3D FEA) to assess how stress distribution is related to different types of plaques.

## II. MATERIALS AND METHODS

### A. Image Acquisition and Geometric Reconstruction

Computed Tomography Angiography (CTA) images of patients undergoing endarterectomy were acquired, and the carotid lumen, together with the plaque lipid and calcific components were segmented. An ad-hoc procedure was used to generate the Computer Aided Design (CAD) model representing the vessel wall and the fibrotic plaque component. This strategy allowed to differentiate the different plaque components and to assign them different mechanical properties. Ultrasound data were also acquired to provide local pressure values from distension waveforms of common carotid artery.

### B. Setting of Computational Simulations

3D FEA was carried out using Abaqus/Standard to compute stress distributions on the plaque and wall. All materials were modelled as incompressible, isotropic, linear elastic. Local carotid blood pressure was considered as a uniform pressure load applied to the lumen surface, and it was set as the difference between systolic and diastolic local carotid pressures. Static analyses were performed.

### C. Results

In Fig. 1, we reported the workflow summarizing the steps implemented to perform the analyses. Results of 3 cases with different plaque composition (A. mostly calcific, B. mostly lipidic, C. mixed plaque) were examined. The high-stress

regions in the artery wall around plaques determine areas of possible rupture. In mostly lipidic and mixed plaques, the highest stresses are localized at the interface between the lipidic components and the lumen, in fibrous cap region, confirming that these locations could potentially be more vulnerable to rupture [3].

## III. CONCLUSION

The obtained results highlight that the mechanical properties of different plaque components, together with patient-specific pressure loads, contribute to the assessment of the carotid plaque vulnerability.

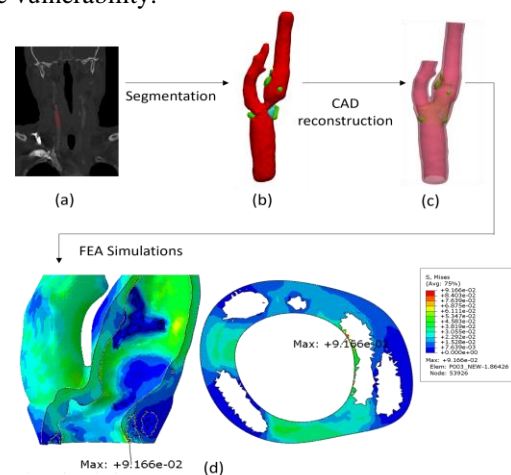


FIGURE I. Workflow implemented to obtain stress distributions on a carotid atherosclerotic wall model derived from CTA images (a). Segmentation result and CAD reconstruction are shown in (b)-(c) respectively. (b) represents the patient-specific lumen and plaque components (calcific in green, lipid in light blue). (c) represents the carotid wall and fibrotic plaque reconstruction. (d) represents von Mises stress [MPa] distributions with a possible site of rupture.

## ACKNOWLEDGEMENT

The research was funded by the Italian Ministry of Health with the financial contribution from the project of Ricerca Finalizzata 2018 (GR-2018-12366862).

## REFERENCES

- [1] Naim C, Douziech M, Therasse E, Robillard P, Giroux MF, Arsenault F, Cloutier G, Soulez G., "Vulnerable atherosclerotic carotid plaque evaluation by ultrasound, computed tomography angiography, and magnetic resonance imaging: an overview." *Can Assoc Radiol J.* 2014 Aug;65(3):275-86.
- [2] Holzapfel GA, Mulvihill JJ, Cunnane EM, Walsh MT. "Computational approaches for analyzing the mechanics of atherosclerotic plaques: a review." *J Biomech.* 2014 Mar 3;47(4):859-69.
- [3] Leach JR, Rayz VL, Soares B, Wintermark M, Mofrad MR, Saloner D. "Carotid atheroma rupture observed in vivo and FSI-predicted stress distribution based on pre-rupture imaging." *Ann Biomed Eng.* 2010 Aug;38(8):2748-65.

# Self-expandable transcatheter aortic valve mechanical performance: Impact of Nickel-Titanium super-elastic material properties

D. Carbonaro<sup>1</sup>, S. Zambon<sup>1</sup>, A. Corti<sup>2</sup>, D. Gallo<sup>1</sup>, U. Morbiducci<sup>1</sup>, A. Audenino<sup>1</sup>, C. Chiastra<sup>1</sup>

<sup>1</sup>PoliTo<sup>BIO</sup>Med Lab, Department of Mechanical and Aerospace Engineering, Politecnico di Torino, Turin, Italy

<sup>2</sup>LaBS, Department of Chemistry, Materials and Chemical Engineering “Giulio Natta”, Politecnico di Milano, Milan, Italy

**Abstract**—Material properties of Nickel-Titanium vary widely according to the chemical composition and processing of the alloy. Accordingly, the study investigated the impact of the material super-elastic characteristics on the mechanical performance of self-expanding transcatheter aortic valves.

**Keywords**— Transcatheter aortic valve implantation, Nitinol, super-elasticity, finite element analysis, sensitivity analysis

## I. INTRODUCTION

Transcatheter aortic valve (TAV) implantation has become an established alternative to open heart surgical aortic valve replacement for the treatment of severe aortic stenosis. Currently, technological advances are investigated to improve the procedural effectiveness and to extend the treatment to low-risk patients. In this regard, self-expanding TAVs, featured by a Nickel-Titanium (NiTi) frame, elastically resume their initial shape when implanted without the need for balloon inflation, by virtue of the NiTi super-elastic properties. These are strongly dependent on the chemical composition and on the metallurgical processing of the alloy. Accordingly, the range of values of the NiTi super-elastic parameters adopted in literature for the finite element (FE) simulation of self-expanding TAVs is large. In this context, this study presents a computational framework to investigate the impact of the NiTi super-elastic properties on the TAV mechanical performance.

## II. METHODS

FE models resembling the NiTi frame of two commercial TAVs were implemented (Fig.1A). A super-elastic material model [1] was considered for the TAV frames, accounting for eight parameters (Fig. 1B). FE analyses of the TAV implantation in three different idealized aortic root models (i.e., healthy, diseased I and II) [2] were conducted in Abaqus (Dassault Systemes). To evaluate the TAV mechanical performance, two FE outputs were computed, namely (1) the pullout force magnitude exerted by the frame and (2) the peak maximum principal stress within the aortic root [2]. The design of experiment method was coupled with the surrogate modelling approach to define an approximate relationship between the NiTi material parameters and the FE outputs. Thereafter, a multi-parametric sensitivity analysis was conducted by computing partial rank correlation coefficients (PRCCs) between the NiTi super-elastic parameters and the two FE outputs. In addition, a multi-objective optimization was performed in relation to the conflicting FE outputs.

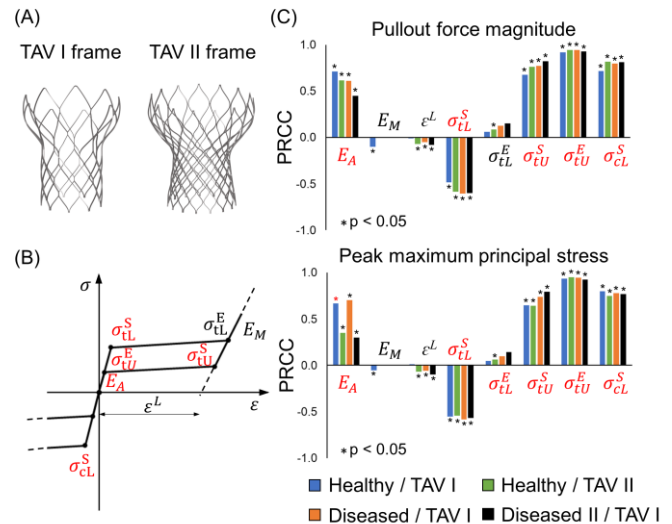


**Fig 1.** FE models of the TAV frames; (B) Uniaxial tension and compression stress vs. strain curve of NiTi, with reference to the super-elastic parameters; (C) PRCCs between the material parameters and the two FE outputs.

## III. RESULTS

Only five out of eight NiTi material parameters (Fig. 1B in red) presented statistically significant and non-negligible PRCCs with both FE outputs (Fig. 1C). Moreover, the TAV frame geometry and the anatomy of the aortic root had a marginal effect on the level of influence of each material parameter (Fig. 1C). Finally, NiTi alloys candidates with optimized characteristics in terms of TAV mechanical performance were successfully identified.

## IV. CONCLUSION

The proposed framework could support the TAV design phase, providing precious data to manufacturers on the relationship between the material characteristics of the supplied NiTi alloys and the mechanical response of the device. Moreover, this study has the potential to be extended to other NiTi cardiovascular devices and to integrate additional features, including material manufacturing data and geometrical optimization of the TAV frame.

## ACKNOWLEDGEMENT

This work has been supported by MIUR (FISR2019\_03221, CECOMES) and Piedmont Region (POR FESR PiTeF 2014-20 351-96, Nitoliera).

## REFERENCES

- [1] F. Auricchio et al., *Comput Methods Appl Mech Eng.* 143:175-94. 1997
- [2] D. Carbonaro et al., *Struct Multidiscip Optim.* 64:1825-42. 2021

# Polymers in Drug Coated Balloon Angioplasty and its Coating Morphology

D. Gunashekar<sup>1</sup>, D. Gastaldi<sup>1</sup>, G. Pennati<sup>1</sup> and P. Vena<sup>1</sup>

<sup>1</sup> Department of Chemistry, Materials and Chemical engineering, Politecnico di Milano, Milan, Italy

**Abstract**— The ideal characteristics of an angioplasty balloon is its strength, flexibility, and biocompatibility. Though these balloons have been in the market for some time, major concern prevails due to the drug loss that occurs during angioplasty. This study provides the first set of experimental data on the difference in mechanical response of the polymer at various stages of manufacturing.

**Keywords**—Angioplasty, Tensile testing, Confocal laser scanning, Pebax.

## I. INTRODUCTION

MANUFACTURING of the angioplasty balloons takes place in various stages, starting from polymer granules which is heated and extruded into a tube. These tubes are then blow moulded into angioplasty balloons with the help of heated jaws and compressed air [1]. Analysis of these polymer materials at different stages of manufacturing is important to understand the adhesion behaviour between the balloon, and the drug coating and the drug transfer pattern. Other than the properties of the polymers there are various drug related parameters like thickness of the drug coating, crystalline structure of the drug, the properties of the excipient used along with the drug that can cause a huge difference in the drug transfer [2]. Thus, adding a layer of coating can also alter the mechanical response of the Drug Coated Balloons. In this research, both the polymer films (comparable to the extruded tubes) and balloon materials are analysed for its mechanical and surface properties, with and without the coating matrix to understand the changes in properties during the manufacturing process and the drug fragmentation during release.

## II. EXPERIMENTAL METHODS

Mechanical analysis on both the films and balloon material were performed by micro-tensile and bulge testing to understand the change in properties at various stages of manufacturing. Here the materials of analysis are Polyamide composites. The experiments were performed in both dry and wet conditions trying to mimic the in vivo conditions. Considering the material to be hyper-elastic, nonlinear data fitting was performed using Finite Element Modelling (FEM). Apart from analysing the mechanical response, fibre orientation during the manufacturing process and change in coating morphologies during experiment are understood by observing it under the laser microscope during and after the testing.

## III. RESULTS AND DISCUSSION

Results from mechanical tests provided information on strength, stiffness and elastic properties of the polymer films and the balloon material. Fig 1 shows the stress-strain curves

from the preliminary ring tests (Left) and strain vs pressure response from the bulge simulation (Right) of the balloon material. With FEM it was possible to reproduce the mechanical behaviour of the balloon materials and compare it with the hyper elastic theoretical models. The morphology of the balloon and the polymer films with and without coating matrix were recorded under laser microscope as in Fig 2. The thickness of the balloon ranged between 43 $\mu$ m and 63 $\mu$ m, whereas the thickness of the polymer films ranged between 60 $\mu$ m and 120 $\mu$ m. The polymer films were opaque while the balloon material was transparent to the monochromatic laser light at 406 nm. Change in surface roughness was also observed which maybe one of the influential parameters for change in mechanical properties. This observation along with further analysis helps in understanding the fragmentation of the coating and its release pattern

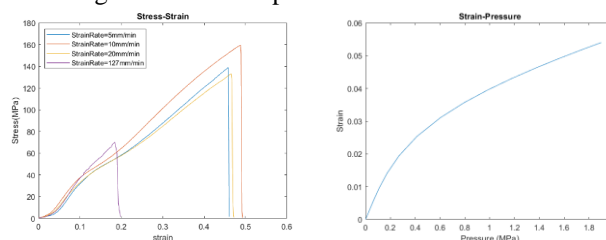


Figure 1: Circumferential stress-strain curves (Left), Pressure-Deflection analysis (Right)

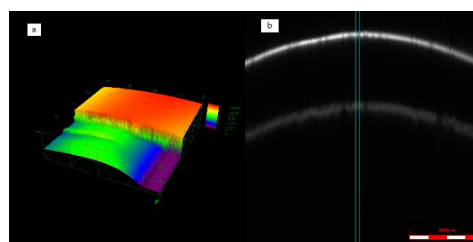


Figure 2: Surface characterization of the balloon material under confocal laser microscope

## ACKNOWLEDGEMENT

This project has received funding from the European Union's Horizon 2020 research and innovation programme under the Marie Skłodowska-Curie grant agreement No 956470.

## REFERENCES

- [1] M. A. Geith, J. D. Eckmann, D. C. Haspinger, et al "Experimental and mathematical characterization of coronary polyamide-12 balloon catheter membranes," in *Plus one*, 6th ed. vol. 12: e0234340. 2020.
- [2] M. Afari, J. Granada *Mechanisms of Action in Drug-Coated Balloons - Endovascular Today*. 2022.

# AI-based pipeline for features extraction and hemodynamic analysis from 3D PC-MRI

S. Garzia<sup>1,2</sup>, M. A. Scarpolini<sup>1,3</sup>, K. Capellini<sup>1</sup>, V. Positano<sup>1</sup>, A. Monteleone<sup>4</sup>, F. Cademartiri<sup>4</sup> and S. Celi<sup>1</sup>

<sup>1</sup> BioCardioLab, Fondazione Toscana G. Monasterio, Massa, Italy

<sup>2</sup> Department of Information Engineering, University of Pisa, Pisa, Italy

<sup>3</sup> Department of Industrial Engineering, University of Rome "Tor Vergata", Roma, Italy

<sup>4</sup> Department of Radiology, Fondazione Toscana G. Monasterio, Massa-Pisa, Italy

**Abstract**— Analysis of blood flow features is a demanding task for cardiovascular disease prevention. The extraction of these features requires the elaboration of patient-specific data that is often affected by issues due to manual segmentation and high time demanding data processing. In this scenario we develop a fully-embedded AI-based pipeline to perform automatic segmentation and to extract morphological and flow features starting from 3D phase contrast magnetic resonance data. This work shows the feasibility to obtain useful results in clinical settings reducing the computational time from hours to a few minutes.

**Keywords**— 3D U-Net, AI, hemodynamics, aorta.

## I. INTRODUCTION

THE analysis of blood flow features plays an important role in the understanding, evaluation, and prevention of cardiovascular diseases [1]. Nowadays, in-vivo hemodynamic analysis is usually performed by processing of 3D phase contrast magnetic imaging (3D PC-MRI). This procedure requires different and not trivial steps such as the segmentation to obtain 3D anatomical models as well as the extraction of significant flow features. Segmentation often requires manual or semi-automatic techniques that are time-consuming and, consequently, difficult to be insert into a clinical workflow. In this regard, methods based on deep learning algorithms turn out to be useful tools to segment 3D PC-MRI in an automatic way [2]. To date, these approaches do not include the feasibility to automatically integrating hemodynamics information with morphological features in a single tool suitable for a clinical setting.

This work aims to develop a novel AI-based pipeline that integrates the automatic segmentation of the aorta and the extraction of morphological and hemodynamic features directly from 3D PC-MRI.

## II. MATERIALS AND METHODS

The developed tool is based on three automatic steps: generation of the phase contrast magnetic resonance angiography (PC-MRA) (i), segmentation with an AI-based algorithm to obtain the 3D surfaces (ii) and hemodynamic and morphological features extraction (iii). The PC-MRA for each patient was generated, and the related manual segmentations were used to train the 3D U-Net. The neural network was developed starting from [3] and fine-tuned for our poupos and image features. A set of 50 different 3D PC-MRI datasets was used for this study. Data were acquired with a 3T MR-scanner. A total of 5 PC-MRA volumes were used as test set for

inference. Starting from the generated 3D surfaces, hemodynamic features were extracted and mapped for each phase of the cardiac cycle together with morphological information such as centerline tortuosity and length, cross sectional areas and diameters at different locations of the centerline.

## III. RESULTS

The results obtained from the trained U-Net revealed a mean accuracy of 0.80 DICE score for the segmentation of the aorta. Figure 1 depicts the developed workflow pipeline from the 3D PC-MRI to the hemodynamic (Fig.1e-f) and morphological features (Fig.1g) extraction. The velocity maps are reported for several cross sections equally spaced along the centerline (Fig.1e) and the corresponding flow rate for the inlet section is shown (Fig.1f). Our pipeline allows to extract patient-specific information in real-time (~5 min.).

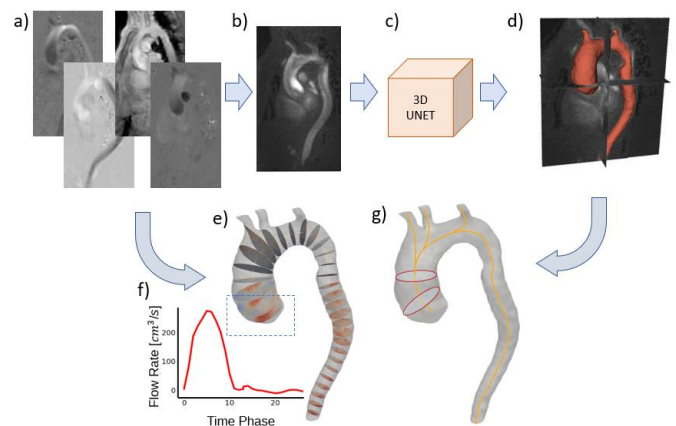


Figure 1: Workflow pipeline: 3D PC-MRI dataset (a), 3D PC-MRA (b), schematic box for the 3D U-Net (c), final segmentation (d). Processing of the segmentation and velocity data for the generation of the flow parameters (e, f) and morphological features (g).

## IV. CONCLUSION

In this work, a specific pipeline was designed to process 3D PC-MRI to obtain automatic segmentation of patient-specific aorta and the related morphological and hemodynamic features in a time compatible whit clinical practice.

## REFERENCES

- [1] P. Quinones et al, *AJH*. 31(10), 1067-1078. (2018).
- [2] H. Berhane et al, *Magn. Reson. Med*. 84(4), 2204-2218. (2020).
- [3] O. Ronneberger et al, *MICCAI*. 234-241. (2015).

# Investigating the effect of drug release on in-stent restenosis: a multiscale model

A. Corti<sup>1</sup>, A. McQueen<sup>2</sup>, F. Migliavacca<sup>1</sup>, C. Chiastra<sup>1,3</sup> and S. McGinty<sup>2</sup>

<sup>1</sup>LaBS, Department of Chemistry, Materials and Chemical Engineering “Giulio Natta”, Politecnico di Milano, Milan, Italy

<sup>2</sup>Division of Biomedical Engineering, University of Glasgow, Glasgow, UK

<sup>3</sup>PoliTo<sup>BIO</sup> Med Lab, Department of Mechanical and Aerospace Engineering, Politecnico di Torino, Turin, Italy

**Abstract**—In-stent restenosis (ISR) following drug eluting stent implantation is still a challenge of percutaneous coronary interventions. The present study proposes a novel multiscale agent-based modelling framework of ISR to investigate the mechanobiological processes underlying the arterial response to the intervention procedure.

**Keywords**—In-stent restenosis, drug-eluting stent, multiscale, agent-based model.

## I. INTRODUCTION

Percutaneous coronary intervention (PCI) with drug-eluting stent (DES) implantation is now the preferred treatment of coronary artery disease. Although the use of DES has significantly improved the treatment outcome compared to bare metal stents, in-stent restenosis (ISR) and the need for subsequent repeat revascularizations remains an unresolved issue, particularly in complex lesions.

ISR is a complex, multifactorial and multiscale vascular adaptation process which is still poorly understood. Multiscale agent-based modelling frameworks, integrating continuum- and agent-based approaches, have recently emerged as promising tools to capture the mechanobiological processes underlying ISR [1]. However, the effect of drug delivery on cellular activities has been under-investigated through these modelling tools [1]. This work proposes a novel multiscale framework of ISR following DES implantation in a coronary artery, by coupling drug transport simulations with an agent-based model (ABM) of cellular dynamics.

## II. METHODS

Figure 1 shows the multiscale framework of ISR. The framework, applied to an idealized 2D stented coronary cross-section, receives as input the artery geometry and a literature-derived post-intervention inflammatory curve, and provides as output a 1-month follow-up artery geometry, by integrating a drug transport and a tissue remodeling module.

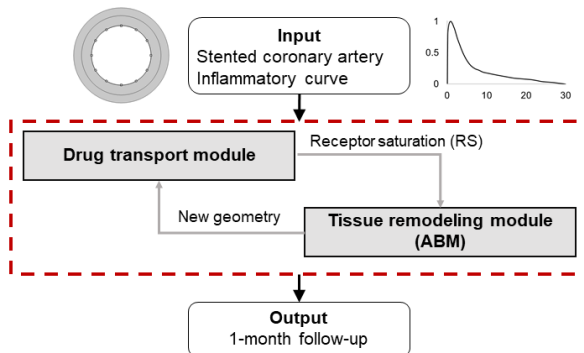


Fig 1. Multiscale framework.

Within the drug module, transient simulations of drug transport are performed in Comsol Multiphysics (Comsol, USA), by coupling Darcy’s law with advection-diffusion-reaction equations [2]. Both non-specific and specific binding sites are considered, representing those within extracellular matrix (ECM) and smooth muscle cells (SMCs), respectively. Receptor saturation (RS), namely the percentage of saturated specific receptors over time, has been strongly linked to DES efficacy. Herein, RS computed by the drug module is used to initialize the tissue remodeling module. Within this module, a 2D ABM implemented in Matlab (MathWorks, USA) replicates SMC and ECM dynamics as a function of the inflammatory curve and the RS, thus simulating the arterial response to the intervention-induced inflammation and to the drug delivered by the DES [3].

## III. RESULTS

The framework simulated a reduced level of ISR when the effect of drug was considered, compared to the case without drug, according to the expectations (Fig. 2). Moreover, different arterial responses were obtained under different combinations of drug mass and release rate.

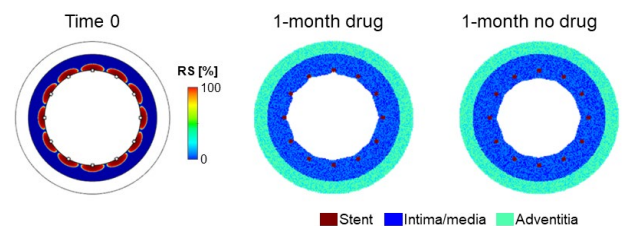


Fig 2. Results of the multiscale framework of ISR.

## IV. CONCLUSIONS

This work presents a novel multiscale framework of ISR for the investigation of the effect of drug delivery in the arterial response to PCI with DES implantation. In the future, patient-specific scenarios will be explored and the potentiality of the framework to identify optimal drug mass and release rate scenarios will be assessed.

## ACKNOWLEDGEMENT

The work has been supported by Fondazione Cariplo, Italy (Grant No. 2017-0792, TIME) and EPSRC (Grant No. EP/S030875/1)

## REFERENCES

- [1] Corti, A. et al. *Front. Bioeng. Biotechnol.* 9:744560, 2021
- [2] McQueen, A. et al. *Int. J. Pharm.* 601:120575, 2021
- [3] Corti, A. et al. *J. R. Soc. Interface* 19:20210871, 2021

# Computational modelling of cardiomyocytes contraction for regenerative medicine

S. Todros<sup>1</sup>, M. Magnussen<sup>2</sup>, D. Scaglioni<sup>2</sup>, A. Urciuolo<sup>3,4</sup>, N. Elvassore<sup>1,2</sup>, and P.G. Pavan<sup>1,4</sup>

<sup>1</sup> Department of Industrial Engineering, University of Padova, Italy

<sup>2</sup> University College London Great Ormond Street Institute of Child Health, London, United Kingdom

<sup>3</sup> Department of Molecular Medicine, University of Padova, Italy

<sup>4</sup> Fondazione Istituto di Ricerca Pediatrica Città della Speranza, Padova, Italy

**Abstract**— In order to evaluate different approaches for cardiac tissue engineering, Finite Element Method (FEM) models are developed to simulate the contractile behaviour of layers of cardiomyocytes on hydrogel scaffolds. The variability of the biomechanical properties of the cardiomyocytes are considered by means of a FEM-stochastic approach to obtain a statistical quantification of the contractile force, depending on cardiomyocytes activation and orientation within the layer. Numerical results are compared with experimental data on human embryonic stem cell-derived cardiomyocytes.

**Keywords**—Cardiomyocyte, contraction, *in silico* analysis.

## I. INTRODUCTION

CARDIAC tissue engineering strategies are based on the development of functional models of heart muscle *in vitro*. The evaluation of the feasibility of different tissue engineering platforms to support the formation of heart muscle can take advantage from *in silico* analysis, to evaluate the contractility properties of cardiomyocytes. Cardiomyocytes are composed of myofibrils bundles containing sarcomeres, consisting of thick and thin myofilaments, myosin and actin proteins. At the microscale, the exchange of calcium between cytosol and the sarcoplasmic reticulum influences the interaction of these myofilaments which onsets the shortening of the sarcomeres and drives the process of excitation-contraction of the whole cardiac cell.

## II. METHODS

FEM models are developed considering different geometries of hydrogel scaffolds, namely flat sheets [1] and microtubes, reconstructed by original data through confocal microscope imaging (Fig.1 a). Microtubes are covered by a layer of cardiomyocytes with a thickness of about 5  $\mu\text{m}$  (Fig. 1 b).

The models are obtained by using ABAQUS CAE software (SIMULIA, Dassault Systems). The geometry is discretized by using linear hexahedral finite elements with hybrid formulation to avoid numerical instabilities due to almost incompressible behaviour. The mechanical response of the hydrogel is described assuming a neo-Hookean hyperelastic constitutive model. The constitutive model of cardiomyocytes is defined by adapting a formulation previously proposed for muscle fibres, based on a phenomenological model of Hill's type [2], and it is implemented with user subroutines in FORTRAN language. Numerical analyses are carried out considering different cardiomyocyte orientation (Fig. 1 c), activation time, and maximum isometric stress, assuming different parameters with specific statistical distribution.

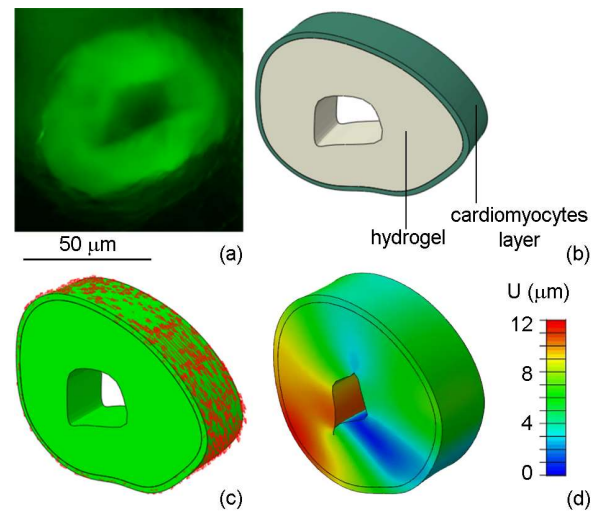


Figure 1. Confocal microscope image of a hydrogel tube covered by an external layer of cardiomyocytes (a); 3D geometric reconstruction of the structure of a tube slice and layer of cardiomyocytes (b); FEM model with red vectors representing the average orientation of cardiomyocytes within the layer (c); contour of magnitude displacement at the time instant of maximum contraction (d).

## III. RESULTS AND DISCUSSION

Typical estimated deformation of the cardiac tube during the excitation of cardiomyocytes, as obtained by FEM analyses, is shown in Fig. 1 d. The deformation at the time instant of maximum contraction depends on the maximum isometric stress, which can be assumed as a characteristic related to contractile functionality of cardiomyocytes. In order to compare numerical results with experimental data obtained in different excitation conditions of cardiomyocytes, a statistical quantification of the contractile force, depending on activation and orientation of cardiomyocytes within the layer, is achieved. The agreement between numerical analyses and experiments is evaluated by considering the deformation of the hydrogel tubes in the transversal sections.

## REFERENCES

- [1] J. Shim, A. Grosberg, J.C. Nawroth, K.K. Parker, K. Bertoldi, "Modeling of cardiac muscle thin films: pre-stretch, passive and active behavior". *J Biomech.* 2012, 15, 45, pp.832–841.
- [2] L. Marcucci, C. Reggiani, A.N. Natali, P.G. Pavan. "From single muscle fiber to whole muscle mechanics: a finite element model of a muscle bundle with fast and slow fibers." *Biomech Model Mechanobiol.* 2017, 16, pp. 1833–1843.

# Computational modelling of a milli-scale perfusion bioreactor for vascular applications

G.M. Di Gravina<sup>1</sup>, R. Pinos<sup>2</sup>, C. Scielzo<sup>2</sup>, and M. Conti<sup>3</sup>

<sup>1</sup> Department of Industrial and Information Engineering, University of Pavia, Pavia, Italy

<sup>2</sup> Division of Experimental Oncology, Malignant B cells biology and 3D modelling Unit, San Raffaele Hospital (IRCCS) Milan, Italy

<sup>3</sup> Department of Civil Engineering and Architecture, University of Pavia, Pavia, Italy

**Abstract**—Vascularization is one of the main problems on which biomedical research is working nowadays. This study proposes a computational study for a milli-scale perfusion bioreactor whose final aim is to support the regeneration of vascularized constructs.

**Keywords**— Computational simulations, perfusion bioreactor, 3D printing, vascularization

## I. INTRODUCTION

Vascularization is one of the most critical challenges of tissue engineering and it is fundamental to establish complex and long-term reliable three-dimensional (3D) models. Current technologies for biomanufacturing the vessel structure still lack standardization to enable a wider adoption of such systems, calling for further activities dealing with the deeper characterization of different physiological or pathophysiological conditions [1]. To fill this gap, a novel 3D printed modular and versatile perfusion bioreactor capable of replicating 3D tissue-like vascularized constructs has been proposed. To this aim, we describe the computational simulation-based study conducted to support the first steps in bioreactor design and its parameters tuning, by avoiding a trial-and-error procedure.

## II. MATERIALS AND METHODS

The device, designed with Fusion 360 (Autodesk) and fabricated with a FDM printer (Crealty CR6 SE), was conceived to easily interchange its components, allowing for the generation of tunable vessels in length and diameter. An in-silico model of the bioreactor was created considering a channel with a diameter and length equal to 2.5 and 5mm, respectively. Numerical simulations to assess the fluid-dynamics of the medium flowing inside the bioreactor and O<sub>2</sub> diffusion were performed by using the commercial software Ansys FLUENT. In particular, for the numerical fluid-dynamic assessment by Computational Fluid Dynamics, two domains were identified: i) a free flow domain (i.e., the channel) modeled with Navier-Stokes equation; ii) a porous flow domain, modeled with Stokes-Brinkman equation. Regarding the diffusion part, Fick's law was used to model oxygen diffusion through the medium and hydrogel and Michaelis-Menten kinetics to model O<sub>2</sub> consumption of HUVECs around the channel and of hepatocytes within the construct. Different flow rate values at the inlet were taken into consideration. Velocity and pressure fields, shear stress, and O<sub>2</sub> concentration distribution throughout the perfusion system were computed and analyzed. Preliminary validation in static with only HUVECs was performed.

## III. RESULTS AND DISCUSSION

The flow pattern, represented by velocity streamlines, is always able to reach internal regions of the scaffold with the value of hydrogel's permeability and porosity considered, irrespective of flow rate. Since closely related, O<sub>2</sub> distribution and shear stress were studied together (Fig. 1a and 1b) and the related critical values of each quantity (>0.04 mM and <5 dyn/cm<sup>2</sup>, respectively) were assessed to prove that such thresholds were not reached by the proposed device. The bioreactor was successfully validated in the short term in static as shown in Fig. 1c, demonstrating the compatibility of the bioreactor with functional endothelial cells (VE-Cadherin expression) and the wall formation.

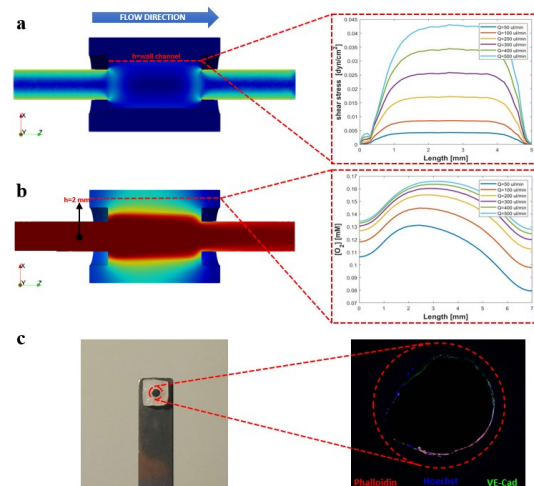


Fig. 1. Distribution of (a) shear stress and (b) oxygen concentration at different flow rate values. c) Confocal imaging of static culture HUVECs in the device at day 1 showing an adequate re-vascularization around the channel.

## IV. CONCLUSIONS

In this preliminary part of computational study, the obtained results were beneficial for optimizing the design specifications and understanding relevant issues, especially in assessing whether the internal parts of the scaffold were perfused and in finding a balance between shear stress, acting directly on the vessel wall and that can provoke the detachment of endothelial cells, and O<sub>2</sub> distribution within the construct, responsible of the cell survival and function. Next tests will see a longer dynamic culture in presence of a selected microenvironment (e.g., the hepatic one) *ad-hoc* created around the endothelial cavity.

## REFERENCES

- [1] A. Szklanny, "3D Bioprinting of Engineered Tissue Flaps with Hierarchical Vessel Networks for Direct Host-To-Implant Perfusion," in *Adv. Mater.*, vol. 33, no. 42, 2021.

# Novel experimental set up to determine the optimal drug-coated balloon angioplasty parameters

E. Stratakos<sup>1</sup>, P. Ravipati<sup>1</sup>, Mohammad Akrami-Hasan-Kohal<sup>2</sup>, Gianluca Poletti<sup>1</sup>, Francesca Berti<sup>1</sup>, L. Vincenzi<sup>1</sup>, E. Pedrinazzi<sup>1</sup>, A. F. Pérez<sup>1</sup>, Tahmer Sharkawi<sup>2</sup>, S. Mantero<sup>1</sup>, L. Petrini<sup>1</sup> and G. Pennati<sup>1</sup> <sup>1</sup>*LABS, Dept. of Chemistry, Materials and Chemical Engineering "Giulio Natta", Politecnico di Milano, Italy* <sup>2</sup>*ICGM, Univ Montpellier, CNRS, ENSCM, Montpellier, France*

**Abstract**—In contradiction to the belief that drug-coated balloons deliver the drug uniformly to the stenosed vessel, literature suggests poor coating adhesion. Evidence indicates that, during the balloon inflation, the balloon-artery interaction has a key role in the efficiency of the treatment. Considering the above, the authors designed an *in vitro* set up able to account for procedural variables and assess their impact on the coating transfer efficacy.

**Keywords**—Drug-coated balloons, drug-coating stamping, mechanical contact, operational parameters

## I. INTRODUCTION

Drug-coated balloons provide a promising minimally invasive solution, by advocating the leave-nothing-behind strategy and offering the potential to deliver the drug-coating homogeneously on the lesion. Nonetheless, studies suggest that the drug-coating is neither uniformly nor adequately delivered on the arterial mural surface, owing to poor mechanical contact [1], [2]. Therefore, it is consequential to comprehend the influence of the operational variables involved during the treatment on the coating transfer rates. On this basis, the authors developed an *in vitro* stamping set up to investigate the contribution of the contact time, pressure values, and balloon stretching rates on the delivered drug-coating percentage, with varying environmental parameters.

## II. MATERIALS AND METHODS

### A. Materials

**Artery:** aortas was dissected from the porcine heart kindly provided by a local abattoir and was longitudinally cut to prepare 10x10 mm samples.

**Artificial Plaque:** 25% w/w gelatin gels [Type B gelatin powder from bovine skin, SIGMA] with and without 15-50% w/w hydroxyapatite [reagent grade synthetic powder, SIGMA ALDRICH] were prepared by using genipin [CHIBIO BIOTECH, China], a crosslinker, to obtain gels of varying stiffness up to 50kPa.

**Balloon samples:** rectangular films of PEBAX 7033 were prepared from granules, using a heat press machine. The PEBAX films were then spray coated with everolimus (EV)/Pluronic solutions of different drug/polymer ratios and then dried under vacuum to yield drug coated PEBAX films as drug coated balloon specimens.

### B. Setup construction

The designed setup had an overall dimension of 100x167x220 mm (Fig.1). All the parts, except for the bolts and the guiding rods, were 3D printed in a Verve Kentstrapper 3D printer with a nozzle size of 0.4 mm and 0.02 mm vertical

resolution.

### C. Set up philosophy

The setup consists of the top bed, where the pig aorta was flattened and glued, and the bottom bed, where the balloon samples were gripped. Each balloon patch was fixed at the grips, while the rotation of the lateral bolt caused a linearly increasing stretch on the sample. To control the contact pressure weights were introduced on the vertical axis of the top bed, considering the buoyancy force in the case of bath immersion. Experiments were performed by altering the parameters shown in Table 1, to study their influence on the coating transfer percentages. The drug coating transfer was studied by imaging the luminal surface of the aorta and the artificial plaque using an Olympus LEXT OLS4100 laser scanning digital microscope.

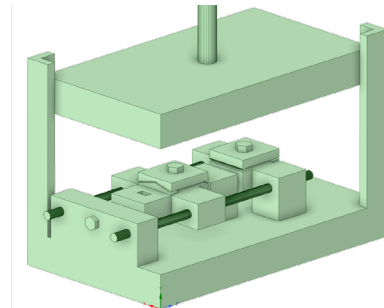


Fig. 1: Coating stamping setup

TABLE I  
VARIABLES FOR THE COATING STAMPING EXPERIMENT

Parameter Type	Parameters
Procedural	Contact time
	Pressure
	Balloon stretching
Environmental	Temperature
	Saline/PBS
	Saline/PBS + Human Serum Albumin
Artificial Plaque	Medium with Fetal bovine Serum
	Stiffness

### ACKNOWLEDGEMENT

This project has received funding from the European Union's Horizon 2020 research and innovation programme under the Marie Skłodowska-Curie grant agreement No 956470.

### REFERENCES

- [1] A. R. Tzafirri, "Balloon-based drug coating delivery to the artery wall is dictated by coating micro-morphology and angioplasty pressure gradients" *Biomaterials*, 2020b, 260, 120337
- [2] G. H. Chang, "Intrinsic coating morphology modulates acute drug transfer in drug-coated balloon therapy" *Scientific Reports*, 2019, 9(1), 6839

# Towards a real-time simulator of flow diverters deployment based on model order reduction

B. Bisighini<sup>1,2,3</sup>, M. Aguirre<sup>1</sup>, B. Pierrat<sup>1</sup>, D. Perrin<sup>2</sup> and S. Avril<sup>1</sup>

<sup>1</sup> Mines Saint-Etienne, Univ Lyon, Univ Jean Monnet, INSERM, U 1059 Sainbiose, Centre CIS, F-42023 Saint-Etienne, France

<sup>2</sup> Predisurge, 10 rue Marius Patinaud, Grande Usine Creative 2, 42000 Saint-Etienne, France

<sup>3</sup> Department of Enterprise Engineering “Mario Lucertini”, University of Rome Tor Vergata, Via del Politecnico, 1, 00133 Rome, Italy

**Abstract**— With the aim of developing a computational tool to assist surgeons in the selection of the best device for patient-specific cerebral aneurysms treatment, here we propose a fast and accurate reduced-order modelling scheme, based on finite element simulations, to compute in real-time the deployed configuration of flow diverters within idealised vessel models.

**Keywords**—Flow diverters, Beam elements, Reduced order modelling, Gaussian process regression.

## I. INTRODUCTION

**F**LOW DIVERTERS (FDs) are very dense braided stents used in the endovascular treatment of cerebral aneurysms. They are available in different sizes, in terms of unconstrained length and radius, and surgeons select the most appropriate one based on the patient’s specific anatomy from 3D images. This choice is not trivial and computational tools could be potentially beneficial to surgeons, especially in complex cases. Any further information should be provided almost in real-time since decisions are taken shortly before and during surgery. Thus, due to the problem complexity, traditional techniques alone, as finite element (FE) modelling, are not suitable because they would exceed the desired computational time. To reach real time, one solution could be to combine FE simulations and reduced-order modelling (ROM). Here, we present a virtual framework that enables real-time computation of the FDs deployed configuration within idealised vessel models.

## II. METHODS

### A. Flow diverter models

The flow diverter is modelled as a tubular net of interlaced thin wires with circular cross-section; the nodal positions and connectivity are defined by a set of parametric equations [1]. The stent structure is discretised using beam elements and simulations are performed using EndoBeams.jl, an in-house and open-source FE solver based on [2] and available at <https://gitlab.emse.fr/pierrat/EndoBeams.jl>.

### B. Vessel models

The centerline of the idealised model is defined using a planar quadratic Bezier curve. Each vessel is parametrised with respect to 4 geometrical parameters: position of the Bezier middle point (2 coordinates), vessel radius (considered constant) and deployment position of the stent along the centreline.

### C. FE simulations and database

The stent deployment procedure is performed as follows: the stent is crimped by imposing a radial displacement to all its

nodes, then it is positioned along the vessel centerline and, finally, it is released within the artery. To create the high-fidelity database, 150 cases for the geometrical parameters are defined using a Latin hypercube method: 100 FE solutions are collected for the training, 50 for the validation.

### D. Reduced order modelling

As in [3], a non-intrusive reduced basis (RBs) method is used: the RBs are extracted from the FE database with the proper orthogonal decomposition and Gaussian process regression, a supervised machine learning algorithm, is used to predict the projection coefficients for new parameters values. The ROM validation is performed by computing the average relative error (ARE) between FE and approximated solutions in the validation database.

## III. RESULTS

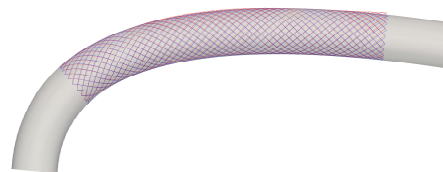


Fig. 1: FE (blue) and predicted solutions (red) for one of the cases in the validation database.

The ARE decays rapidly as more RBs are considered and, around 11 basis, reaches a stable plateau equal to 0.003, which results in an acceptable approximation (Fig. 1).

## IV. CONCLUSIONS

Using the proposed scheme, the computational cost is reduced from ca 30 minutes to few ms with a controlled loss of accuracy. Future efforts will be oriented at creating more complex vessel models, introducing an idealised aneurysm and a varying vessel radius.

## ACKNOWLEDGEMENTS

This project is carried on in the framework of the MeDiTaTe Project, which has received funding from the European Union’s Horizon 2020 research and innovation programme under Grant Agreement 859836.

## REFERENCES

- [1] A. Zaccaria, F. Migliavacca, G. Pennati, and L. Petrini, *J. Biomech.*, vol. 107, p. 109841, 2020.
- [2] M. Aguirre and S. Avril, *Comput. Methods Appl. Mech. Eng.*, vol. 371, p. 113275, 2020.
- [3] M. Guo and J. S. Hesthaven, *Comput. Methods Appl. Mech. Eng.*, vol. 341, pp. 807–826, 2018.

# An *in silico* method to evaluate bone remodelling after total hip arthroplasty: a six years longitudinal study

V. Betti<sup>1</sup>, L. Cristofolini<sup>1</sup>, H. Jónsson<sup>2</sup>, M. K. Gíslason<sup>3</sup>, and P. Gargiulo<sup>3</sup>

<sup>1</sup> Department of Industrial Engineering, University of Bologna, Italy

<sup>2</sup> Department of Orthopaedics, Landspítali University Hospital, Iceland

<sup>3</sup> Institute of Biomedical and Neural Engineering, Reykjavik University, Iceland

**Abstract**—The standard practice to assess the bone mineral density (BMD) uses DXA scans, resulting in an information loss since bone remodelling is a 3d mechanism. The aim of this study was to develop a protocol to assess BMD evolution 24 hours, 1 and 6 years after total hip arthroplasty using CT-scans, localising the changes in the different Gruen zones. The method was implemented and tested on five patients with a cemented implant, seven with an uncemented ones. Good results were obtained in terms of reproducibility and efficiency, proving that the method can be easily used to assess how bone remodels over time.

**Keywords**—bone remodelling, total hip arthroplasty.

## I. INTRODUCTION

Research on bone remodelling after total hip arthroplasty (THA) is a key element to (i) improve THA design by locating where the changes in bone mineral density (BMD) occur, and (ii) investigate the mechanisms of bone remodeling in the long term [1]. Existing studies use DXA scans and look at the density in two dimensions [2], which can lose some pivotal features of how bone remodels since it is a 3D mechanism [3]. The aim of this work was to develop a method to quantitatively assess femur's BMD evolution in the long-term after THA based on CT scans, localising the changes in the seven standard Gruen zones (GZs).

## II. MATERIALS AND METHODS

Spiral CT scans of THA patients were taken 24 hours, 1 year and 6 years post-operatively. Scans were calibrated using a phantom to convert the Hounsfield unit (HU) to BMD. A segmentation (*Mimics*) with threshold [300-2999] HU was performed to isolate the region of interest, creating a mask from the greater trochanter to 2 cm below the implant. In order to assess the inter-operator variability in the segmentation, ten operators were recruited. The error in the volume of the mask was calculated as:

$$Err\% = \frac{|V_{op}-V_r|+|V_r-V_{op}|}{V_r} \cdot 100, \quad (1)$$

where  $V_{op}$  and  $V_r$  are respectively the volume of the mask of each operator and the volume of the mask of the author set as the reference mask. To identify the GZs, each mask was set to the frontal view and the planes identified as per protocol [4]. The average value of BMD was calculated in each GZ, for each subject at the three timepoints, to assess the gain/loss in BMD over time. To better assess any change from the previous dataset, post-1y data were normalised by post-24h; post-6y data by post-1y ones. To test the method, twelve subjects (six males, six females), five with a cemented implant, seven with an uncemented one, were analysed.

## III. RESULTS

The  $Err\%$  between operators was on average 1.75%. The mean time spent to create the mask was 1 hour. Changes in BMD[%]

grouped and averaged according to the type of fixation are reported in Table 1. No statistically significant changes over time were observed in the cemented group. For the uncemented one, variations were statistically significant only in few regions (GZs 4-6 after one year, GZs 1 and 4 after six years).

TABLE I: Average BMD gain/loss [%] in each GZ for the cemented and uncemented groups. Negative values state for an average loss, positive values for an average gain. \*statistically different from previous dataset ( $p<0.05$ ).

GZs	BMD <sub>CEMENTED</sub>		BMD <sub>UNCEMENTED</sub>	
	$\mu_{\frac{1-24}{24}}[\%]$	$\mu_{\frac{6-1}{1}}[\%]$	$\mu_{\frac{1-24}{24}}[\%]$	$\mu_{\frac{6-1}{1}}[\%]$
1	0,45	-0,95	0,98	-2,08*
2	-1,91	-2,12	-1,54	0,09
3	-1,49	-0,63	-2,17	1,88
4	-0,69	0,71	-1,03*	1,03*
5	-0,41	1,14	-2,81*	3,45
6	-2,3	-1,25	-3,37*	1,87
7	-1,41	-0,52	-2,32	0,07



## IV. DISCUSSION

The *in silico* method presented in this study can be easily employed as a tool to evaluate long-term bone remodelling in the femur. The protocol showed good results in terms of reproducibility ( $Err\%$ ) and efficiency (time) [5].

While the BMD changes for the cemented group were not statistically relevant, our findings for the uncemented one in GZs 4-6 one year post-op are in line with other prospective studies, which reported a bone loss of BMD in the medial part of the femur, more pronounced in the proximal area [6]. The significant changes in GZs 1 and 4 after six years are likely caused by load transfer being shifted from the proximal part of the femur, through the rigid implant to the distal area.

These results may depend on the small number of subjects analysed. Future analyses on more data will be performed to assess (i) the potential statistical significance of other areas, and (ii) the relationship between BMD gain/loss and several features (e.g. age, sex, pathologies).

## REFERENCES

- [1] Gíslason et al, *Clin Biomech*, 2020, 78:105092.
- [2] Kröger et al, *JMBR*, 2009, 11:1526-1530.
- [3] Albanese et al, *Hip Int*, 2006, 16:9-15.
- [4] Gruen et al, *Clin Orthop Relat Res*, 1979, 141:17 - 27.
- [5] Patijn, *Man Med*, 2019, 57:451-479.
- [6] Nyström et al, *Acta Ortho*, 2022, 93:206-2011.

# Musculoskeletal model evaluates the effect of spinal fixation length on vertebral joints

S. Borrelli<sup>1,2</sup>, F. Argentieri<sup>1,2</sup>, G. Putame<sup>1,2</sup>, A. L. Audenino<sup>1,2</sup>, M. Terzini<sup>1,2</sup>

<sup>1</sup> Polito<sup>BIO</sup>Med Lab, Politecnico di Torino, Turin, Italy

<sup>2</sup> Department of Mechanical and Aerospace Engineering, Politecnico di Torino, Turin, Italy.

**Abstract** - A musculoskeletal model of the upper body was used to evaluate the compression loads on intervertebral joints in case of long and short lumbar fixations in different spinal positions.

**Keywords** - Musculoskeletal lumbar model, multibody modelling, spinal fixation, adjacent level effects.

## I. INTRODUCTION

Spinal stability is commonly restored through segmental pedicle-screw short or long fixations [1]. To further characterize the biomechanical effects of this surgical choice, this study explores the variation of vertebral compressive loading recurring to a musculoskeletal multibody model.

## II. METHODS

A healthy subject-specific musculoskeletal model developed in OpenSim4.2 was extracted from the “Framingham Heart Study” (n. 246) [2]. The model was scaled from the Bruno model, and it included only the upper body; each lumbar vertebra was represented as a single rigid body. A long (L1-L5, *Lf model*) and a short (L2-L4, *Sf model*) lumbar fixations were modelled by introducing weld joints in the corresponding intervertebral discs. Static optimizations were performed for neutral posture, 30° of flexion, 15° of extension, and 30° of torsion (Figure 1). The total motion was preserved also in *Sf* and *Lf* models: compensation was performed by redistributing the 75% of the motion to the first mobile adjacent cranial level and the 25% to the adjacent caudal levels [3]. Compression forces along the lumbosacral joints were then calculated and compared to the control model.

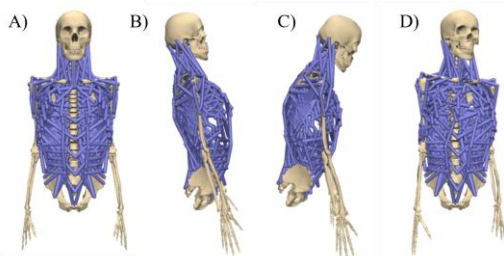


Figure 1 The upper body musculoskeletal model in all the configurations analysed: A) neutral posture, B) 15° of extension, C) 30° of flexion, D) 30° of axial torsion.

## III. RESULTS

Figure 2 reports the compression load distribution along L1-S1 segment as a percentage of the load at the corresponding cranial T12-L1 adjacent level. The figure clearly states that fixation lengths impact on vertebral joints loads for all the motions studied. Long fixation registers a linear cranio-caudally incrementing pattern, even in neutral posture.

Conversely, in the control and *Sf* models, the lumbar levels are loaded uniformly, deviating less than the 15% in neutral posture, flexion, and torsion. Lumbosacral joint are always the most loaded level and the adherence between the control and the *Sf* model is maintained.

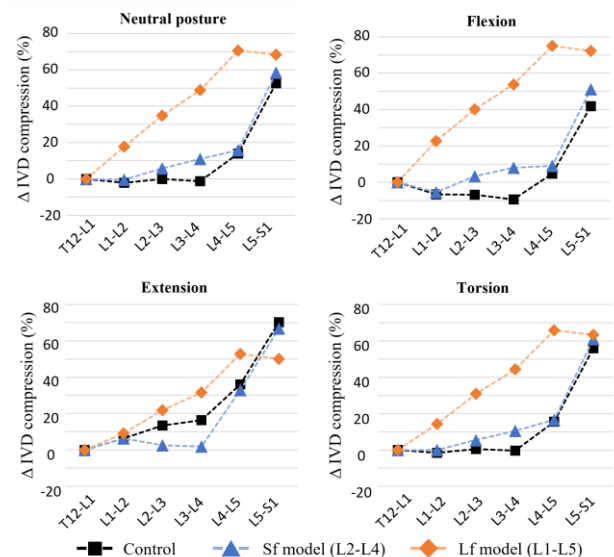


Figure 2 Compression component in L1-S1 intervertebral discs (IVD) expressed as percentage variation with respect to the T12-L1 level.

## IV. CONCLUSIONS

Although this study modelled surgery fixation outcomes through a simplified strategy (i.e., translating the whole procedure into an ideal fixed joint), it permitted to highlight a dependency between compressive loads on lumbar joints and the length of spinal fixations, providing in this way direct implications in the clinical sphere. Indeed, the computed compressive loads are closely correlated to *intervertebral disc pressures*, which in turn play a crucial role in the long-term success of the fixation and in the onset of disc injuries [4].

## REFERENCES

- [1] X. Shao, “A retrospective comparative study of postoperative sagittal balance in isthmic L5-S1 spondylolisthesis using single segment or two-segment pedicle screw fixation”, *BMC Musculoskeletal Disorders*, vol. 23(1), 2022.
- [2] H. Mokhtarzadeh, “Patterns of Load-to-Strength ratios along the spine in a population-based cohort to evaluate the contribution of spinal loading to vertebral fractures”, *Journal of Bone and Mineral Research*, vol. 36(4), 2020, pp.704-711.
- [3] M. Malakoutian, “Do in vivo kinematic studies provide insight into adjacent segment degeneration? A qualitative systematic literature review”, *European Spine Journal*, vol. 24, 2015, pp.1865-1881.
- [4] C. Zhou, “Investigation of alterations in the lumbar disc biomechanics at the adjacent segments after spinal fusion using a combined in vivo and in silico approach”, *Annals of Biomedical Engineering*, vol. 49(2), 2021.

# Development of a contrast-enhanced microtomography protocol for meniscal tissue

G. Marchiori<sup>1</sup>, M. Maglio<sup>1</sup>, M. Berni<sup>1</sup>, A. Grassi<sup>1</sup>, S. Zaffagnini<sup>1</sup>, C. Falsina<sup>2</sup>, N.F. Lopomo<sup>2</sup>,  
A. Visani<sup>1</sup>, M. Baleani<sup>1</sup> and M. Fini<sup>1</sup>

<sup>1</sup> IRCCS Istituto Ortopedico Rizzoli, Bologna (Italy)

<sup>2</sup> Università degli Studi di Brescia, Brescia (Italy)

**Abstract**—Aim of the study is to reveal the peculiar microstructure of the meniscus in a reliable way. Specifically, a contrast-enhanced microtomography protocol is under development to provide full 3D information of wide tissue portions with a sufficient spatial and contrast resolution for the structures of interest, reducing the workload for sample preparation, increasing the throughput potential thanks to fast image acquisition and volume reconstruction, limiting the destructiveness of the methodology as not to alter the investigated object itself nor prevent the complementarity with histology or other assays.

**Keywords**—meniscus, contrast-enhanced microtomography, unconfined compression

## I. INTRODUCTION

THE meniscus plays an important role in knee biomechanics. Its mechanical function is defined by extracellular inhomogeneity and anisotropy along its entire three-dimensional anatomy [1]. However, a validated 3D imaging of the whole complex meniscus' microstructure is still lacking, while the literature is still based on meniscus descriptions aggregating local information, e.g. from histomorphometry or electron microscopy.

To overcome such a limitation, contrast-enhanced microtomography (CE- $\mu$ CT) should be explored [2], focusing on validation, i.e. capability of revealing original microarchitecture, and on complementarity with other assays.

## II. MATERIALS AND METHODS

This study preliminarily moves from two different techniques proposed to enhance X-ray attenuation properties – i.e., by phosphotungstic acid (PTA) staining [3] or by hexamethyldisilazane (HMDS) drying [4] – of meniscal tissue, which however had been limited to small tissue portions.

In the first protocol, tissue sample is fixed in 4% formalin, stained with 1% (w/v) PTA in 70% ethanol solution for 21 days and then  $\mu$ CT scanned (source voltage 70 kV and current 140  $\mu$ A; filter Al 0.5 mm). In the second protocol, tissue sample is fixed in 4% formalin, dehydrated in ascending ethanol concentrations (4 days), treated with HMDS (2 days), air-dried in a fume hood overnight and then  $\mu$ CT scanned (40 kV, 250  $\mu$ A; no filter).

The two protocols were applied on the halves of an ovine meniscus to evaluate and compare their contrast capacity.

To evaluate the macroscopic effect of the contrast-enhancement treatments on meniscal tissue and the chance of reversing them, two cubic samples from human meniscus (ethical approval 952/2021/Sper/IOR) underwent unconfined compression 1) in fresh condition (PRE), 2) following PTA or

HMDS treatment (INTERMED), and 3) after rehydration in PBS overnight (POST).

## III. RESULTS AND DISCUSSION

PTA treatment did not reach the core of the ovine meniscus even after 21 days of staining. Therefore, the internal microstructure was not visible (Figure 1).

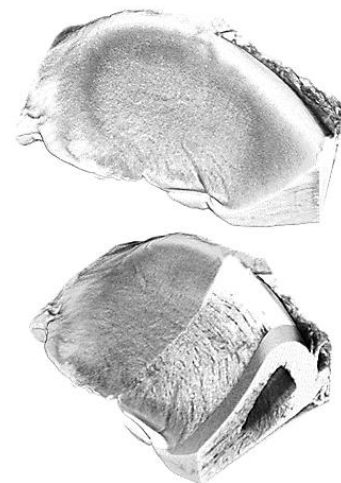


FIGURE 1: full (above) and sectioned (below)  $\mu$ CT volume reconstruction (pixel size 18  $\mu$ m) of the ovine meniscus half, treated by PTA, highlighting a core not penetrated by the staining.

HMDS treatment instead permitted a full imaging of the ovine meniscus architecture (Figure 2), in front of a more rapid sample preparation (7 days).



FIGURE 2: full (above) and sectioned (below)  $\mu$ CT volume reconstruction (pixel size 5  $\mu$ m) of the ovine meniscus half treated by HMDS.

## REFERENCES

- [1] M. Berni et al., "Anisotropy and inhomogeneity of permeability and fibrous network response in the pars intermedia of the human lateral meniscus", *Acta Biomaterialia*, 2021, vol. 135, pp. 393-402.
- [2] S. de Bournonville et al., "Contrast-Enhanced MicroCT for Virtual 3D Anatomical Pathology of Biological Tissues: A Literature Review", *Contrast Media & Molecular Imaging*, 2019, 2019:8617406.
- [3] I. Ribitsch et al., "Structure-Function relationships of equine Menisci", *PLoS one*, 2018, vol. 13,3, e0194052.
- [4] I. Kestilä et al., "Three-dimensional microstructure of human meniscus posterior horn in health and osteoarthritis", *Osteoarthritis and Cartilage*, 2019, vol. 27, pp. 1790-1799.
- [5] G. Marchiori et al., "Integration of micro-CT and uniaxial loading to analyse the evolution of 3D microstructure under increasing strain: application to the Anterior Cruciate Ligament", *Materials Today: Proceedings*, 2019, vol. 7, pp. 501-507.
- [6] S. Zhu et al., "Microstructure Analysis and Reconstruction of a Meniscus", *Orthopaedic Surgery*, 2021, vol. 13, pp. 306-313.

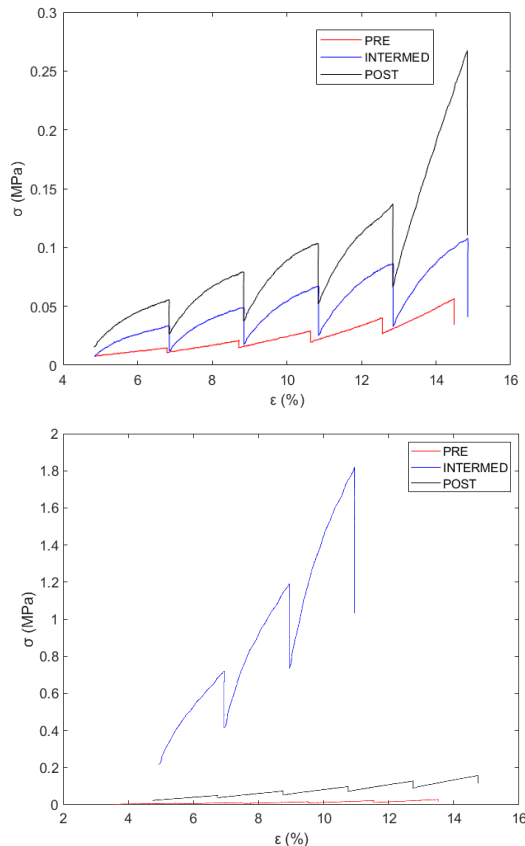


FIGURE 3: stress-strain ( $\sigma$ - $\epsilon$ ) curves of unconfined compression for PTA (above) and HMDS (below) treatment (PRE: before treatment; INTERMED: after treatment; POST: after dehydrating).

## IV. CONCLUSION

An experimental campaign with statistical power is under design to screen various aspects of the meniscus CE- $\mu$ CT protocol introduced in this work, thus to reduce the workload for sample preparation, to find the best treatment and to validate the protocol. For instance, in the case of PTA, an aqueous instead of an alcoholic solution could be useful in preserving the mechanical behaviour of the tissue [5]; for the same reason, rehydration could be more effective after freeze-[6] respect to chemical-drying.

## ACKNOWLEDGEMENT

We acknowledge the Italian Ministry of Health 5x1000 2019 (2018 incomes) "Medicina rigenerativa e riparativa personalizzata per le patologie dei tessuti muscolo-scheletrici e la chirurgia ricostruttiva ortopedica" project for the financial support.

# Fracture risk assessment in healthy and pathological human vertebra: a computational study

D. Bianchi<sup>1</sup>, C. Falcinelli<sup>2</sup>, L. Molinari<sup>3</sup>, A. Di Martino<sup>4,5</sup> and A. Gizzi<sup>1</sup>

<sup>1</sup> Department of Engineering, University of Rome Campus Bio-Medico, Rome Italy

<sup>2</sup> Department INGEO, University “G. D’Annunzio” of Chieti-Pescara, Pescara, Italy

<sup>3</sup> Department of Mathematics and Computer Science, Emory University, Atlanta, United States

<sup>4</sup> Department of Biomedical and Neuromotor Science, DIBINEM, University of Bologna, Italy

<sup>5</sup> 1st Orthopaedic and Traumatologic Clinic, IRCCS Istituto Ortopedico Rizzoli, Bologna, Italy

**Abstract**—Metastatic lesions compromise the mechanical integrity of vertebrae, increasing the fracture risk. Screw fixation is usually performed to guarantee spinal stability and prevent dramatic fracture events. Accordingly, predicting the overall mechanical response in such conditions is critical to planning and optimizing surgical treatment. This work proposes an image-based finite element computational approach describing the mechanical behavior of a patient-specific instrumented metastatic vertebra by assessing the effect of lesion size, location, type, and shape on the fracture load and fracture patterns under physiological loading conditions.

**Keywords**— metastatic vertebra; finite element analysis; constitutive modeling; fracture risk.

## I. INTRODUCTION

IN the last decade, mechanics-based computational tools, such as image-based finite element (FE) modeling [1,2], have been developed to improve the fracture risk assessment of vertebra. A more profound comprehension of the mechanical response of healthy and metastatic vertebra could help develop accurate clinical tools for making decisions about the treatment and evaluating its efficacy. The present work aims to evaluate the mechanical behavior of instrumented metastatic vertebra through the development of an image-based FE computational tool. Considering the critical configurations found in [3,4], we present a FE comparative analysis investigating physiological and pathological scenarios (i.e., presence of metastatic lesion, size, location).

## II. MATERIALS AND METHODS

A custom Matlab code has been developed and integrated within Comsol Multiphysics to simulate the vertebral fracture. The main steps of the developed computational approach are shown: i) geometry reconstruction of vertebra (from Computed Tomography images) and screws, ii) inclusion of metastasis simulating the bone-metastasis interaction and thus accounting for the possible effect of tumoral lesion on bone material properties, iii) choice of boundary conditions, and iv) computational discretization.

## III. RESULTS

The influence of size, position, and metastasis presence on the mechanical response of the vertebra has been evaluated. For example, in Figure 1, the progression of fracture patterns in extension loading condition for osteolytic lesions 10 mm located in the right-lateral position is reported. Numerical results show that a wider metastasis close to the screw leads to

a more extended fracture zone that involves a large portion of the vertebral body than a smaller lesion.



Figure 1: Progression of fracture patterns in case of osteolytic lesion and screw fixation. Failed elements are highlighted by red color

## IV. CONCLUSION

In the present study, a new image-based computational FE approach that accounts for the effect of metastasis on bone material properties has been developed and used to evaluate the impact of size, location, and type of metastasis on the mechanical response of an instrumented vertebra. We highlight how these parameters significantly affect the fracture load predictions and the fracture pattern.

## ACKNOWLEDGEMENT

The authors acknowledge the support of the Italian National Group for Mathematical Physics (GNFM-INdAM). Daniele Bianchi and Cristina Falcinelli acknowledges the funding by the Italian Ministry of University and Research (MUR) within the PON “Ricerca e Innovazione” 2014–2020 (azione IV.6) - FSE-REACT EU.

## REFERENCES

- [1] Costa, M.C.; Eltes, P.; Lazary, A.; Varga, P.P.; Viceconti, M.; Dall’Ara, E. Biomechanical assessment of vertebrae with lytic metastases with subject-specific finite element models. *J Mech Behav Biomed Mater* 2019, 98, 268–290.
- [2] Stadelmann, M.A.; Schenk, D.E.; Maquer, G.; Lenherr, C.; Buck, F.M.; Bosshardt, D.D.; Hoppe, S.; Theumann, N.; Alkalay, R.N.; Zysset, P.K. Conventional finite element models estimate the strength of metastatic human vertebrae despite alterations of the bone’s tissue and structure. *Bone* 2020, 141, 115598.
- [3] Molinari, L.; Falcinelli, C.; Gizzi, A.; Di Martino, A. Effect of pedicle screw angles on the fracture risk of the human vertebra: A patient-specific computational model. *J Mech Behav Biomed Mater* 2021, 116, 104359.
- [4] Molinari, L.; Falcinelli, C.; Gizzi, A.; Di Martino, A. Biomechanical modeling of metal screw loadings on the human vertebra. *Acta Mech Sin* 2021, 37, 307–320.

# Permeability test bench for characterizing tissue engineering scaffolds: design and validation

B. Masante<sup>1,2</sup>, C. Massini<sup>1</sup>, S. Gabetti<sup>1</sup>, F. Mochi<sup>3</sup>, C. Del Gaudio<sup>3</sup>, A. Schiavi<sup>4</sup>, A. Audenino<sup>1</sup>, D. Massai<sup>1</sup>

<sup>1</sup> Polito<sup>BIO</sup>Med Lab, Department of Mechanical and Aerospace Engineering, Politecnico di Torino, Italy

<sup>2</sup> Bone and Dental Bioengineering Lab, CIR-Dental School, Department of Surgical Sciences, University of Torino, Italy

<sup>3</sup> Hypatia Research Consortium, Rome, Italy

<sup>4</sup> INRiM-National Institute of Metrological Research, Turin, Italy

**Abstract**— Permeability is a crucial feature for tissue engineering scaffolds however, a standardized protocol to assess this property is still missing. Here we propose a novel permeability test bench for characterizing hard and soft samples.

**Keywords**—Permeability, test bench, Darcy's law, hard and soft tissue engineering scaffolds.

## I. INTRODUCTION

GEOMETRICAL properties such as porosity, pore size, tortuosity, and interconnectivity strongly influence the ability of tissue engineering scaffolds to be permeated by fluids (permeability) and consequently to be colonized by cells. Characterizing the scaffold permeability could thus provide crucial information in view of the biological tests [1,2]. In literature, several methods have been proposed for assessing scaffold permeability, however, defined protocols are still missing also because soft scaffolds pose challenging tasks due to their deformability. Here, we present a versatile permeability test bench designed for characterizing hard and soft scaffolds. The test bench was developed and preliminarily validated by testing two different hard scaffolds and comparing the results with a reference test bench [3].

## II. MATERIALS AND METHODS

The proposed permeability test bench (PTB) is based on the pump method [1]. The permeability chamber (PC) consists of 2 parts coupled by screws with an internal cylindrical geometry. Interchangeable silicone holders and a grid allow housing hard or soft cylindrical samples (height = 1-14 mm, diameter = 8-27 mm). The PC is part of a closed-loop hydraulic circuit, composed of a reservoir, a peristaltic pump (Masterflex), silicone tubing, 3-way stopcocks, and two pressure sensors (HJK) located upstream and downstream the PC, respectively. The sensor signals are acquired by a DAQ (National Instruments), controlled by a computer running a purpose-built LabView interface (Fig. 1A). Demineralized water was used as test fluid. Upon imposing a defined flow rate (guaranteeing laminar flow), permeability ( $k$ ) was calculated by using the Darcy flow transport model:

$$\Delta P/L = \mu/k \cdot (Q/A) \quad (1)$$

where  $\Delta P$  is the pressure drop across the sample,  $L$  is the sample thickness,  $Q$  is the flow rate, and  $A$  is the area of the sample cross-section. For validating the PTB, a 3D-printed PLA scaffold (Fig. 1B) and a commercial biomimetic scaffold (SmartBone IBI S.A, Fig. 1C) were tested at 5 mL/min for at least 4 repetitions. Tests were performed with and without samples. The results were then compared with the ones obtained from a reference test bench (RTB) [3].

## III. RESULTS

Performance tests demonstrated that the PC design allows holding several types of samples, preventing deformations and ensuring watertightness. The mean permeability values of the PLA scaffold tested within the PTB and the RTB resulted to be  $3.7 \cdot 10^{-10} \pm 1.59 \cdot 10^{-10} \text{ m}^2$  and  $3.7 \cdot 10^{-10} \pm 3.1 \cdot 10^{-11} \text{ m}^2$ , respectively, while the mean permeability values of the SmartBone scaffold were  $2.9 \cdot 10^{-10} \pm 2.6 \cdot 10^{-10} \text{ m}^2$  (PTB) and  $2.7 \cdot 10^{-10} \pm 3.6 \cdot 10^{-11} \text{ m}^2$  (RTB) (Fig. 1D). The normalized errors between the mean permeability values obtained with the PTB and the RTB resulted to be less than 1.

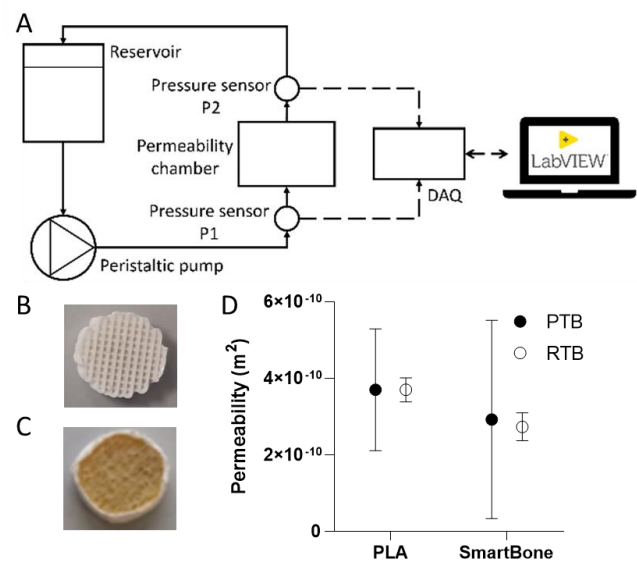


Fig. 1. A) Schematic drawing of the PTB; B) PLA scaffold; C) SmartBone scaffold; D) Permeability test results.

## IV. CONCLUSION

A versatile test bench for characterizing the permeability of hard and soft scaffolds has been developed. Although the PTB measurements were affected by a higher dispersion, preliminary validation tests demonstrated that the permeability values obtained using the PTB and RTB setups were compatible. For reducing measurement uncertainty, the optimization of the PTB data acquisition system is in progress. In parallel, tests varying the imposed flow rates and using soft scaffolds are ongoing.

## REFERENCES

- [1] F. Pennella, "A survey of methods for the evaluation of tissue engineering scaffold permeability," *Annals of Biomedical Engineering*, vol. 41(10), pp 2027–2041, 2013.
- [2] J. Santos, "On the permeability of TPMS scaffolds," *Journal of the Mechanical Behavior of Biomedical Materials*, vol. 110, 2020
- [3] A. Schiavi, "Acoustic method for permeability measurement of tissue-engineering scaffold," *Measurement Science and Technology*, vol. 23, 2012.

# Replicating the alveolar interface in-vitro using spherical, transparent and stretchable membranes

P. Signorello<sup>2</sup>, L. Cacopardo<sup>1</sup>, N. Guazzelli<sup>1,2</sup> and A. Ahluwalia<sup>1,2,3</sup>

<sup>1</sup>Research Center 'E. Piaggio', University of Pisa, Pisa, Italy

<sup>2</sup>Department of Information Engineering, University of Pisa, Italy

<sup>3</sup>Centro 3R, Italy

**Abstract**— Replicating the alveolar spherical geometry is essential for investigating substance and drug deposition in physiological relevant conditions. Here, the developed a strategy for the fabrication of spherical membranes, which are also transparent and stretchable, allowing their use for cell culture applications in dynamic conditions.

**Keywords**— inhalation testing, lung in-vitro models, membrane fabrication, curvotaxis

## I. INTRODUCTION

In-vitro models of the pulmonary barrier are commonly based on flat, 2D semipermeable membranes at the air-liquid interface. Only recently some studies have attempted to replicate the spherical alveolar geometry. For instance, curved polycarbonate membranes were fabricated via microthermoforming achieving the formation of confluent lung epithelial layers in microwells [1-2]. However, they still lack many physiological properties such as stretchability. Here we describe transparent spherical membranes which replicate the alveolar architecture in a more accurate manner, and which can be used in dynamic breathing conditions.

## II. MATERIALS AND METHODS

The membranes were fabricated by casting 1% w/v agarose in custom moulds obtained by stereolithographic 3D printing (Fig.1). After agarose crosslinking (1h at 4°C), the samples were dried overnight at 37°C.

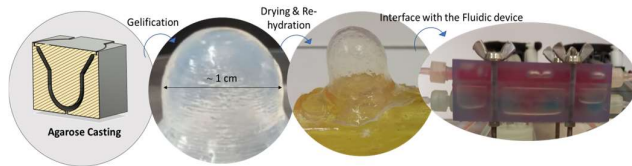


Figure 1. Workflow for membrane fabrication

Mechanical tensile tests at break were performed at a constant strain rate ( $0.2 \text{ s}^{-1}$ ) on flat membranes, which were prepared by casting in petri dishes and maintained for 7 days in incubator. Cyclic tests at 5% strain, typical of physiological breathing, were also performed. Membrane thickness was measured using a micrometer guage. Dry and hydrated weight was also measured to calculate water content. Permeability tests with methylene blue ( $30 \mu\text{g}/\text{mL}$ ) were then performed using transwell supports. To assess their cytocompatibility, the membranes were sterilized under UV for 30 mins and coated with 5%w/v gelatin overnight. A549 cells were seeded with at a density of  $200\,000/\text{cm}^2$  using polyethylene (PET) transwells as control. After 7 days, bright field images were acquired

(Olympus microscope) and cell viability was evaluated with the Alamar blue assay.

Finally, the membranes were interfaced with an alveolar duct (air) and a blood compartment (with media flow).

## III. RESULTS

Figs.2A-B show the flat membranes used for the characterization. They are transparent. In hydrated conditions, the membranes have a thickness of  $33.2 \pm 1.8 \mu\text{m}$  and a water content of  $89.4 \pm 0.6 \%$ . Their permeability to methylene blue is similar to that of transwell membranes. They are also highly elastic in the range of physiological strains and the apparent elastic modulus ( $26.5 \pm 5.0 \text{ MPa}$ ) was stable over typical cell culture times. Cyclic tensile testing also demonstrated a good fatigue behaviour with a low residual strain (under 1%). Cell viability on the membranes was not significantly different with respect to PET controls. Fig.2C shows cell adhesion after 7 days of culture.

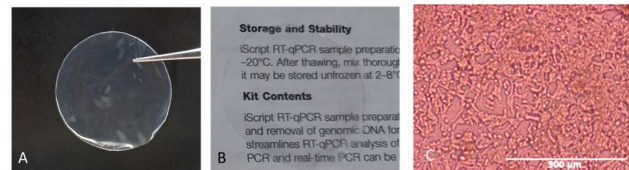


Figure 2. Flat membrane on dark (A) and text (B) background; C) A549 cells on the membrane at day 7.

## IV. CONCLUSION

Spherical agarose membranes were fabricated and characterized, demonstrating their suitability for in-vitro applications. In addition to the geometrical factor, the main advantages are their transparency and their elastic behaviour over the range of physiological strains observed in the lung (~5 to 15%).

Membrane deformation tests through over pressurization or other strategies are currently on going to replicate breathing. In conclusion, the fabrication of these membranes provide an innovative solution for alveolar models, which paves the way for more reliable and physiologically relevant inhalation tests and for a reduction of animal tests in line with the 3R principles.

## REFERENCES

- [1] Nossa R., Costa J., Cacopardo L., Ahluwalia A., "Breathing in vitro" in *J. Tissue Engineering*, 12:1-28, 2021.
- [2] Baptista D., Teixeira L., Birgani Z. et al., "3D alveolar in vitro model" in *Biomaterials*, 266: 120436, 2021.

# Do corneal mechanical properties play a role in Photorefractive Keratectomy outcome?

Benedetta Fantaci<sup>1</sup>, Miguel Ángel Ariza-Gracia<sup>3</sup>, Iulen Cabeza-Gil<sup>1</sup>, Jorge Grasa<sup>1,2</sup>, Begoña Calvo<sup>1,2</sup>

<sup>1</sup> Applied Mechanics and Bioengineering (AMB), Instituto de Investigación en Ingeniería de Aragón (I3A), Spain.

<sup>2</sup> Bioengineering, Biomaterials and Nanomedicine Networking Biomedical Research Centre (CIBER-BBN), Spain.

<sup>3</sup> ARTORG, University of Bern, Switzerland.

**Abstract**— Excimer lasers are widely used in refractive surgery for correcting vision errors by reshaping the corneal surface. However, the post-surgical mechanical consequences of removing the tissue have to be addressed. In this work, a finite element (FE) model has been developed to reproduce Photorefractive Keratectomy (PRK), in order to investigate surgery's outcomes depending on mechanical parameters.

**Keywords**—PRK, corneal mechanics, diopters, laser surgery.

## I. INTRODUCTION

PRK is one of the most performed procedures for correcting vision defects and consists of reshaping the anterior corneal surface with a laser. The removal of the ablation tissue affects the biomechanics of the cornea, causing deformations and stresses on the tissue, due to the action of the intraocular pressure (IOP). In this work, a FE model of the cornea has been developed to address the influence of geometrical, physiological and material parameters on the final outcome of PRK surgery simulation.

## II. MATERIALS AND METHODS

A 3D conicoid finite element (FE) model of the cornea was built using average geometrical parameters (Figure 1.a-b). A non-linear anisotropic Holzapfel-Gasser-Ogden constitutive model was chosen to model the behavior of corneal tissue, including in-plane and out-of-plane dispersion of the corneal collagen fibers [1]. A pre-stretch iterative algorithm was applied to introduce stromal pre-stresses. The PRK surgery simulation consisted of removing corneal tissue from the anterior surface following a specific ablation profile. The ablation depth was calculated using a conic ablation profile [2], in order to obtain a correction of 4 D. All mechanical simulations were calculated using ABAQUS 6.13-1.

To study the effect of the corneal mechanical properties on the PRK surgery's outcome, a  $2^k$  full factorial design was conducted, considering as key factors of the FE simulation the following variables: the materials constants ( $C_{10}$ ,  $k_1$ ,  $k_2$ ), the IOP and the thickness of the cornea (with  $k = 5$ , resulting in 32 simulations). The material constants were considered within a 50% variation with respect to the reference values [2] ( $C_{10-Ref} = 30$  kPa,  $k_{1-Ref} = 20$  kPa,  $k_{2-Ref} = 400$  [-]), whilst IOP and corneal thickness were changed within average physiological values, 13-18 mmHg and 490-550  $\mu\text{m}$ , respectively. The simulations' outcomes were analyzed by considering the diopters corrected with the PRK and the apex displacement of anterior corneal surface. An ANOVA statistical analysis was performed to interpret the results of the full factorial design.

## III. RESULTS

The results obtained from the statistical analysis are shown in Figure 1.c. The constant  $k_2$  turned out to be the most influential factor for both the corrected diopters and the apical displacement. This underlines the highly non-linear contribution of the anisotropic component of the material to

the behavior of the FE model and, therefore, the need of incorporating the collagen fibers when modeling the corneal tissue, as previously demonstrated in [3]. The IOP and the corneal thickness gave a lower effect with respect to the material parameters. In general, the material constants and their interactions have shown the major influence in determining the behavior of the corneal model and must be set properly.

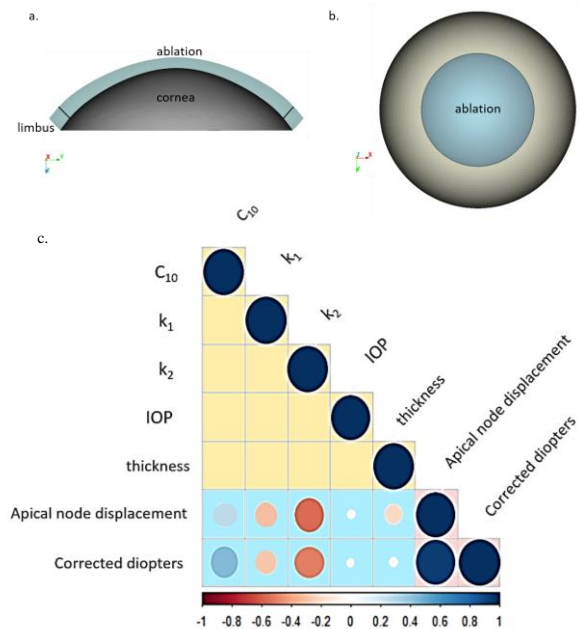


**Figure 1. a. and b. FEM model; c. Pearson correlation matrix - the color of each circle depicts whether the linear correlation is direct (blueish palette) or inverse (reddish palette). The larger the circle diameter, the higher the correlation.**

## IV. CONCLUSION

From the statistical analysis it turned out that the material constants do play a role on the final result of the PRK FE simulations. Consequently, it is of major importance to set the correct material constants in order to perform a reliable PRK simulation, having as final goal the post-surgical optical quality of the patient. To achieve this goal, post-surgery mechanical deformations cannot be neglected.

## ACKNOWLEDGEMENT

This project has received funding from the European Union's Horizon 2020 research and innovation program under grant agreement No 956720.

## REFERENCES

- [1] Wang, S., & Hatami-Marbini, H. (2021). Constitutive Modeling of Corneal Tissue: Influence of Three-Dimensional Collagen Fiber Microstructure. *Journal of Biomechanical Engineering*, 143(3).
- [2] Cano, .. Barbero, S., & Marcos, S. (2004). Comparison of real and computer-simulated outcomes of LASIK refractive surgery. *Journal of Optical Society of America*.
- [3] Pandolfi, A., Holzapfel, G. (2008). Three-Dimensional Modeling and Computational Analysis of the Human Cornea Considering Distributed Collagen Fibril Orientations. *Journal of Biomedical Engineering*.

# Biomechanical characterization of plantar skin

S. Pettenuzzo<sup>1</sup>, F. Toschetti<sup>2</sup>, A. Berardo<sup>1,3,4</sup>, E. Belluzzi<sup>4,5</sup>, A. Pozzuoli<sup>4,5</sup>, P. Ruggieri<sup>4,5</sup>, C.G. Fontanella<sup>2,4</sup>

<sup>1</sup> Department of Civil, Environmental and Architectural Engineering, University of Padova, Italy

<sup>2</sup> Department of Industrial Engineering, University of Padova, Italy

<sup>3</sup> Department of Biomedical Sciences, University of Padova, Italy

<sup>4</sup> Centre for Mechanics of Biological Materials, University of Padova, Italy

<sup>5</sup> Orthopedics and Orthopedic Oncology, Department of Surgery, Oncology and Gastroenterology (DiSCOG), University-Hospital of Padova, Italy

**Abstract**— Plantar skin is a complex structure, which covers and protects the plantar soft tissues. This study reports the results of experimental tests performed on foot skin, allowing to compare the different behaviour between samples taken from different foot regions and orientations, highlighting skin anisotropy.

**Keywords**—Foot skin, tensile tests, mechanical behaviour

## I. INTRODUCTION

THE plantar skin is a complex multi-layered structure whose main functions are to protect body against mechanical injuries, to act as a sensory organ and to withstand and adapt to the external stresses during physical activities [1]. It is composed of elastic and collagen fibres whose distribution and properties determine a non-linear, time-dependent and anisotropic behaviour [3]. Since skin plays a relevant role, it is important to maintain its integrity. Unfortunately, some diseases, such as diabetes, can cause skin damage, e.g. plantar ulcers, leading to a loss of its function [2]. In this context, the aim of this work is to describe the mechanical behaviour of foot skin in relation with its microstructure.

## II. MATERIALS AND METHODS

Skin plantar tissues were collected from healthy male human donors, (61±21 years). Plantar skin samples were collected from posterior, medial, lateral and metatarsal regions according to foot directions: anterior-posterior and lateral-medial (Fig. 1a). Tensile tests were carried out using a multi-step procedure (Fig. 1b). In stress relaxation protocol, after preconditioning, each step was composed of 7% strain at 10%/s strain rate with a subsequent 400 s of resting to allow the almost complete development of relaxation phenomena. With regard to failure tests, after preconditioning, samples were tightened at a 1%/s strain rate until rupture.

TABLE I  
PLANTAR SKIN MECHANICS

Region	UTS [MPa]	E [MPa]	Failure Strain [%]
P	5.93	21.56	38.51
L-LM	3.96	13.99	35.11
L-PA	11.73	33.43	45.69
M-LM	5.14	15.17	44.56
M-PA	6.81	22.50	41.43
Met-LM	2.82	6.74	65.64
Met-PA	3.60	9.26	54.60

P: posterior, L: Lateral, M: Medial, Met: Metatarsal; LM: lateral-medial, PA: posterior-anterior; UTS: ultimate tensile stress.

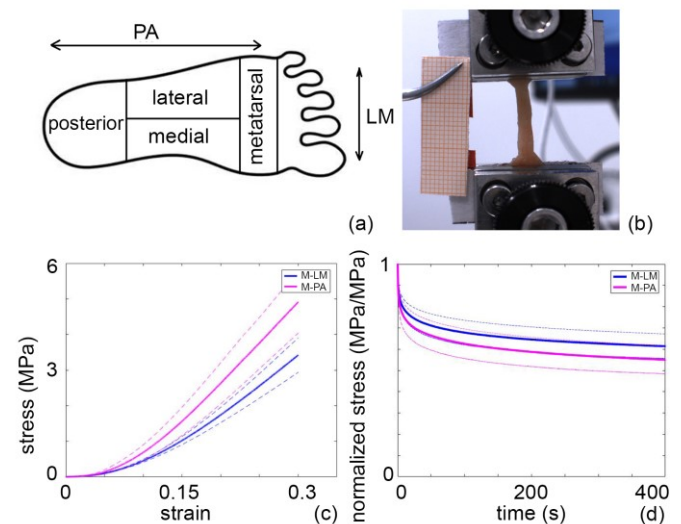


Figure 1: (a) samples orientation; (b) tensile tests; an example of (c) stress-strain and (d) stress-relaxation data (mean ± SD).

## III. RESULTS

Experimental results showed a non-homogeneous mechanical response between foot regions, e.g. in the metatarsal ones. Results highlighted the viscoelastic behaviour and tissue anisotropy (Fig. 1c-d), in terms of ultimate tensile stress, failure strain, and elastic modulus (Table I).

## IV. CONCLUSION

All the information will be useful to develop in silico tools to investigate interactions between foot and footwear, or to compare the mechanical response of tissues in healthy and pathologic conditions, e.g. in diabetic patients.

## ACKNOWLEDGEMENT

Project N° FISR2019\_03221, titled CECOMES: Centro di studi sperimentali e Computazionali per la ModelliStica applicata alla chirurgia.

## REFERENCES

- [1] F. Hashmi et al., “Characterising the biophysical properties of normal and hyperkeratotic foot skin” in *Journal of Foot and Ankle Research*, 2015; 8 (35): pp. 1-10.
- [2] L. Brady et al., “The compressive, shear, biochemical, and histological characteristics of diabetic and non-diabetic plantar skin are minimally different” in *Journal of Biomechanics*, 2021; 129: pp. 1-8
- [3] C.G. Fontanella et al., “Biomechanical response of the plantar tissues of the foot in healthy and degenerative conditions” in *Muscles, Ligaments and Tendons Journal*, 2017;7 (4): pp. 503-509

# Mechanical characterization of soft tissues from the lower urinary tract in male: a case study

M. V. Mascolini<sup>1</sup>, M. Todesco<sup>2</sup>, R. Boscolo Berto<sup>3,4</sup>, V. Macchi<sup>3,4</sup>, A. Porzionato<sup>3,4</sup>, R. De Caro<sup>3,4</sup>,  
C. G. Fontanella<sup>1,4</sup>, E. L. Carniel<sup>1,4</sup>, A. Berardo<sup>2,4,5</sup>

<sup>1</sup> Department of Industrial Engineering, University of Padova, Italy

<sup>2</sup> Department of Civil, Environmental and Architectural Engineering, University of Padova, Italy

<sup>3</sup> Department of Neuroscience, University of Padova, Italy

<sup>4</sup> Centre for Mechanics of Biological Materials, University of Padova, Italy

<sup>5</sup> Department of Biomedical Sciences, University of Padova, Italy

**Abstract**— The mechanical characterization of the human urinary tract is still a challenge, due to the variety of biological tissues involved and the difficulties in sample availability. At the same time, the development of effective *in-silico* models for this anatomical tract represents a key point to study and validate alternative and innovative solutions for most pathologies, reducing also the wide use of animal trials. This work reported a full characterization of the human tissues involved in the lower urinary tract in male, to obtain the constitutive parameters which are fundamental for these purposes.

**Keywords**—Lower urinary tract, human soft tissue, urethral tissues, mechanical tests.

## I. INTRODUCTION

THE mechanical behavior of many human tissues has already been extensively investigated, but the urinary tract is still a challenge. In fact, only few works analyzed the mechanics of urethra [1], bladder or prostate [3], but other soft tissues have never been studied yet. Moreover, the close relationship with these tissues and their physiological function during micturition address a clear interest from the scientific community in assessing their mechanical response and thus identifying the constitutive parameters. These latter are fundamental to develop *in-silico* models for the lower urinary tract and thus propose alternative and innovative solutions for most pathologies, such as benign prostatic hyperplasia or urinary incontinence, that nowadays are not always optimized either effective. For these reasons, the here presented work is a comprehensive study on the mechanical characterization of the soft tissues of the lower urinary tract in male, thanks to the combination of multiple mechanical tests (uniaxial tensile tests up to failure or stress-relaxation, compression and indentation) on seven different tissues from a cadaver donor, according to Body Donation Program of the Institute of Anatomy of the University of Padua.

## II. MATERIAL AND METHODS

Within this work we tested samples from: (i) bladder, (ii) tunica albuginea, (iii) Buch's fascia, (iv) prostate, (v) urethra, (vi) corpus cavernosum and (vii) glans penis. All the samples were obtained from one fresh-frozen cadaver. With reference to the tissue structure and function, a variety of mechanical tests were applied, such as uniaxial tensile tests, compression and indentation tests. *Ad-hoc* protocols were developed, when possible, with reference to previous works. Anisotropy was also investigated for urethral tissue, prostate and tunica albuginea, with significant outcomes.

## III. RESULTS

Uniaxial tensile tests revealed a non-negligible anisotropy in some of the studied tissues, such as the urethral samples, with a stiffer behavior along the longitudinal direction with respect to the circumferential one, and in the prostate. We observed no prevalent directions for the bladder and the other tissues, but results provided the mechanical identification of some materials never studied yet.

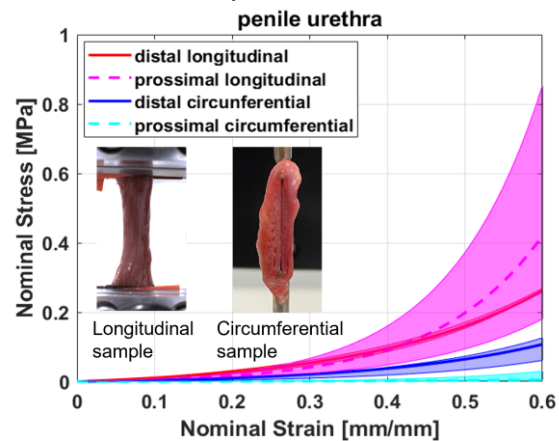


**Figure 1:** Performed mechanical tests. Stress-strain curves at the equilibrium for both longitudinal and circumferential urethral samples after stress-relaxation and corresponding confidence intervals (first and third quartile).

## IV. CONCLUSION

These results will serve as a complete mechanical description of the lower urinary tract in male for the development of more suitable computational models aimed at improving the existing solutions for the urinary pathologies and diseases.

## ACKNOWLEDGEMENTS

Project N° FISR2019\_03221, titled CECOMES: CEntro di studi sperimentali e Computazionali per la ModelliStica applicata alla chirurgia.

## REFERENCES

- [1] E.M. Cunnane et al., *Mechanical, compositional and morphological characterisation of the human male urethra for the development of a biomimetic tissue engineered urethral scaffold*, *Biomaterials* 2021, DOI: 10.1016/j.biomaterials.2021.120651
- [2] A.N. Natali et al., *Bladder tissue biomechanical behavior: experimental tests and constitutive formulation*, *Journal of Biomechanics*, 2015, DOI: 10.1016/j.jbiomech.2015.07.021
- [3] J. Ma et al., *Prostatic Fibrosis is Associated with Lower Urinary Tract Symptoms*, *The Journal of Urology*, 2016, DOI: 10.1016/j.juro.2012.06.007

# Biomechanical characterization of human superficial fascia from abdomen: A case study

L. Bonaldi<sup>1</sup>, A. Berardo<sup>1,2,5</sup>, C. Stecco<sup>3,5</sup>, and C.G. Fontanella<sup>4,5</sup>

<sup>1</sup> Department of Civil, Environmental and Architectural Engineering, Via F. Marzolo 9, 35131 - Padova, Italy;

<sup>2</sup> Department of Biomedical Sciences, Via U. Bassi 58/B, 35131 – Padova;

<sup>3</sup> Department of Neuroscience, Via A. Gabelli 65, 35121 - Padova, Italy;

<sup>4</sup> Italy Department of Industrial Engineering, Via Venezia 1, 35121 - Padova, Italy;

<sup>5</sup> Centre for Mechanics of Biological Material (CMBM), Via F. Marzolo 9, 35131 - Padova, Italy.

**Abstract**—The Superficial Fascia (SF) is a lamina of connective tissue found throughout body subcutis, that creates a link between the skin and the muscles. The protective role of SF in the integrity of subcutaneous tissue to external/internal forces (from skin to muscles and vice versa) could be compromised during aging or in pathological conditions. However, even if a clear biomechanical characterization of SF is critical for clinical practice, the literature is still poor in experimental outcomes from mechanical tests. For this reason, we would like to offer an in-depth study on this topic.

**Keywords**—Superficial Fascia, Abdomen, Biomechanical properties.

## I. INTRODUCTION

**S**UPERFICIAL FASCIA (SF) is a fibrous lamina of connective tissue (as network of collagen fibers and abundant elastin fibers arranged irregularly) between layers of superficial (SAT) and dense (DAT) adipose tissues, that is connected to the skin and deep fascia through fibrous septa (Fig. 1) [1]. The mechanical properties of SF depend on its structure. Its arrangement and thickness vary according to body location and gender [2]. The functional role of SF in supporting the integrity of subcutaneous structures through stress adaptation could be modified with aging or in pathological conditions, thus leading to alterations e.g., in vascular patency, in sliding/transmission of the forces between the muscles and the skin [1]. Despite the clinical importance of SF, to date literature is still poor of experimental data for its biomechanical characterization.

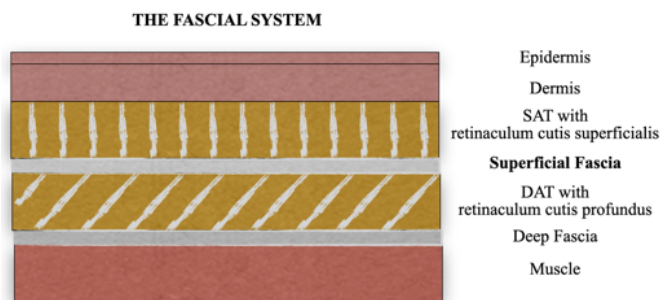


Fig. 1: The fascial system.

## II. MATERIAL AND METHODS

SF was harvested and stored from the abdomen of a human fresh-frozen donor, according to *Body Donation Program* of the Institute of Anatomy of the University of Padua [3]. After thawing, the sample was cut into strips, mounted on Mechanical Tester (Model Mach-1, ©Biomomentum Inc) and

loaded for the uniaxial tensile tests. Ten preconditioning cycles were performed before stress relaxation (strain rate: 15%/s, resting time: 300s) and failure (strain rate: 1%/s) protocols. Results have been analyzed with MATLAB [4]. Statistical analyses were performed for the different subgroups of specimens (according to different loading directions).

## III. RESULTS

Experimental results show a time-dependent and anisotropic behavior between longitudinal (a) and transverse (b) directions. Strain at break [mm/mm] values: (a)  $0.475 \pm 0.085$  (b)  $0.500 \pm 0.107$ . Stress at break [MPa] values: (a)  $0.348 \pm 0.116$  (b)  $0.719 \pm 0.390$ . See Fig. 2.

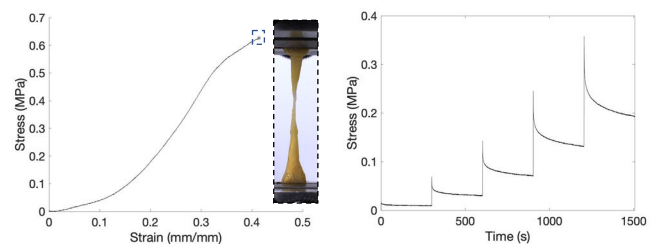


Fig. 2: Failure (left) and Stress-Relaxation (right) curves, as examples.

## IV. CONCLUSION

The proof of specific tissue anisotropy and viscoelastic behaviour is fundamental information for deepening the knowledge of SF arrangements, as a key connection between skin and deep muscle layer for the transmission of mechanical loads from multidirectional forces.

## ACKNOWLEDGEMENTS

This work was supported by MIUR, FISR 2019, Project n° FISR2019\_03221, titled CECOMES (*CEntro di studi sperimentali e COmputazionali per la ModElliStica applicata alla chirurgia*).

## REFERENCES

- [1] C. Stecco, *Functional Atlas of the human fascial system*. Churchill Livingstone, Elsevier Ltd, 2015, pp. 21-49.
- [2] M.F. Abu-Hijleh et al, "The membranous layer of superficial fascia: evidence for its widespread distribution in the body", in *Surgical and radiologic anatomy: SRA*, vol. 28 issue 6, 2006, pp. 606–619.
- [3] A. Porzionato et al, "Quality management of Body Donation Program at the University of Padova", in *Anat Sci Educ*, vol. 5 issue 5, 2012, pp. 264-272.
- [4] The MathWorks, Inc., *MATLAB and Statistics Toolbox Release 2021b*, Natick, Massachusetts, United States.

# Analysis of the mechanical behaviour of native and decellularized human diaphragmic tissue

M. Pelosin<sup>1</sup>, S. Todros<sup>1</sup>, S. Barbon<sup>2,3</sup>, E. Stocco<sup>2,3</sup>, V. Vindigni<sup>2</sup>, A. Porzionato<sup>2,3</sup>, P. Pavan<sup>1</sup>

<sup>1</sup> Department of Industrial Engineering, University of Padova, Italy

<sup>2</sup> Section of Human Anatomy, Department of Neuroscience, University of Padova, Italy

<sup>3</sup> Life Lab Program, Consorzio per la Ricerca Sanitaria, Padova, Italy

**Abstract**— In this work, the elastic and viscoelastic mechanical behaviour of human diaphragmic tissue is evaluated in native and decellularized conditions, to verify that the mechanical properties are maintained. This work represents one of the first studies focusing on the mechanical properties of scaffolds derived by decellularized human diaphragm and paves the way towards their use for muscular tissue engineering purposes.

**Keywords**— Human diaphragm; muscular tissue engineering; mechanical testing; viscoelasticity.

## I. INTRODUCTION

CELLULAR scaffolds derived from diaphragmic tissue's extracellular matrix (ECM) may represent a valid therapeutic solution for the reconstruction of lost or damaged muscular tissue. One of the main issues in diaphragm tissue engineering is related to the design of the optimal decellularization protocol: this should guarantee that, while removing all the antigenic elements from the tissue, the ECM's ultrastructure and biomechanical properties are preserved. In this sense, mechanical characterization of decellularized scaffolds is of key importance, given that the role of mechano-transduction in conditioning all aspects of cell behaviour has been demonstrated. The aim of this work is to compare the mechanical properties of human diaphragmic tissue in its native condition and after processing through four different decellularization protocols.

## II. MATERIALS AND METHODS

Four protocols were adopted for decellularization, differing in the detergents that were used; experimental details are reported in [1]. Considering the spatial distribution of diaphragmic muscle fibres, patches from a single cadaveric donor were cut into rectangular samples in longitudinal and transversal directions with respect to the muscle fibres. Tensile tests involved the application of five loading-unloading cycles up to a maximum nominal strain of 20%, at a constant strain rate of 1% s<sup>-1</sup>. Stress relaxation test were performed by applying an almost instantaneous 20% strain and maintaining it constant for the subsequent 600 s.

## III. RESULTS AND DISCUSSION

As shown in Fig. 1, both in the longitudinal and transversal directions, protocols n. 1, n. 2 and n. 3 caused a reduction of tissue stiffness, while samples obtained via protocol n. 4 reached higher stiffness values. Native tissue showed the highest anisotropy degree, with a higher secant modulus  $E_s$  along the direction transversal to muscle fibres; anisotropy was slightly decreased after decellularization with protocol n. 4, while the other decellularized samples displayed an almost isotropic behaviour. Fig. 2 shows the mean stress-relaxation curves obtained for each type of considered tissue.

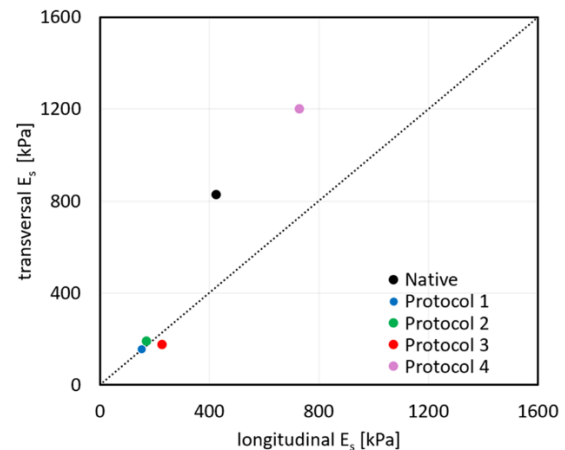


Figure 1. Mean values of secant elastic modulus ( $E_s$ ) at 20% strain: longitudinal vs. transversal  $E_s$  for native and decellularized tissues.

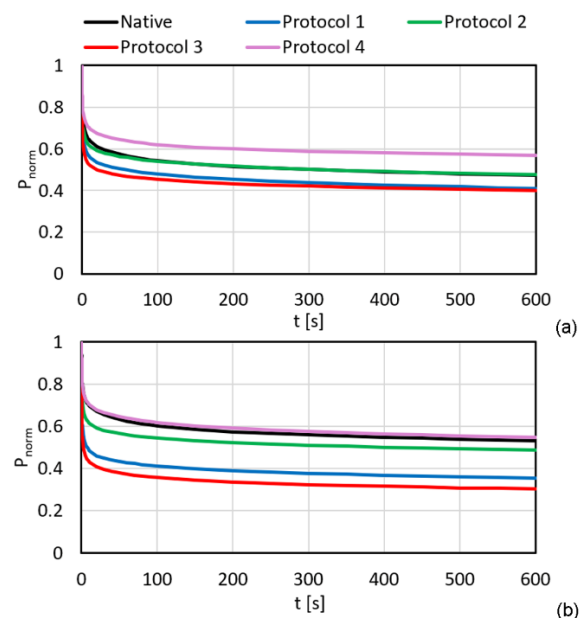


Figure 2. Mean normalized stress  $P_{norm}$  vs. time for native and decellularized tissues in longitudinal (a) and transversal (b) directions.

Analysis of variance on the values of  $P_{norm}$  at the end of the tests revealed a significant difference among the different groups of samples, both in longitudinal and transversal directions ( $p$ -value = 0.0207 and 0.036, respectively), although *post-hoc* analyses did not give significant results. These data showed that decellularization treatments affected the tensile mechanical response of human diaphragm in different ways, while a larger amount of samples will be needed to evaluate the effects on viscoelastic properties.

## REFERENCES

- [1] S. Barbon *et al.*, "Preclinical Development of Bioengineered Allografts Derived from Decellularized Human Diaphragm". *Biomedicines*, 2022, 10, 739.

# Fracture mechanics approach for fatigue life prediction of NiTi stent-like components considering experimental measurements and numerical simulations

Alma Brambilla<sup>1,2</sup>

<sup>1</sup>LaBS - Department of Chemistry, Materials and Chemical Engineering, Politecnico di Milano, Piazza Leonardo da Vinci 32, 20133 Milan, Italy

<sup>2</sup>Department of Mechanical Engineering, Politecnico di Milano, Via La Masa 1, 20156 Milan, Italy

**Abstract**—The fatigue failure of Nickel-Titanium stents, adopted to treat occlusive peripheral disease, is still an open issue of major concern. Despite total life approaches and many phenomenological methods have been proposed, the current literature lacks extensive knowledge on the fracture modality of NiTi thin struts under cyclic loads. This work aims at increasing awareness of the fatigue failure of NiTi devices. A fracture mechanics predictive tool is proposed to assess the fatigue life of NiTi stent-like specimens obtaining promising results.

**Keywords**—Nickel-Titanium, Shape memory alloy, Peripheral stents, Crack propagation

## I. INTRODUCTION

Nickel-Titanium (NiTi) alloy is a near-equiatomic shape memory alloy adopted in many engineering sectors including the biomedical field, where its pseudoelastic properties are exploited. Pseudoelasticity allows accommodating large strains, with a complete shape recovery at the unloading, when the working conditions are above a certain threshold of temperature. This enables the lattice to transform between two solid states, austenite and martensite. NiTi alloys find their main application in the cardiovascular field for manufacturing self-expandable peripheral stents for mini-invasive deployment in occluded vessels. Stents implanted in lower limb arteries undergo a complex set of cyclic loads related to leg movement, with frequently reported failures [1] associated with dramatic drawbacks [2].

NiTi fatigue assessment is usually performed by adopting total life approaches, monitoring the device lifetime as a function of the applied strain [3]. The presence of manufacturing-related defects on the surface of the stent suggests as an alternative a damage tolerant method accounting for the crack growth. This study is intended to investigate a fracture mechanics approach to assess the fatigue response of NiTi stent-like structures by coupling experimental tests with analytical and numerical tools.

## II. MATERIALS AND METHODS

The static and fatigue behavior of a Ni<sub>50.8</sub>Ti<sub>49.2</sub> alloy, provided as an as-cast billet, was extensively characterized. Given the influence of temperature on mechanical behavior, different thermal treatments were studied to tune the transformation temperatures of the material, assessed through differential scanning calorimetry. Uniaxial tensile tests were performed on dog-bone samples to characterize the mechanical properties, adopting Digital Image Correlation

(DIC) to evaluate the strain field. Crack propagation tests were carried out on C(T) specimens, exploiting DIC to measure the strain field at the crack tip. Fatigue crack growth properties were determined by adopting the Paris Law, using both the stress intensity factor range  $\Delta K$  and the cyclic J-integral  $\Delta J$  as crack driving forces. The propagation tests were supported by 2D finite element (FE) simulations, using a properly calibrated constitutive model and a node-release technique for crack growth. Lastly, a fracture mechanics predictive tool was developed. Starting from the experimental fatigue data collected on multi-wires stent-like samples, the  $\Delta J$  was computed to account for the deformation energy in the various loading regimes, following the elastic-plastic fracture mechanics approach proposed in [4]. The fracture surfaces were examined to highlight pre-existing defects and the  $\Delta J$  was finally implemented as the crack driving force parameter in a crack propagation algorithm to predict the fatigue life.

## III. RESULTS AND DISCUSSION

The agreement between experimental and numerical strain fields during crack propagation allowed to validate the FE model, which predicted the amount of stress-induced martensite at the crack tip at different load ratios. Crack propagation properties resulted slightly lower than those reported in the literature for textured materials [5] due to a microstructure effect. The final application of the  $\Delta J$  to stent-like samples fatigue data gave promising fatigue life predictions, accounting for the coupled role of mean strain and strain amplitude on the number of cycles to failure.

## REFERENCES

- [1] A. Kurayev, S. Zavulunova, and A. Babaev, "Role of nitinol stent fractures in the development of in-stent restenosis in the superficial femoral artery," *JACC Cardiovasc. Interv.*, vol. 7, no. 2, pp. 35, 2014, doi: 10.1016/j.jcin.2014.01.089.
- [2] D. Scheinert et al., "Prevalence and clinical impact of stent fractures after femoropopliteal stenting," *J. Am. Coll. Cardiol.*, vol. 45, no. 2, pp. 312–315, 2005, doi: 10.1016/j.jacc.2004.11.026.
- [3] S. W. Robertson, A. R. Pelton, and R. O. Ritchie, "Mechanical fatigue and fracture of Nitinol," *Int. Mater. Rev.*, vol. 57, no. 1, pp. 1–36, 2012, doi: 10.1179/1743280411Y.0000000009.
- [4] L. Patriarca, S. Foletti, and S. Beretta, "A comparison of DIC-based techniques to measure crack closure in LCF," *Theor. Appl. Fract. Mech.*, vol. 98, no. September, pp. 230–243, 2018, doi: 10.1016/j.tafmec.2018.09.020.
- [5] J. M. Stankiewicz, S. W. Robertson, and R. O. Ritchie, "Fatigue-crack growth properties of thin-walled superelastic austenitic Nitinol tube for endovascular stents," *J. Biomed. Mater. Res.*, vol. 81A, no. 3, pp. 685–691, 2007. <https://doi.org/10.1002/jbm.a.31100>.

# Perfusion and electromagnetic stimulation bioreactor for bone tissue engineering: optimization, characterization and validation tests

B. Masante<sup>1,2</sup>

<sup>1</sup> Polito<sup>BIO</sup>Med Lab, Department of Mechanical and Aerospace Engineering, Politecnico di Torino, Italy

<sup>2</sup> Bone and Dental Bioengineering Lab, CIR-Dental School, Department of Surgical Sciences, University of Torino, Italy

**Abstract**—We developed a versatile bioreactor that allows combining direct perfusion and pulsed electromagnetic stimulation, for bone tissue engineering applications. Iterative process of design, modeling, prototyping and testing allowed the culture chamber optimization. Preliminary biological tests validated the bioreactor in terms of ease of use, versatility, and functionality.

**Keywords**—Perfusion bioreactor, PEMF stimulation, Bone tissue engineering.

## I. INTRODUCTION

IN bone tissue engineering, physical stimuli, such as fluid flow-induced shear stress or pulsed electromagnetic field (PEMF), have been shown to be crucial *in vitro* for stimulating cells differentiation towards bone tissue [1,2]. However, many biological mechanisms and signalling pathways modulated by PEMF stimulation remain unknown leading to empirical treatments [3]. With a view to develop a reliable *in vitro* investigation methodology for studying the precise combination of physical parameters needed to reach a desired biological effect, the aim of this work was the optimization and validation of a versatile bioreactor that combines tunable direct perfusion and PEMF stimulation for *in vitro* investigating three-dimensional (3D) bone-like tissues under defined physical stimuli.

## II. MATERIALS AND METHODS

The bioreactor, to be incubated, is composed of: 1) culture chamber (CC) (Fig. 1A); 2) perfusion unit; 3) PEMF stimulation unit. The 3D-printed CC (priming volume = 2.5ml) consists of two screwable cylindrical parts and allows housing scaffolds of different sizes press-fit in tailored silicone holders, for guaranteeing direct perfusion. The CC is part of a closed-loop perfusion circuit (Fig. 1B), based on a peristaltic pump and controlled by a customized Arduino-equipped control box, which enables uni- or bi-directional flow (0.006-24ml/min) for scaffold cell seeding or perfusion culture. The PEMF stimulation is provided by a commercial device (1.5mT, 75Hz). To support the design optimization phase, multiphysics simulations (COMSOL Multiphysics) were performed, enabling characterizing the flow and magnetic fields developing within the CC. As exploratory biological tests, human mesenchymal stem cells were seeded into commercial porous scaffolds and, after 48 h of static culture, the constructs were transferred into the CC and exposed to unidirectional flow (0.3ml/min, 2h/day w/o PEMF stimulation) for additional 15 days. Control constructs were statically cultured for 15 days. During the culture, cell viability and release of the early osteogenic marker alkaline phosphatase (ALP) were assessed.

## III. RESULTS

Adopting an iterative process of design, CFD modeling, prototyping, and testing, the CC internal geometry was optimized and validate. Magnetic field modeling showed that the construct is exposed to a homogeneous magnetic field of 1.5mT (Fig. 1C). The cell viability analysis showed no significant differences between perfused and control constructs, while direct perfusion significantly increased the ALP release compared to control, promoting the formation of a bone-like construct (Fig.1D).

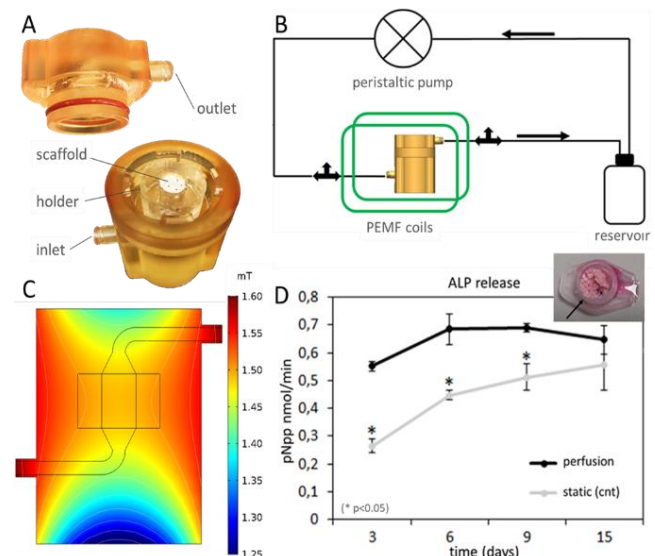


Fig. 1. A) Bioreactor culture chamber; B) Bioreactor set-up schematic drawing; C) Contour plot of the magnetic field distribution; D) ALP release analysis.

## IV. CONCLUSION

The proposed bioreactor provides, for the first time, a controlled 3D dynamic culture environment in which direct perfusion and PEMF stimulation can be combined, allowing an in-depth investigation of the biological effects exerted by PEMF exposure on bone tissue, with the final goal of providing guidelines for improved therapeutic treatments.

## REFERENCES

- [1] C. Wittkowske, "In Vitro Bone Cell Models: Impact of Fluid Shear Stress on Bone Formation." *Frontiers in bioengineering and biotechnology* vol. 4 87, 2016
- [2] H. Hu "Promising application of Pulsed Electromagnetic Fields (PEMFs) in musculoskeletal disorders." *Biomedicine & pharmacotherapy*, vol. 131, 2020
- [3] K. Varani, "Pulsed Electromagnetic Field Stimulation in Osteogenesis and Chondrogenesis: Signaling Pathways and Therapeutic Implications," *International journal of Molecular Science*, vol. 22,2 809, 2021

# Statistical Shape Analysis of the Thoracic Aorta with supra-aortic vessels: development of a Non-Rigid Registration Algorithm and correlation with CFD simulation results

Marilena Mazzoli<sup>1,2</sup>

<sup>1</sup> *BioCardioLab – Bioengineering Unit, Ospedale del Cuore, Fondazione Monasterio, Italy*

<sup>2</sup> *Department of Information Engineering, University of Pisa, Pisa, Italy*

**Abstract**—Ascending thoracic aortic aneurysm (aTAA) is a permanent dilation of the aorta. In most cases the aneurysm occurs without obvious symptoms, so the preventive diagnosis remains the most effective strategy for to prevent its aggravation. It is in this clinical context that both the studies based on Statistical Shape Models (SSMs) that those of Computational Fluid Dynamics (CFD) are inserted. The combination of these tools allows to relate the main geometric features, characterizing a certain group of patients, with hemodynamic features, related to the particular geometry of the aorta under examination [1].

**Keywords**—SSM, non-rigid registration, CFD.

## I. INTRODUCTION

Several studies based on SSM are present in the literature [2], however they do not include the total complexity of the thoracic aortic tract, excluding the supra-aortic vessels from analysis. This limitation is also reflected in the subsequent CFD clustering studies. The purpose of this thesis has been to overcome the main limitations of the literature for the implementation of SSMs and CFD analysis.

## II. MATERIAL AND METHODS

A total of 28 segmented aortas were considered, originated from CT scans. The segmented geometries were used to assess the SSM. This approach methods, in fact, require, as a first step, a set of geometries on which to define a source mesh that is deformed, through a non-rigid registration process, on all the other target meshes of the dataset. Starting from previous work of Nicolet et al. [2] for the rendering of images, we have implemented an in-house algorithm for non-rigid registration. Our approach is characterized by (i) a modified gradient descent approach of the second order, (ii) a loss function based on the minimization of chamfer distance and (iii) four steps of remeshing. The second step for the definition of a SSM consists in an efficient description of each shape of the aorta using the fewer parameters that accurately represent individual characteristics in terms of size, curvature, orientation and so on. Therefore, to reduce the dimensionality of the problem to few meaningful features, Principal Component Analysis (PCA) was applied to the new registered dataset. The first 16 principal components (or modes), significant for about 98% of the total variance, were used to reconstruct 5 new geometries varying the first mode -2 to +2 standard deviation (SD). A progression in the shape from healthy (-2SD) to completely aneurysmatic (+2SD) aorta was observed. The results of our code were firstly compared with those obtained by using software reported in literature such as Deformetrica and Gias2, and used to assess the morphological effects of computational fluid dynamics

(CFD). Volumetric meshes were generated in ANSA BETA CAE with polyhedral elements and six inflation layers. Simulations were carried out using ANSYS Fluent, considering the fluid as Newtonian and a laminar flow. An ideal flow was imposed to the inlet and, for each outlet, the Windkessel model with concentrated parameters. For the analysis of hemodynamics of the aneurysmal aorta, several parameters were used, such as the wall shear stress, the oscillatory shear index, the time averaged wall shear stress, the endothelial cell activation potential and the relative residence time. Finally, an analysis of correlation was performed between the change in the first mode of the SSM and the results obtained from the CFD simulations to derive a relationship between form, fluid dynamics and pathology.

## III. RESULTS

By applying the new proposed algorithm, it can be observed that, even in the case of a very peculiar target geometry shape distant from that of the source mesh, excellent results are obtained also with regard to the registration of the supra-aortic vessels, as reported in Figure 1.

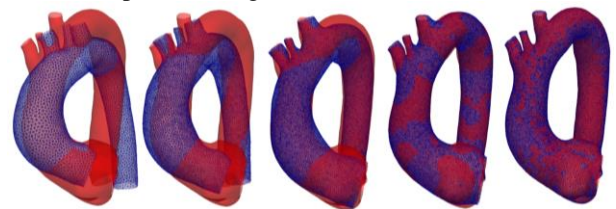


**Figure 1.** Frames of the registration process achieved with our algorithm.

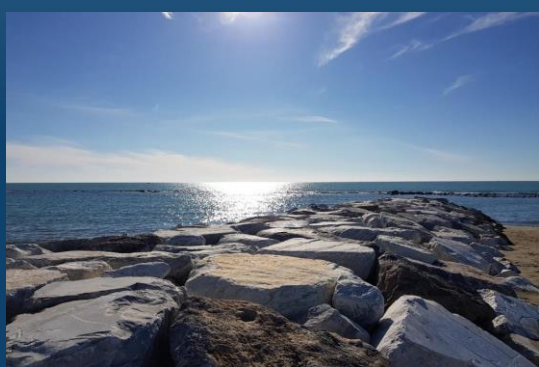
Significant correlations between the variation of the first mode, and hence the variation in size, and hemodynamical parameters were discovered. In conclusion, the presented methods and tools for the analysis of shape and function have the potential to contribute to a better understanding of complex structural disease, which may lead to the development of novel diagnosis and risk stratification strategies and, potentially, of new surgical approaches.

## REFERENCES

- [1] Rodero, Cristobal, et al. "Linking statistical shape models and simulated function in the healthy adult human heart." *PLoS computational biology* 17.4 (2021): e1008851.
- [2] Bruse, Jan L., et al. "How successful is successful? Aortic arch shape after successful aortic coarctation repair correlates with left ventricular function." *The Journal of thoracic and cardiovascular surgery* 153.2 (2017): 418-427.
- [3] Baptiste Nicolet, Alec Jacobson, and Wenzel Jakob. Large steps in inverse rendering of geometry. *ACM Transactions on Graphics (TOG)*, 40(6):1–13, 2021.



ESB-ITA2022  
XI ANNUAL MEETING - MASSA 6-7 OCTOBER 2022



Congress venue

Centro Congressi della Provincia di Massa-Carrara

Via S. Leonardo, 492

Marina di Massa